"Broadband" Plasma Waves in the Boundary Layers

G. S. Lakhina
Indian Institute of Geomagnetism,

Colaba, Mumbai - 400 005, India.

B.T. Tsurutani
Jet Propulsion Laboratory,

Pasadena, California, USA

H. Kojima, and H. Matsumoto
Radio Atmospheric Science Center, Kyoto University, Kyoto, Japan.

Short title: BOUNDARY LAYER PLASMA WAVES

Abstract. Boundary layers are commonly encountered in space and astrophysical plasmas. For example, interaction of solar wind plasma with the planets and comets produces magnetopause and cometopause boundary layers, respectively. Generally, the boundary layers are formed when plasmas with different characteristics interact with each other. The plasma sheet boundary layer in the Earth's magnetotail is formed due to the interaction of hot, dense plasma in the plasma sheet region with the rarified plasma of the lobe region. Boundary layers are the site where energy and momentum is exchanged between two distinct plasmas. Boundary layers occurring in space plasmas can support a wide spectrum of plasma waves spanning a frequency range of a few mHz to 100 kHz and beyond. The purpose of the review is to describe the main characteristics and the possible generation mechanisms of the broadband plasma waves (with frequencies > 1 Hz) observed in the Earth's magnetopause boundary layer, the Jovian magnetopause boundary layer, the plasma sheet boundary layer, and in the Earth's polar cap boundary layer. The rapid pitch angle scattering of energetic particles via cyclotron resonant interactions with the waves can provide sufficient precipitated energy flux to the ionosphere to create the dayside aurora at Earth, and a weak high-latitude auroral ring at Jupiter. In general, the broadband plasma waves may play an important part in the processes of local heating/acceleration of the boundary layer plasma. Recent exciting high time resolution results on the broadband plasma waves coming from Geotail, Polar and FAST will be discussed.

1. Introduction

The boundary layers in space and astrophysical plasmas are generally formed when plasmas with different characteristics interact with each other. For example, interaction of solar wind plasma with the planets and comets produces magnetopause and cometopause boundary layers, respectively. For the case of the Earth, the magnetopause boundary is formed by the interaction of the shocked solar wind plasma in the magnetosheath with the hot plasma in the magnetosphere. The magnetosheath is a region of shocked solar wind plasma downstream of the bow-shock that is formed ahead of the magnetopasue to deflect the oncoming super-Alfvénic and supersonic solar wind plasma smoothly around the Earth, as the geomagnetic field forms an an obstacle in its flow. At the bow shock, the solar wind gets heated and compressed. Several plasma measurements have identified the existence of a boundary layer, inside of and adjacent to the magnetopause, consisting of plasma with temperature and flow properties intermediate between the magnetosheath and the magnetosphere proper [*Hones et al.*, 1972; *Akasofu et al.*, 1973; *Eastman et al.*, 1976; *Haerendel et al.*, 1978]. The plasma in this region is a mixture of solar wind/magnetosheath plasma (H^+, He^{++}) and magnetosphere/ionosphere (H^+, He^+, O^+). This boundary layer is referred to as magnetospheric boundary layer [*Eastman et al.*, 1976; *Lundin*, 1987]. The low latitude portion of this boundary layer is known as the low latitude boundary layer (LLBL) and the high latitude part as the high latitude boundary layer (HLBL) which includes the plasma mantle (PM), entry layer (EL) and the polar cusp (PC) [*Hones et al.*, 1972; *Rosenbauer et al.*, 1975; *Eastman et al.*, 1976; *Haerendel and Paschmann*, 1982]. On the other hand, the plasma sheet boundary layer is formed due to the interaction of hot and dense plasma in the plasma sheet region with the rarified plasma of the lobe region of the magnetotail[*Haerendel and Paschmann*, 1982]. Figure 1 shows various boundary layers in the Earth's magnetosphere.

The magnetopause boundary layer is the region where solar wind energy and momentum is transferred into the magnetosphere. Two main processes by which the solar wind plasma can cross the magnetopause are 1) direct entry involving magnetic reconnection and 2) the cross-field transport due to the scattering of particles by the waves across the closed magnetopause field lines. Several processes, like impulsive penetration of the magnetosheath plasma elements with an excess momentum density [*Lemaire and Roth*, 1978; *Heikkila*, 1982; *Owen and Cowley*, 1991], plasma entry due to solar wind irregularities [*Schindler*, 1979], Kelvin-Helmholtz instability [*Miura*, 1987], and plasma percolation due to overlapping of a large number of tearing islands at the magnetopause [*Galeev et al.*, 1986], have been suggested for the plasma entry across the magnetopause. We will devote this paper to the topic of diffusion of particles due to boundary layer waves.

As mentioned above, solar wind plasma can cross the magnetopause and enter the magnetosphere either by a direct entry due to flow along reconnected, open field lines or by cross-field transport due to scattering across closed magnetopause field lines [*Tsurutani and Thorne*, 1982; *Baumjohann and Paschmann*, 1987; *Lee et al.*, 1994]. The first process is more likely to be important when IMF is directed southward, in this case the solar wind and magnetospheric field lines are anti-parallel and the magnetic reconnection can occur rather easily. Magnetic reconnection, due to southwardly directed fields lead to 5 to 10 % solar wind ram energy input into the Earth's magnetosphere [*Weiss et al.*, 1992; *Gonzalez et al.*, 1989] during substorms and storms. However, during northward interplanetary magnetic field (IMF) intervals, the energy injection due to magnetic reconnection is considerably reduced, and the wave-particle cross-field transport may become dominant. *Tsurutani and Gonzalez* [1995] have estimated that about 0.1 to 0.3 % of the ram energy gets transferred to the magnetosphere during northward IMF.

The boundary layers (BLs) occurring in space plasmas can support a wide spectrum of waves depending upon their plasma and field properties. In the magnetopause boundary layer, plasma waves with frequencies less than 1 Hz to 100 kHz and higher have been observed. These boundary layer waves can play an important role in the cross-field transport processes. These waves can diffuse the magnetosheath plasma across the closed magnetospheric field lines at a rate rapid enough to create the low latitude boundary layer (LLBL) itself [*Tsurutani and Thorne*, 1982; *Gendrin*, 1979, 1983; *Thorne and Tsurutani*, 1991; *Tsurutani et al.*, 1997]. This would provide a specific mechanism for "viscous interaction" [*Axford and Hines*, 1961, *Eviatar and Wolf*, 1968; *Tsurutani and Gonzalez*, 1995] in which the solar wind flow enery is transferred to the magnetosphere. These broadband waves may be important for the cross-scale coupling [*Ashour-Abdalla et al.*, 1995; *Horwitz et al.*, 1996]. *Tsurutani et al.* [1981] have shown that cyclotron resonant interaction of the LLBL waves with the energetic particles can put protons and electrons on near-strong to strong pitch angle diffusion to create the dayside aurora at the Earth, a phenomena that is ever present and is independent of substorms. The broadband plasma waves have large enough power to explain the boundary layer formation during non-reconnecting times [*Treumann et al.*, 1991]. At the same time, the magnetopause boundary layer waves may give rise to enough dissipation, and, thus, act as a trigger for magnetic reconnection to occur [*Cattell et al.*, 1995].

Similar waves have been detected at the Jovian LLBL by the Ulysses magnetometer and plasma wave instrument [*Tsurutani et al.*, 1997]. Although the Jovian waves are many order of magnitude less intense than those at Earth, due to the lower boundary layer field strengths near the Jovian magnetopause, the waves have sufficient intensities to create the Jovian LLBL from crossfield diffusion of magnetosheath plasma. The Jovian wave electric and magnetic fields have spectral shapes that are quite similar to those at the Earth.

Earlier, broadband electrostatic noise (BEN) has been observed in the neutral sheet by IMP-7 [*Scarf et al.*, 1974], and in the plasma sheet boundary layer (PSBL) by IMP-8 [*Gurnett et al.*, 1976]. These broadband plasma waves have been suggested as the source of hot ions in the central plasma sheet (CPS) [*Eastman et al.*, 1984].

Recent Polar plasma wave observations indicated that similar waves are present on magnetic field lines that penetrate the LLBL but are near the Polar apogee of 6-8 R_E and also near Polar perigee at ~ 2 R_E [*Pickett et al.*, 1997; *Ho et al.*, 1997; *Tsurutani et al.*, 1998]. The region of wave activity bounds the dayside (05 and 18 MLT, where MLT is the magnetic local time) polar cap magnetic field lines, thus these waves are called polar cap boundary layer (PCBL) waves.

Lakhina and Tsurutani [1999a] have summarized the the properties of broadband plasma waves in the magnetopause and polar cap boundary layers. Here we shall review the characteristics of high-frequency (wave frequency, $f > 1$ Hz) broadband plasma waves observed in the magnetopause boundary at Earth and Jupiter, the polar cap boundary layer, and in the plasma sheet boundary layer. In all the above three regions, the waves could play a crucial role in the heating, acceleration and cross-field diffusion of the electrons and ions. Section 2 describes the broadband plasma waves observed in the Earth's magnetopause boundary layer, and their possible role in the cross-field particle transport which sustains the boundary layer itself and in the formation of dayside aurora. Sections 3, 4 and 5 deal with the PCBL waves, the PSBL waves, and Jovian boundary layer waves, respectively. Various possible generation mechanisms for the boundary layer waves are discussed in Section 6. Section 7 summarizes the results, and gives a brief description of the latest results on the high time resolution of the broadband plasma waves.

2. Earth Magnetopause Boundary Layer

2.1. Broadband Plasma Wave Observations

The Earth's magnetopause represents a complex variable boundary. The ultra-low frequency (ULF) waves at the magnetopause have been studied by several workers [*Holzer et al.*, 1966; *Anderson et al.*, 1968; *Cummings and Coleman*, 1968; *Smith and Davis*, 1970; *Aubry et al.*, 1971]. Thedr long period waves are thought to be generated either by the magnetopause boundary motions or by the Kelvin-Helmholtz instabilities, tearing instabilities, or by drift wave type instabilities [*Holzer et al.*, 1966; *Miura*, 1987; *Sckopke et al.*, 1981; *Lakhina et al.*, 1993; *Anderson*, 1995; *Lakhina and Schindler*, 1996]. *Neugebauer et al.* [1974] reported whistler-mode waves at the magnetopause using wave magnetic field measurements from OGO-5. Magnetic waves near the ion cyclotron frequency ($f_{ci} \approx 1$ Hz) were reported by *Fairfield* [1976] from IMP 6 magnetic field measurements. *Bahsen* [1978] analysed the HEOS-2 magnetic data and showed that the wave amplitudes, in the frequency range 20 -235 Hz, peaked at the magnetopause, and the power spectral density falls off with increasing frequency. Here we will focus mainly on the high frequency plasma waves ($f > 1$ Hz) BL waves.

The results on both the plasma wave electric and magnetic fields in the vicinity of magnetopause were first reported by *Gurnett et al.* [1979] by using measurements from the ISEE 1 and 2 spacecrafts. They found that the maximum plasma wave intensities usually occur at the magnetopause. An example is shown in Figure 2. They observed magnetic waves in the frequency range of 5.6 to 1 kHz charcterized by a $f^{-3.3}$ power law spectrum. The electric field turbulence occurred in the frequency range 5.6 to 100 kHz and had a featureless spectrum obeying a $f^{-2.2}$ power law. Typical electric and magnetic field spectra of the magnetopause boundary layer waves are shown in Figure 3. In a few cases, *Gurnett et al.* [1979] could determine the polarization of the wave electric field

from the spin modulation of the electric field intensity. In cases where spin modulation was clearly present, the electric field had perpendicular polarization. *Gurnett et al.* [1979] suggested that the magnetic waves are whistler modes, and that the electric component is a superposition of some electrostatic emissions and the electric component of the whistler mode. From the analysis of 10 ISEE 1 and 2 magnetopause crossings, *Tsurutani et al.* [1981] reported an average magnetic wave spectrum to be 10 $f^{-3.9}$ nT^2 Hz^{-1} for the frequency range of (10 - 1000) Hz. A typical electric waves spectrum in the frequency range (10 - 10^5) Hz was characterized by $3 \times 10^{-5} f^{-2.8}$ $V^2m^{-2}Hz^{-1}$. However, both the spectra varied by an order of magnitude in amplitude from case to case. *Anderson et al.* [1982] studied the morphology of plasma waves associated with the magnetopause, from the magnetosheath to the outer magnetosphere using high time resolution measurements from ISEE 1 and 2. They found little difference in the plasma wave characteristics at the magnetopause, in the boundary layer, and in flux transfer events (FTEs).

The boundary layer magnetic wave spectrum at frequencies below 11 Hz, during an unusual event when the magnetopause penetrated to the geosynchronous orbit of GEOS-2, was analyzed by *Gendrin* [1983]. The wave intensity was found to decrease monotonically with increasing frequency which is consistent with the previous ISEE results at higher frequencies. *Rezeau et al.* [1986] extended the work of *Gendrin* [1983] and made a comparison of magnetopuse boundary waves and magnetosheath waves as shown in Figure 4. The upper panel in Figure 4 is the magnetosheath spectrum for the 3 directional components whereas the lower panel is the same for the magnetopause boundary layer. The average magnetosheath spectrum is indicated by the dashed line in the lower panel for easy comparison. Figure 4 clearly indicates that the boundary layer spectrum is enhanced above the magnetosheath spectrum (above 1 Hz) and has a similar frequency dependence. Recently, *Rezeau et al.* [1999] have shown that the

magnetic fluctuations at the magentopause exhibit power law spectra up to the lower hybrid frequency.

LaBelle and Treumann [1988] analyzed the AMPTE/IRM plasma wave data and found that the spectrum of electric as well as magnetic fluctuations decreases with frequency. Figure 5 shows an example of their AMPTE plasma wave data for an unusual event when the magnetopause boundary layer was pushed into AMPTE distances. The top panel shows the electric field in a frequency range of 30 Hz - 10 kHz, and the next panel the 0-16 Hz magnetic fields. The other panels show plasma and ambient field parameters. The vertical lines indicate the positions of the three magnetopauses. The dashed vertical line indicates the location of a diamgnetic structure or a magnetic "hole" in the magnetosheath region. The plasma waves are clearly enhanced in the last two crossings. A comparison of many spacecraft observations for the magnetopause boundary layer waves as summarized by *LaBelle and Treumann* [1988] is shown in Figure 6. Although the figure contains measurements from different instruments sampling different latitudes, local times, and radial distances of the dayside magnetopause for different time periods, together all of the measurements generally fit power law spectra for both electric and magnetic components. The various measurements all agree with one an other, within an order of magnitude in power, which is the typical variation of the spectra from one event to another as found by *Tsurutani et al.* [1981].

From a statistical study of the broadband plasma waves at the magnetopause using ISEE 1 plasma wave data, *Tsurutani et al.* [1989] reported enhanced wave intensities at 85% of all magnetopause crossing. Although wave amplitudes were highly variable from event to event, the wave spectra averaged over many passes are remarkably similar at dawn, noon and dusk local hours as seen from Figures 7 and 8. They found that the average wave intensity has a little or no dependence on latitude (-2° to +25°), magnetosheath field strength , or on magnetopause position. The wave were found to be

more intense during negative magnetosheath (interplanetary) B_z than during positive B_z. *Zhu et al.* [1996] studied the ELF-VLF waves within the current layer of the dayside magnetopause using ISEE 1 data. Their database consists of 272 crossings of the dayside magnetopause from 1977 to 1979. They find a nearly linear relationship between the local magnetic shear angle and the wave amplitudes (both electric and magnetic components) as shown in Figure 9. The magnetic shear angle θ is calculated from the magnetic field vectors ($\mathbf{B_1}$, $\mathbf{B_2}$) from the magnetometer at the starting and ending times for a given magnetopause crossing, using the formula $\cos\theta = \mathbf{B_1} \cdot \mathbf{B_2}/(|\mathbf{B_1}||\mathbf{B_2}|)$. They estimated the phase velocity $v_{ph} = E(\omega)/B(\omega)$ for different frequency channels by assuming that the electric perturbations are perpendicular to the propagation direction (i.e., ambient magnetic field direction). Their dispersion relation for different shear angles is shown in Figure 10. The dispersion relation has the characteristics of parallel propagating whistler modes, namely a rising tone and a cutoff at the electron cyclotron frequency. They, therefore, suggested that the waves are parallel propagating whistler modes. However, it should be noted that quantitatively the estimated v_{ph} from the observed amplitude ratio is more than three times greater than that calculated from the parallel propagating whistler mode dispersion relation (cf. curve labelled v_{w2} in Figure 10). Recently, *Song et al.* [1998] have found that most of the wave power in the current layer is in the magnetic fluctuations rather than the electric field fluctuations. Further, they found a clear correlation between the broadband waves and the electron plasma beta as shown in Figure 11a, but no clear correlation between the wave amplitudes and the electron anisotropy as seen from Figure 11b. In a case study, *Song et al.* [1998] found the wave electric field to be polarized nearly perpendicular to the ambient magnetic field as found by *Gurnett et al.* [1979].

2.2. Cross-Field Diffusion

The magnetopause boundary is more or less a collisionless plasma system. However, the interaction of broadband plasma waves with the charged particles can cause scattering of the particles thereby changing particles' momenta and energies. Thus wave-particle interactions in a collisionless plasma can play a role similar to direct particle-particle collisions in a collisional plasma. If there is no particle scattering by the waves, the magnetosheath ions are not expected to penetrate the boundary to a distance larger than a Larmor radius or so. Since the magnetopause thickness is generally much greater than an ion Larmor radius, the particle cross-field transport due to the wave-particle interaction has been invoked to explain the formation of the boundary layer.

2.2.1. Resonant wave particle interactions. A particle can interact strongly with the waves when it senses the wave Doppler-shifted to its cyclotron frequency (or its harmonics). This process is known as cyclotron resonance. The condition for the cyclotron resonance between the waves and the particles can be written as

$$\omega - k_{\|} v_{\|} = n\Omega, \tag{1}$$

where ω and $k_{\|}$ are the wave frequency and the parallel component of the wave vector $\mathbf{k}$, $v_{\|}$ is the parallel component of the particle velocity, $\Omega = qB_0/mc$ is the cyclotron frequency of the charged particle, B_0 is the magnetic field, q and m are particle charge and mass, respectively, c is the speed of light, and n is an integer equal 0, $\pm$ 1, $\pm$ 2, $\cdots$. The $k_{\|}v_{\|}$ term is the Doppler shift effect due to the particle motion relative to the wave. The case of $n = 0$ corresponds to the Landau resonance. When condition (1) is satisfied, the waves and particles remain in phase, leading to energy and momentum exchange between them.

Tsurutani and Thorne [1982] have given general expressions for cross-field diffusion of electrons and ions via resonant interaction with either electromagnetic or electrostatic waves. The cross-field diffusion rate due to the magnetic component of electromagnetic waves can be written as [*Tsurutani and Thorne*, 1982; *Thorne and Tsurutani*, 1991; *Tsurutani and Lakhina*, 1997]

$$D_{\perp,B} = 2\eta \left(\frac{B}{B_0}\right)^2 D_{max}, \tag{2}$$

where B is the amplitude of the wave magnetic field at the resonant frequency given by (1), η is a a dimensionless scaling factor indicating what fraction of time the particles stay in resonance with the waves, and

$$D_{max} = \frac{cmv_\perp^2}{2eB_0}, \tag{3}$$

is the Bohm diffusion rate [*Bohm*, 1949]. Here, $v_\perp$ denotes perpendicular velocity of the charged particles relative to the ambient magnetic field $\mathbf{B}_0$.

The cross-field diffusion rate due to the electrostatic waves is given by

$$D_{\perp,E} = 2\eta \left(\frac{E}{B_0}\right)^2 \left(\frac{c}{v}\right)^2 D_{max}, \tag{4}$$

where E is the amplitude of the wave electric field at the resonant frequency given by (1), and v is the magnitude of the particle velocity.

For the boundary layer parameters, $B_0 \approx 50$ nT, $N \approx 20$ cm^{-3}, protons of energies ~ 1 keV can be in cyclotron resonace with the wave at $\omega/\Omega_p \sim 1$ (Ω_p is the proton cyclotron frequency), i.e., at frequencies close to 1 Hz. At these frequencies, $B \approx 5$ nT [*Gendrin*, 1983; *Rezeau et al.*, 1986], then (2) gives $D_{\perp,B} = 260$ km^2 s^{-1} for 1.3 keV protons. On the other hand, 1 keV electrons will be resonant with the waves at frequency $\omega \sim \Omega_e/3$ (here Ω_e is the electron cyclotron frequency). As there is much less power at such high frequencies, therefore 1 keV electron diffusion due the cyclotron resonant

process will be negligible. The observations of *Tsurutani et al.* [1981] indicate amplitude of broadband electrostatic waves to be ~ 3 mV/m near Ω_p and $\sim 3 \times 10^{-3}$ mV/m near Ω_e. Then, from (4), the cross-field diffusion rates for the magnetosheath plasma ($\sim$ 1 keV protons and electrons) due to their cyclotron resonance with the electrostatic waves are $D_{\perp,E} \approx 4 \times 10^2$ km^2 s^{-1} for ~ 1 keV protons, and $D_{\perp,E} \approx 4 \times 10^{-4}$ km^2 s^{-1} for $\sim$1 keV electrons [*Tsurutani and Thorne*, 1982]. Once again the electron diffusion is insignificant compared to the ion diffusion. It should be noted that theoretical models of either a viscous momentum transfer [*Axford*, 1964] or mass diffusion across the magnetopause [*Sonnerup*, 1980] require a kinematic viscosity or diffusion coefficient comparable to 10^3 km^2 s^{-1} to account for the observed magnetopause boundary layer thickness. The cross-field diffusion rates for the magnetosheath ions due to resonant interaction with the electromagnetic or electrostatic waves are comparable to the value required to maintain the typical thickness of the boundary layer. Since the broadband waves show significant variability in the power spectral densities for both magnetic and electric components [*Gurnett et al.*, 1979; *Tsurutani et al.*, 1981; *Gendrin*, 1983; *LaBelle and Treumann*, 1988; *Tsurutani et al.*, 1989], this could lead to substantially different rates of cross-field diffusion thereby explaining the observed variations in the thickness of the magnetopause boundary layer.

The intense broadband wave in the magnetopause boundary layer can cause rapid isotropization of both the electron and ion distributions. *Tsurutani et al.* [1981] found a strong correlation between intense broadband waves and 1-6 keV electrons and protons. The observed wave power was found to be sufficient to scatter the 1-6 keV electrons and protons near the limit of strong pitch angle diffusion. On using the measured spectrum of the ISEE 1 electrons and ions and integrating from 1 to 10 keV, the precipitated energy flux into the atmosphere was estimated to be 0.15 erg cm^{-2} s^{-1}. When the presence of enhanced ion fluxes at energies from 300 to 500 eV is taken into account,

the precipitated energy flux is increased to ≈ 1.0 erg cm^{-2} s^{-1} [*Tsurutani et al.*, 1989]. These numbers are comparable to the dayside auroral energy input. It appears that resonant cyclotron interactions between the waves and particles in the boundary layer can provide a reasonable explanation for the nearly continuous presence of dayside aurora.

2.2.2. Anomalous diffusion from plasma instabilities. A process complementary to the resonant wave-particle interactions described above, is the stochastic scattering of particles by microscopic plasma turbulence. This process can lead to anomalous collision frequency, ν_{an}, in a collisionless plasma. Current driven plasma instabilities are found to be the best candidate for generating sufficiently high anomalous collision frequencies in space plasmas. Two most important sources of free energy for the excitation of plasma instabilities are the field-aligned currents and the cross-field currents due to the presence of a plasma density gradient perpendicular to the magnetic field [*LaBelle and Treumann*, 1988; *Thorne and Tsurutani*, 1991]. The anomalous collision frequency due to plasma instabilities driven essentially by field-aligned currents, is typically a fraction of the ion cyclotron frequency, i.e., $\nu_{an} \sim \Omega_p$ [*Dum and Dupree*, 1970; *Treumann et al.*, 1991], whereas it can be substantially higher for the case of perpendicular current driven instabilites [*LaBelle and Treumann*, 1988; *Thorne and Tsurutani*, 1991]. Anomalous collision freequencies can be used to estimate the cross-field diffusion coefficient [*Ichimaru*, 1973],

$$D_\perp = \frac{1}{2}\rho_e^2 \nu_{an} \left(1 + \frac{T_p}{T_e}\right), \tag{5}$$

where $\rho_e$is the electron gyroradius, and T_P, T_e are the respective proton and electron temperatures. Based on the quasi-linear theory, *LaBelle and Treumann* [1988] derived a simple general approximate formula for anomalous collison frequencies due to various

perpendicular current driven instabilities,

$$\nu_{an} \approx \frac{W}{m_e n V_D}\left(\frac{\gamma_m k_m}{\omega_m}\right), \tag{6}$$

where $W = \int W_k d^3k$ is the average wave energy density, n is the plasma density, V_D is the perpendicular current drift velocity, γ_m is the maximum growth rate, ω_m and k_m are respectively wave frequency and the wave number corresponding to the maximum growth. The wave spectral energy density is given by,

$$W_k = \left(\frac{\partial \omega \epsilon(\omega, k)}{\partial \omega}\right)\frac{1}{2}\epsilon_0 |\delta E_k|^2, \tag{7}$$

where $\epsilon(\omega, k)$ is the linear dielectric constant of the plasma for the wave mode under consideration, and δE_k is the linear wave amplitude. The above expressions are quite general, and applicable to a wider range of nonlinear waves if the dielectric constant and the amplitude are replaced by their nonlinear counterparts.

Estimates for anomalous diffusion coefficients for four plasma instabilities, namely, the modified two-stream instability (MTSI), the lower-hybrid drift instability (LHDI), the ion-acoustic instability, and the electron cyclotron drift instability (ECDI), based on their nonlinear saturation level as predicted by the quasi-linear theory, indicate that none of these four instabilities could provide adequate diffusion to maintain the boundary layer [*LaBelle and Treumann*, 1988]. *Gary and Sgro* [1990] and *Thorne and Tsurutani* [1991] pointed out an error in the estimation of the diffusion coefficient for the lower-hybrid instability in *LaBelle and Treumann* [1988]. The corrected estimates yield diffusion coefficients large enough to explain the thickness of the magnetopause boundary layer [*Treumann et al.*, 1991, 1995]. The correct expression for the anomalous collision frequency for the lower-hybrid instability is reproduced below.

The dielectric constant, $\epsilon(\omega, k)$, for the lower hybrid waves is given by [*Lakhina and*

Sen, 1973; *Davidson*, 1978; *Revathy and Lakhina*, 1977],

$$\epsilon(\omega, k) = 1 + \frac{\omega_{LH}^2\,\omega}{k^2 v_{tp}^2\,(\omega - kV_D)} = 0, \tag{8}$$

where v_{tp} is the ion (proton) thermal speed and $\omega_{LH} = \omega_p/(1 + \omega_e^2/\Omega_e^2)^{1/2}$ is the lower-hybrid frequency. Here ω_e and ω_p are the electron and proton plasma frequencies, respectively. Then, from (7) we get,

$$W_k = \left(1 + \frac{\omega_e^2}{\Omega_e^2}\right)\left(1 + \frac{k^2 v_{tp}^2}{\omega_{LH}^2}\right)\frac{\epsilon_0}{2}|\delta E_k|^2, \tag{9}$$

The solution of (8) yields the maximum growth rate $\gamma_m \approx (\sqrt{2\pi}/8)(V_D/v_{tp})^2\omega_{LH}$ and corresponding $\omega_m \approx k_m V_D/2$. On substituting these in (6), we obtain the following expression for the anomalous collision frequency for the lower-hybrid instability,

$$\nu_{an}^{LH} = \left(\frac{\pi}{8}\right)^{\frac{1}{2}}\frac{m_p}{m_e})\left(1 + \frac{\omega_e^2}{\Omega_e^2}\right)\frac{W}{nT_p}\omega_{LH} \tag{10}$$

Variation of the theoretical diffusion coefficients versus electric field power for four electrostatic modes considered by *LaBelle and Treumann* [1988] is shown in Figure 12 (this is a corrected version of their Figure 6). An average magnetic field strength of 50 nT, density $n = 10$ cm^{-3}, temperatures $T_e = 25$ eV, $T_p = 1$ keV have been assumed. The dots on each curve show the theoretically derived saturation levels of the respective instabilities. The vertical line is the upper limit of measured wave electric field intensity as deduced from the available satellite measurements of ISEE and AMPTE/IRM spacecraft. The horizontal dashed line gives the required Sonnerup diffusion limit. It is clear that the diffusion coefficient caused by the LHDI comes marginally close to Sonnerup diffusion limit. However, the diffusion coefficients from the rest of the instabilities are too low to be significant for the maintenance of the low latitude boundary layer. Hence, the LHDI could, in principle, provide sufficiently high diffusion rates, based on observed wave power, to account for the existence of

the LLBL under the conditions when reconnection in the vicinity of the subsolar stagnation point does not occur. It is interesting to note that all the four electrostatic instabilities shown in Figure 12, and LHDI in particular, may provide the dissipation necessary to initiate reconnection at the magnetopause under southward, or inclined IMF conditions. Observations from ISEE 1 and Geotail also indicate that the amplitudes of the magnetopause boundary layer waves are large enough to provide the dissipation required for reconnection to occur [*Cattell et al.*, 1995]. Recently, *Treumann* [1997] has suggested that in the region of strong plasma wave activity, particles undergo Lévy flight interactions caused by scale invariant turbulence. Plasmas containing Lévy flight intractions may possess super- diffusivity which is enahnced over the anomalous. Therefore, the strong broadband plasma wave activity at the magnetopause may lead to super-diffusive (of the order of or even greater than the Bohm diffusion) particle transport across the magnetopause to populate the inner LLBL.

The lower hybrid drift instability at the magnetopause has been studied, using a 2D hybrid computer simulation (particle ions, fluid electron with nonzero mass) code, by *Gary and Sgro* [1990]. The magnetopause wave generation (at low-frequencies, i.e., $\omega \ll \Omega_p$, as well as at lower hybrid wave frequencies) and particle transport using a 2D hybrid code with particle ions and massless fluid electrons as been investigated by *Winske and Omidi* [1995] and *Winske et al.* [1995]. The free energy source in all the above computer simulation studies was the density gradient. It is found that lower hybrid waves could give rise to diffusion comparable to the Bohm rate as required by *Sonnerup* [1980] to populate the low latitude boundary layer. However, the diffusion remained quite localized, meaning that diffusion per se leads only to some local relaxation of the gradients, and not to the formation of an extended boundary layer.

3. Polar Cap Boundary Layer

3.1. Wave Observations

Plasma wave data from the Plasma Wave Instrument (PWI) [*Gurnett et al.*, 1995] on the POLAR spacecraft indicate the presence intense broadband plasma waves on the polar cap magnetic field lines which map to LLBL. These waves are spiky, and their frequency dependence and intensities are quite similar to those of the low latitude boundary layer (LLBL) waves detected at and inside the low latitude dayside magnetopause (cf. section 2). These waves, therefore, are called polar cap boundary layer (PCBL) waves [*Tsurutani et al.*, 1997].

Figure 13 shows the POLAR orbit, which has an inclination of 86° with an apogee of $\sim 9\ R_E$ and perigee of $\sim 1.8\ R_E$ and covers the noon-midnight sector. Under ordinary circumstances the POLAR spacecraft does not intercept the magnetopause [Pickett et al., 1997], but as shown in the figure, the spacecraft does cross field lines that map into the LLBL.

Plate 1 is a frequency-time color spectrogram of the data obtained on April 7, 1996 from the POLAR Plasma Wave Multichannel Analyzer (MCA). This plot covers 24 hours as shown along the horizontal axis, and a frequency range of 5 Hz to 311 kHz, as shown along the vertical axis. The electric field power spectral density is plotted according to the color bar to the right of the spectrogram. The Universal Time (UT), radial distance from the center of the earth (R_E), magnetic latitude (λ_M), magnetic local time (MLT), and approximate L-shell value, are indicated at the bottom of the plot. The wave intervals of interest are indicated by two sets of arrows along the time axis, and are designated as "Dayside PCBL" and "Nightside PCBL" within Plate 1. These intervals of intense waves bound magnetic fields that map into the polar cap region. Both wave events occur in the northern hemisphere near apogee. The dayside

PCBL event occurs near 13.0 MLT and the other near 0.3 MLT, as the spacecraft orbit is in a near noon-midnight orientation. The PCBL waves are characterized by bursts of "turbulence" covering a broad frequency range extending from $f < 10^1$ to 2×10^4 Hz as shown in the MCA electric field spectrum of Plate 1. The magnetic field spectrum for these waves shows similar bursts (not shown). The region between the dayside PCBL and the nightside PCBL (about 0555 to 1450 UT) is identified as the northern polar cap. In this region there is typically a lack of strong signals although a few bursts of electrostatic noise are seen, as well as auroral hiss (3 kHz) and auroral kilometric radiation (100 kHz).

Figure 14 shows the fractional amount of time that the waves are present from March 13 to August 31, 1996 on the dayside (05 to 18 GMT) near POLAR apogee. During this period the spacecraft apogee was in the northern hemisphere. For this statistical study, the total number of "crossings" was 254. For each hourly bin, the number of passes are indicated, as well as the number of times PCBL waves were detected. The plot shows that enhanced waves were present 100 % of the time near local noon with a slightly lower occurrence rate at dawn and dusk. The overall percentage of wave occurrence during this time interval was 96 %.

The region of PCBL wave activity is located in a relatively narrow band of latitudes from 70° to 85° as seen from Figure 15a. The wave location is slightly lower than cusp field lines. There is a trend for the PCBL waves to extend to slightly lower latitudes in both the dawn and dusk sides relative to the noon sector. The PCBL waves occur predominantly in the region with $L \sim 10$ or larger as seen from Figure 15b.

The spectral density plots for both electric and magnetic field are found to have rough power-law shapes, even though the intensities and spectral shapes vary from event-to-event. The electric component has on average a $f^{-2.2}$ frequency dependence, and the wave frequency extends from $\sim 10^1$ Hz to $\sim 2 \times 10^4$ Hz, whereas the wave

magnetic component has on average a $f^{-2.7}$ frequency dependence and appears to have an upper frequency cutoff at the electron cyclotron frequency. The electric and magnetic spectra of a typical event occurring near the apogee in the northern hemisphere on day 98, 1996 at 1302 MLT at 78.8° N invariant magnetic latitude is shown in Figures 16. For this event, the wave frequency of the electric component extends to $\sim 2 \times 10^4$ Hz (Fig. 16a), and that of the wave magnetic component extends to $\sim 3 \times 10^3$ Hz (Fig. 16b). Note that the electric component of the waves extends to frequencies above the electron cyclotron frequency. Although it appears that the wave magnetic component cuts off at the electron cyclotron frequency, f_{ce}, this is too close to the noise floor of the receiver to make any definite determination.

The PCBL waves are found to be very bursty when seen in high time resolution wideband receiver (WBR) data. They last from a few milliseconds to tenths of seconds, with the latter probably composed of several bursts occurring in succession or simultaneously [*Tsurutani et al.*, 1998a]. Further, the average power spectra and the wave intensities for the electric and magnetic components for the events near the POLAR perigee in the southern hemisphere were found to be similar to those of the apogee events in the northern hemisphere.

Figure 17 shows the B/E ratios for two events occurring on Day 98 and 114, 1996. Two representative curves for the whistler refractive index for parallel propagation ($\psi = 0°$) and for oblique propagation (at $\psi = 60°$) are added for comparison. These curves asre calculated from the following expression for the refractive index,η, for the obliquely propagating whistler waves in a cold uniform plasma:

$$\eta = \frac{f_{pe}}{f^{1/2}(f_{ce}\cos\psi - f)^{1/2}}, \tag{11}$$

where $f = \omega/2\pi$, and $f_{pe} = \omega_e/2\pi$ are, respectively, the wave frequency and the electron plasma frequency expressed in Hz, and ψ is the angle of propagation with respect to the

magnetic field direction. The cold plasma density values fluctuated considerably during the wave events. For example, N_e values varied from 0.7 to 3.8 cm^{-3} for day 98, and 0.9 to 6 cm^{-3} for day 114. The maximum value of N_e has been used while computing the whistler refractive indices.

It is seen from Figure 17 that the B/E amplitude ratio generally fits the parallel propagating ($\psi = 0°$) whistler wave curve at the lowest frequencies ($f < 100$ Hz). At mid (10^2 Hz $< f < 10^3$ Hz) and high ($f > 10^3$ Hz) frequencies, the B/E ratio shows considerable departure from the ψ =0° curve and a somewhat better fit with the ψ = 60° curve. This clearly indicates that there could be considerable (off-axis) refraction associated with the higher frequency components. The B/E ratios lie in the range of 10 to 100. Thus, the wave phase velocities range from 3×10^3 to 3×10^4 km s^{-1}. These velocities are much higher than plasma convection speeds measured in this region of space, so Doppler shift effects on the phase velocities or on the B/E ratios should be negligible.

The broadband plasma waves are found to be well correlated with enhanced ion fluxes (H^+, O^+, He^+ and He^{++}), whenever these ions are presents on the PCBL field lines, as detected by the toroidal imaging mass-angle spectrograph (TIMAS) [*Shelley et al.*, 1995] experiment on POLAR. An example is shown in Plate 2 for April 7 (day 98), 1996. Prior to 0500 UT, the energy and angular distributions of ions reveal primarily hot quasi-isotropic ion populations characteristic of the dayside magnetosphere. The energy-latitude(time) dispersion in the H^+ and He^{++} populations beginning about 0505 and 0530 UT, are characteristic of the entry of magnetosheath plasma into the cusp or boundary layer. The regions of most intense wave activity (0500 to 0515 UT) is associated with significant changes in the angular distributions in the upflowing O^+ ions. Specifically, in these regions, the upflowing, relatively low energy O^+ ions have angular distributions that are peaked at 50 to 70 degrees relative to the magnetic field direction.

They have energies of a few hundred eV. The most probable mechanism for which the O^+ ions can gain significant energy transverse to the local magnetic field is through interactions with waves. Assuming that heating occurs primarily in the perpendicular direction, we can estimate the location of the region below the spacecraft. Because the magnetic field strength falls off roughly as r^{-3} and the first adiabatic invariant $mv_\perp^2/2B$ is conserved, we can estimate the maximum distance below the spacecraft where the transverse energy was possibly acquired. For conic angles of 50, 60, and 70 degrees at an altitude typical for these observations (5.5 R_E), the maximum distances below the spacecraft where the transverse energy could be acquired are 0.9, 0.5, and 0.2 Earth Radii (R_E), respectively. These locations are quite close to the spacecraft, so the energization process is essentially a local one.

3.1.1. Characteristics of PCBL waves. The PCBL waves occur on field lines that map into or close to the LLBL field lines, and the wave characteristics (cf. Figure 14-17) are quite similar to those of the LLBL waves. An inter-comparison between the POLAR wave power spectra and the LLBL waves as measured by ISEE-1 and 2 and GEOS is given in Table 1. The GEOS event, which is much more intense than either ISEE-1 and -2 or POLAR wave intensities, is somewhat anomalous as it occurred during a magnetic storm when the magnetopause was pushed in to the spacecraft orbit (6.6 R_E). It is possible that the extraordinarily high solar wind ram pressure and intense southward interplanetary magnetic field B_s may have led to unusually high wave power during this event. Such LLBL wave intensity dependences on interplanetary parameters have been discussed at Earth and Jupiter by Tsurutani et al. [1989] and Tsurutani et al. [1997], respectively. Table 1 also lists a spectrum for day 103, 1996 for POLAR when it was near the southern hemisphere dayside perigee at $\sim 2\ R_E$. We note that the wave intensities are of the same order as the high altitude northern hemispherical events. Table 1 also lists a typical spectrum for the Jovian wave event recorded by Ulysses for

comparison.

The main charactersitics of the PCBL waves are summarized below:

1. The PCBL wave regions are located at 70° to 80° invariant magnetic latitude. This location is just below the cusp fields (75° to 85° latitude) and thus corresponds to LLBL field lines. The PCBL waves detected at low $\sim 2\ R_E$ altitudes are similar to those detected at high altitudes (6 to 8 R_E).

2. The emissions are bursty, but when averaged over longer time intervals, they fit a rough power law with a $f^{-2.2}$ dependence for E and $f^{-2.7}$ dependence for B waves, on average. The electric component extends from $\sim 10^1$ Hz to $\sim 2 \times 10^4$ Hz and the magnetic component from $\sim 10^1$ to $\sim 5 \times 10^3$ Hz.

3. The waves have very similar intensities, spectral shapes and E and B dependences as the LLBL waves. The PCBL waves are similar to the broadband noise on auroral field lines [Gurnett and Frank, 1977; Gurnett et al., 1984], but unlike the latter, the PCBL waves do not have any clear peaks at any frequency.

4. The B/E ratio is consistent with the parallel propagating whistler mode waves for the low frequency (10^1 - 10^2 Hz) component. However, the B/E ratio is often higher at mid- (10^2 - 10^3 Hz) and high- (10^3 - 10^4 Hz) frequencies, consistent with off-axis propagating waves.

5. The intense noon sector wave events are well correlated with enhanced fluxes of 10 to 200 eV H^+, He^{++} and O^+ ions.

A schematic of the magnetic field lines, the PCBL wave locations and the LLBL wave locations is shown in Figure 18. Although to date such waves have been identified at only three regions along the field lines (PCBL, LLBL and POLAR near-perigee), one can argue that the waves most likely exist along the entire length of the field lines

provided that the field lines are "closed" and extend from one hemispherical ionosphere to the other. The PCBL wave field lines must be configured as indicated in Figure 18, where they map into the earth's ionosphere over a broad region of local times. The three-point intensity (LLBL, POLAR near-apogee, POLAR near-perigee) measurements put strong constraints on the wave source location. An ionospheric source can be ruled out because if wave generation occurs in the ionosphere, upward wave propagation would lead to wave intensity decreases (from POLAR perigee to LLBL location) by orders of magnitude due to flux tube expansion alone. Wave damping and scattering would decrease intensities further. Some other possibilities are the magnetosheath magnetosonic waves couple into LLBL Alfvén waves [Johnson and Cheng, 1997] and magnetosheath waves that are amplified at the magnetopause and propagate down the magnetic field lines [Belmont et al., 1995]. However, these wave-coupling mechanisms would work only for ultra-low-frequency (ULF) waves which are much below the PCBL broadband plasma wave frequencies. The most likely scenario appears to be the wave generation by a local source of free energy existing along field lines. Two possible sources are field-aligned currents and density gradients [*Drake et al.*, 1994a,b; *Lakhina et al.*, 1997; *Lakhina and Tsurutani*, 1999b].

4. Plasma Sheet Boundary Layer (PSBL)

4.1. Broadband Electrostatic Noise (BEN)

The broadband electrostatic emissions near the neutral sheet were observed during the substorms, for the first time, by *Scarf et al.* [1974] using the IMP 7 spacecraft . *Gurnett et al.* [1976] showed that such broadband electrostatic emissions are commonly observed around the plasma sheet. They referred to these emissions as "broadband electrostatic noise (BEN)." *Gurnett et al.* [1976] reported BEN's detailed features using

the plasma wave data observed by IMP-8, which passes through the magnetotail at radial distances ranging from about 23 R_E to 46 R_E. Figure 19 shows a typical spectrum of BEN reported by *Gurnett et al.* [1976]. BEN usually occurs over a broad range of frequencies extending from about 10 Hz to a few kHz with intensities ranging from about 50 μV/m to 5 mV/m. An interesting feature shown in Figure 19 is a quasi-upper cutoff around a few hundred Hz. *Gurnett et al.* [1976] pointed out that this quasi-upper cutoff frequency is almost equal to the local electron cyclotron frequency (f_{ce}). They also noted that the BEN spectra have a lower cutoff at the local lower hybrid resonance frequency.

The wave features of BEN reported by *Gurnett et al.* [1976] are summarized as follows:

1. The noise usually occurs over a broad range of frequencies from very low values up to the local electron plasma frequency.
2. BEN consists of many discrete bursts lasting from a few seconds to several minutes.
3. The spectrum shows a marked decrease in intensity at the electron cyclotron frequency.
4. BEN has a low frequency cutoff corresponding to the local lower hybrid resonance frequency.
5. The electric field is oriented within $\pm 20°$ from perpendicular to the magnetic field.
6. BEN is commonly observed in the plasma sheet boundary layer with a strong correlation with high energy ion flows.

Gurnett et al. [1976] found a good correlation between BEN and ion streams observed in the plasma sheet boundary layer (PSBL). This correlation has lead to many

possible theoretical mechanisms for BEN generation. Proposed mechanisms include ion beam instabilities such as ion-ion two stream instability [*e.g., Akimoto and Omidi*, 1986; *Schriver et al.*, 1990; *Grabbe*, 1987], the ion beam acoustic instability [*e.g., Dusenbery and Lyons*, 1985; *Omidi*, 1985; *Akimoto and Omidi*, 1986; *Ashour-Abdalla and Okuda*, 1986a, b; *Dusenbery*, 1986; *Grabbe and Eastman*, 1984; *Grabbe*, 1987; *Burinskaya and Meister*, 1989, 1990], the Buneman instability [*Grabbe*, 1985, 1989], and their combinations [*Schriver and Ashour-Abdalla*, 1987; *Schriver and Ashour-Abdalla*, 1990]. *Tsutsui et al.* [1991] considered ion flow as the plasma bulk flow to provide the Doppler shift, and they attempted to explain the broad frequency characteristics of BEN by the Doppler shifted ion acoustic potential bubbles convecting with the plasma bulk flow.

On the other hand, *Parks et al.* [1984] demonstrated the relation of the BEN and electron beams based on the observations by ISEE-1 spacecraft. Further detailed analyses on the relation of BEN and electron distributions were conducted by *Onsager et al.* [1993]. They showed that BEN can be observed in the electron layer of the outer PSBL without energetic ions. They pointed out that the ion streaming is not essential for the excitation of BEN, and stressed that BEN has a close relationship to the electron dynamics.

The above proposed generation mechanisms address the destabilization of normal modes due to ion and/or electron beams. On the other hand, *Nishida et al.* [1985] have argued that the high frequency part ($f > f_{ce}$) of BEN is not a normal mode. They suggested the possibility that this high frequency component corresponds to potential structures picked up very closed to electric field antennas.

In spite of the above observational and theoretical efforts, the clear answers to the generation mechanism of BEN have not been obtained. The main difficulty in explaining BEN excitation comes from the broadness of its spectrum. In order to explain this wide frequency band, scientists had resorted to assuming that several different instabilities

were responsible.

4.2. Electrostatic solitary waves

Most of the above observation results and data analyses of BEN were discussed in the frequency domain. However, using waveform observations by GEOTAIL, *Matsumoto et al.* [1994] and *Kojima et al.* [1994] revealed that BEN involves a series of solitary bipolar waveforms.

Plate 3(a) shows the frequency-time spectrogram of BEN observed in the PSBL at (–118 R_E, 4.3 R_E, 0.7 R_E) on April 1, 1993. The coordinate system is GSM. One can clearly see intense BEN spectra extending all the way to the electron plasma frequency ($f_{pe} \sim 2$ kHz) during the intervals from 13:30 to 13:36 (UT), from 13:41 to 13:53 (UT), from 13:54 to 14:00 (UT) and from 14:12 to 14:22 (UT). Plate 3(b) shows waveforms observed by the Wave-Form Capture (WFC) receiver at 13:55:43.241 (UT). The observed waveforms are completely different from that of incoherent random noise. The pulse width shown here is about 2 msec. One of the interesting points shown in Plate 3(b) is that observed solitary waves detected by the two orthogonally crossed set of electric field antennas, E_U and E_V, have coherent structures.

Because the most frequently observed BEN emissions have isolated pulse waveforms and no obvious corresponding magnetic component, *Matsumoto et al.* [1994] termed them "PSBL Electrostatic Solitary Waves (PSBL ESW)" after their waveforms. However, note that the PSBL ESW mainly contributes to the high frequency portion of the BEN spectra. Wave amplitudes of the ESW at lower frequencies as shown in Plate 3, are too small to explain the low frequency component.

Based on the results of detailed analyses *Matsumoto et al.* [1994] and *Kojima et al.* [1997] concluded that ESW correspond to isolated electrostatic potentials traveling along the ambient magnetic field. The nature of the PSBL ESW are summarized as

follows:

1. Typical pulse widths are a few milliseconds.
2. The orientation of the electric field is parallel to the ambient magnetic field.
3. The PSBL ESW waveform corresponds to an isolated potential structure flowing along the ambient magnetic field.
4. The PSBL ESW appear very bursty and intermittently. The bursty nature of the BEN's high frequency range is due to the bursty nature of the PSBL ESW.

Computer simulations using a one-dimensional full particle code succeeded in reproducing ESW waveforms [*Matsumoto et al.*, 1994; *Omura et al.*, 1994]. They showed that the nonlinear evolution of electron beam instabilities lead to the formation of isolated electrostatic potentials traveling along the ambient magnetic field. The reproduced potential structures are very stable, and are equivalent to the Bernstein-Greene-Kruskal (BGK) solution [*Bernstein et al.*, 1957]. *Omura et al.* [1996] extensively examined several different types of electron beam instabilities and found that the most plausible and realistic generation mechanism of the ESW is the electron bump-on-tail instability.

Figure 20 shows the time evolution of the bump-on-tail instability obtained by the one-dimensional computer simulations. The right- and left-panels display the time series of electron phase diagrams and reduced electron velocity distributions. The vortices shown in the bottom left panel are electron holes formed by trapped electrons due to isolated electrostatic potentials, which are generated by the nonlinear evolution of the bump-on-tail instability. As shown in Figure 20, the energies of trapped electrons are much smaller than those of background electrons. This means that the isolated potentials formed do not play an important role in thermalizing the electrons. This

result can be confirmed in the velocity distribution shown in the bottom right panel of Figure 20.

The ESW explain the high frequency part of the BEN spectra and computer simulation results strongly suggest that the ESW are the results of the nonlinear evolution of the electron bump-on-tail instability. However, the ESW do not explain all of the features of the BEN reported by *Gurnett et al.* [1976]. For example, *Gurnett et al.* [1976] reported that the electric field is oriented within ±20° from perpendicular to the ambient magnetic field. This feature cannot be explained by the ESW, because the electric field orientation of the ESW is almost parallel to the ambient magnetic field. On the other hand, *Onsager et al.* [1993] reported that the intense high frequency part of BEN are oscillating in the parallel direction to the ambient magnetic field. Using these results, we can conclude that while the high frequency portion of the BEN spectra correspond to the ESW, the low frequency part of the BEN are different mode waves from the ESW. The exact mode of the low frequency part is still unclear.

4.3. Scattering of electrons/ions due to the BEN

Eastman et al. [1984] suggested that the source of hot ions in the central plasma sheet (CPS) are warm ions from the PSBL. The best candidate which is responsible for scattering ions in the PSBL are the plasma waves. Further, since the most intense waves in the PSBL is BEN, one can arrive at the speculation that the BEN scatters the warm ions in the PSBL and the scattered warm ions are convected into the central plasma sheet (CPS).

As we discussed in the previous section, the high frequency portion of the BEN consist of the ESW. Further, *Omura et al.* [1996] demonstrated that the most plausible generation mechanism of the ESW is the electron-bump-on tail instability. As we can see in Figure 20, significant scatter of electrons or ions does not take place in the

bump-on-tail instability, because the generated potential energies are relatively small to the background plasma thermal energies. This model predicted by computer simulation is supported by Geotail observation results. *Kojima et al.* [1999] statistically examined the ESW potential energies using Geotail waveform and plasma measurements and concluded that potential energies of the ESW are mostly less than 10 eV. The value of 10 eV is much less than the background ion and electron thermal energies of 1 keV and 300 eV, respectively. Thus, we can conclude that the ESW, as the high frequency portion of the BEN, do not have a significant role of scattering PSBL ions/electrons.

There exists the possibility that the low frequency part of the BEN, which carry most of the wave energy, causes the diffusion of warm PSBL ions. *Grabbe and Eastman* [1984] and *Dusenbery and Lyons* [1985] argued that BEN can be generated due to ion beam instabilities and that the excited electrostatic waves possibly scatter warm ions in the PSBL. *Dusenbery and Lyons* [1989] evaluated the ion diffusion coefficients due to the ion beam instabilities. They solved the unmagnetized dielectric function with ion beams and showed that ion-sound waves can be generated under the coexistence of cold and hot ion beam components. They also examined the parametric dependence of diffusion rate of ions due to the resonance with excited ion-sound waves, and concluded that significant diffusion should occur resulting in isotropization of the warm ions in the PSBL.

The wave mode of the low frequency part of BEN still remains to be explained. The above discussion on scattering the PSBL ions strongly depend on the wave mode or the generation mechanism of the BEN's low frequency component. However, *Kojima* [1998] reported that the waveforms corresponding to the BEN low frequency component are continuous and that their electric field orientation is almost perpendicular to the ambient magnetic field. Further, their peak frequencies are almost equal to the local lower hybrid resonance frequency. These results obtained from Geotail waveform

observations are consistent with the BEN characteristics reported by *Gurnett et al.* [1976]. These facts are very suggestive to the generation of whistler mode-type waves. The results from the detailed waveform analyses on the BEN low frequency component are expected in the near future.

5. Jovian Magnetopause Boundary Layer

The presence of the magnetopause boundary layer in the Jovian magnetotail has been inferred from the Voyager measurements [*Lanzerotti et al.*, 1979; *Gurnett et al.*, 1980]. *Sonnerup et al.* [1981] reported the existence of a boundary layer near the dayside Jovian magnetopause by analyzing Pioneer 10 and 11 plasma and magnetic field data. Recently, *Bame et al.* [1992] have reported the detection of magnetopause boundary layer using the plasma measurements during Ulysses flyby. Because of solar wind ram pressure variations, the magnetopause boundary layer was crossed several times on both the inbound and outbound portion of the Ulysses flyby trajectory [*Phillips et al.*, 1993], and this provided a wealth of information on the boundary layer waves.

5.1. Wave Observations

Low-frequency (LF) electromagnetic waves in and near the Jovian magnetosphere have been reported by several authors [*Smith et al.*, 1976, 1983; *Smith and Tsurutani*, 1983; *Goldstein et al.*, 1983; *Smith and Lee*, 1986; *Glassmeier et al.*, 1989]. *Tsurutani et al.* [1993] were the first to report the enhanced broadband noise in LF frequencies in a Jovian boundary layer (JBL) using Ulysses magnetometer data [*Balogh et al.*, 1992]. They reported the detection of enhanced electromagnetic waves at the proton cyclotron frequency, a feature similar to that found by *Gendrin* [1983] for the Earth's LLBL waves. The local peak power in the magnetic wave spectrum was found to be ~ 1 nT^2 Hz^{-1} occurring at $\sim 2 \times 10^{-2}$ Hz, and a total power of $\sim 10^{-1}$ nT^2 was determined

assuming a bandwidth of 10^{-1} Hz.

Recently, *Tsurutani et al.* [1997] have reported the plasma wave spectra from 10^{-3} to 10^{2} Hz for the 14 time intervals of the Ulysses Jovian magnetopause BL crossings identified by *Phillips et al.* [1993]. They combined the dc magnetometer (MAG) [*Balogh et al.*, 1992] and ac search coil data from Ulysses radio and plasma wave (URAP) instrument [*Stone et al.*, 1992] to cover the frequency range from essentially dc to ELF frequencies for the magnetic (B) component of the wave. Data from the URAP electric field sensors were used for the electric (E) component of the wave spectra.

Figure 21 shows both the E and B wave for all 14 JBL events. The top 4 panels show the E spin average 9.3-, 14-, 19-, and 28-Hz channel wave intensities, the next 4 panels show the B spin average wave intensities for the same frequency channels, the next 2 panels show B 1-min and 10-min variance (taken from dc magnetometer), and the bottom two panels show the spacecraft location relative to Jupiter. The shaded events are the BL intervals, the vertical dashed lines indicate the bow shock crossings, and magnetosheath/BL intervals are shown by horizontal bars in the top panel. Enhanced wave intensities are sometimes present in frequency channels ranging from 9.3 Hz (displayed) up to electron cyclotron frequency, $\sim$ 140 Hz. The signals are more intense in the lowest frequency channels shown. The magnetosheath signals are generally less intense than those in the boundary layer, a situation similar to that for the Earth's BL/magnetosheath waves [*Gurnett et al.*, 1979; *Anderson et al.*, 1982]. The waves are more intense on the outbound pass than the inbound pass. This has been speculated to be due to the unusually low solar wind ram pressure during the inbound pass.

Power spectra for the B and E waves for the event 10, which was one of the intense intervals that occurred around 1820 - 1910 UT on day 043, 1992, are shown in Figure 22. The electric wave spectra is shown in the left-hand panels, and the combined MAG and URAP magnetic spectra are shown in the right-hand panels. The instrument

background noise and the best-fit power law curves for E as well as B waves are also shown. The E spectrum has a $4.1 \times 10^{-9} f^{-2.4}$ V^2 m^{-2} Hz^{-1} fit, and is broadbanded with no obvious peaks within the frequency range shown here, the later property is typical of all the 14 events shown in Figure 21. The overall combined B spectra for this event have a $1.8 \times 10^{-4} f^{-2.4}$ V^2 m^{-2} Hz^{-1} fit, and the wave intensities are greatest at low-frequencies.

Figure 23 shows the B/E ratio for the event 10 shown in Figure 22. At 1 Hz, $B/E \sim 200$, and the ratio decreases with increasing frequency but increases from 10^1 Hz to above 10^2 Hz. Overall, the ratio remains relatively constant near the value ~ 100.

For purely electromagnetic, parallel propagating waves, $B/E = \eta = c/V_{ph}$, where η is the refractive index, c is the velocity of light, and V_{ph} is the phase velocity of the wave. At low-frequencies, $V_{ph} \sim V_A$, the Alfvén velocity, and η decreases with a $f^{-1/2}$ dependence as long as $f \ll f_{ce}$(cf. equation (11)). A typical measured value of the Alfvén velocity in JBL is $V_A = 2.4 \times 10^7$ cm s^{-1}, and this would give $\eta = 870$. The measured values of B/E ratio is reasonably close to the theoretical value, given the errors in the measurements of B and E. The B/E ratio curve in Figure 23 shows a $f^{-1/2}$ dependence for the frequency range of 10^0 - 10^1 Hz. However, for 10^1- to 10^2- Hz range, the B/E ratio has a positive slope. Since clear E wave signals were not detected at frequencies above the electron cyclotron frequency ($\sim$ 140 Hz), there is a possibility that the JBL waves might be purely electromagnetic in nature.

A comparison of Jovian waves and the Earth's BL waves is given in Table 1. The wave power at Jupiter is lower by several orders of magnitude than the Earth's BL waves. There are, however, several similarities of the waves for the two different magnetospheres. Both the JBL and the Earth's BL waves have power law type spectra without any obvious spectral peaks, and the slopes of the electric field spectra are quite similar. In addition, the measurements of Jovian magnetic field spectral slopes fall

within the range of the terrestrial spectral slopes. Further, the Jovian BL waves have been detected at approximately noon and also at approximately dusk, two different local time regions. It is quite likely that the waves are present at all locations on the dayside magnetopause. If this happens to be true, the situation would be the same as that for the Earth's BL waves [*Tsurutani et al.*, 1989].

5.2. Cross-field Diffusion and Boundary Layer Formation

Although the intensity of the JBL waves is much smaller than that of LLBL, the magnitude of the ambient magnetic field is also low at the Jupiter magnetopause BL. This could lead to appreciable cross-field diffusion of magnetosheath plasma across the Jovian magnetopause due to resonant wave-particle interactions. At the JBL, $B_0 \simeq 5$ nT, and assuming a proton kinetic energy of 1 keV, we get from (3), the maximum diffusion rate, $D_{max} = 10^5$ km^2 s^{-1}. Then, taking the magnetic wave power of $\sim 10^{-1}$ nT^2 at resonance, the cross-field diffusion as calculated from (2), is $D_{\perp,B} \approx 10^3$ km^2 s^{-1}. Now, for the time scale of cross-field diffusion, *Tsurutani et al.* [1997] used the convection time of magnetosheath plasma from the magnetopause nose to the dawn/dusk flank. Considering magnetosheath flow velocity of 100 km s^{-1} and a distance of 150 R_J (where R_J is the radius of the Jupiter), they obtained a JBL thickness of 10,700 km or ~ 0.1 R_J thick. This value agrees very well with the measured value of JBL thickness of 9,100 to 13,000 km as determined by *Sonnerup et al.* [1981] from the analysis of a Pioneer 10 triple crossing of the Jovian magnetopause/plasma boundary layer. Assuming a reasonable contraction factor of magnetic fields of ~ 60 ($L \sim 60$), the corresponding latitudinal width at ionosphere/atmosphere altitudes would be of ~ 180 km. This is quite similar to the width of Jovian auroral high-latitude ring measured by Hubble.

5.2.1. Particle precipitation rates. *Tsurutani et al.* [1997] considered the effects of both E and B component of the waves in terms of effectiveness for pitch angle scattering rates via resonant wave-particle interactions. From the analyses of the pitch angle diffusion rates due to both the magnetic component and the electric component of the waves, they found that the JBL waves were intense enough to scatter 1-to 5-keV electrons and 1-keV to 1-MeV protons onto the strong diffusion limits. The 10-keV electrons could be scattered to near-strong to weak diffusion limits, while the higher-energy electrons only to weak diffusion limits. On the other hand, the lower-energy, $<$ 1-keV plasma could be scattered to strong diffusion limit by the JBL waves. The energy precipitation rate from the resonant JBL wave-particle interactions have been calculated by *Tsurutani et al.* [1997]. It was found that the total energy of precipitating ions from 1-keV to 1-MeV is 0.11 erg cm^{-2} s^{-1}, whereas for electrons in the same energy range it is 0.02 erg cm^{-2} s^{-1}. Thus, a total energy flux of 0.013 erg cm^{-2} s^{-1} is associated with the precipitating particles. This energy flux is only sufficient for a weak high-latitude auroral ring, and not for the main auroral ring which requires energy deposition rate of $\sim$ 100- 200 erg cm^{-2} s^{-1}.

6. Generation Mechanisms

The plasma waves observed in the Earth's BL, the Jovian BL, the PSBL, or in the PCBL are broadbanded with no obvious spectral peaks which could be used to identify the plasma instabilities exciting these modes. As the boundary layers are the site of many free energy sources existing simultaneously, it is not an easy task to identify which free energy source could be dominant for a given event. The changing interplanetary conditions can further complicate the identification of the free energy source and relevant plasma instability driven by it. The gradients in density, temperature, velocity and magnetic field, sometimes all together, are present at the boundary layers. These

gradients could act as sources of free energy for wave generation. In addition, the boundary layers can support strong currents, particle beams, and anisotropic velocity space distributions, which again can drive many plasma instabilities.

A number of possible wave modes have been put forth in the literature for the BL waves. We will mention only some of the important modes briefly here.

6.1. Lower Hybrid Drift Instability

The lower hybrid drift instability (LHDI) is driven essentially by the density gradients present in the boundary layer [*Gary and Eastman*, 1979; *Huba et al.*, 1981; *Revathy and Lakhina*, 1977]. *Gary and Sgro* [1990], *Winske and Omidi* [1995] and *Winske et al.* [1995] studied the lower hybrid drift instability at the magnetopause using a 2D hybrid computer simulation (particle ions, fluid electron) code. The LHDI is basically an electrostatic instability, and the waves are generated near the lower hybrid wave frequencies. These short wavelength waves could be Doppler-shifted to form a broadband spectrum. This instability is a plausible candidate that can give rise to cross-field plasma transport.

6.2. Modified Two Stream and Alfvén Wave Instabilities

The modified two-stream instability (MTSI) is very similar to the LHDI and is driven by the presence of both density gradient and the currents [*Krall and Liewer*, 1971; *McBride et al.*, 1972; *Lakhina and Sen*, 1973; *Revathy and Lakhina*, 1977; *Papadopoulos*, 1979]. Like the lower hybrid drift instability, this instability also leads to anomalous resistivity and cross-field particle diffusion. The density gradients, whether weak or strong, are always present in the boundary layers. In addition to exciting MTSI, these density gradients can also drive low-frequency electromagnetic drift Alfvén wave or drift kinetic Alfvén wave instabilities in the boundary layers [*Chmyrev et al.*, 1988; *Lakhina et*

al., 1993; *Johnson and Cheng*, 1997]. The frequencies generated by this mechanism fall in the range of ULF frequencies, and therefore the mechanism is suitable for explaining the lowest frequencies of the broadband wave spectrum.

6.3. Ion-Acoustic Instability

This is the current-driven electrostatic instability. The instability is excited when the field-aligned drift velocity exceeds the ion-acoustic speed [*Kindel and Kennel*, 1971]. This instability has been suggested to explain the generation of broadband electrostatic noise (BEN) in the magnetotail [*Gurnett et al.*, 1976; *Akimoto and Omidi*, 1986]. However, this instability requires $T_e \gg T_i$, a condition which is not met in the boundary layers. This makes the ion-acoustic instability an unlikely mechanism for the BL waves.

6.4. Ion Cyclotron Instability

This is an electrostatic instability propagating nearly perpendicular to $\mathbf{B_0}$, and is driven by the field-aligned currents [*Ashour-Abdalla and Thorne*, 1977, 1978; *Swift*, 1977]. The instability can occur even when $T_e \sim T_i$. Since sufficiently strong field-aligned currents are expected to be present in the Earth's and the Jovian magnetopause BLs as well as in PCBL, this instability is a good candidate for the generation of BL waves. The main problem with this instability is that it requires very high harmonics to explain the observed broadband spectrum.

6.5. Ion Beam Instabilities

The presence of ion beams in the boundary layer can give rise to various type of electromagnetic and electrostatic instabilities. The electromagnetic instabilities generate long-wavelength, low-frequency waves, which can be either resonant or nonresonant with the beam ions [*Gary et al.*, 1984; *Verheest and Lakhina*, 1991, 1993]. On the

other hand, the electrostatic modes generate modes at some what higher frequencies and shorter wavelengths as compared to the electromagnetic modes [*Lakhina*, 1993]. Various kinds of ion beam-driven modes have been studied to explain the generation of BEN in the plasma sheet boundary layer [*Grabbe and Eastman*, 1984; *Dusenbury and Lyons*, 1985; *Akimoto and Omidi*, 1986; *Ashour-Abdalla and Okuda*, 1986a, b; *Schriver and Ashour-Abdalla*, 1987]. In most of these mechanism, the wave power is generally concentrated towards the lowest frequencies. To explain the wave power at higher frequencies, one has to invoke strong Doppler shifts as well as some cascade mechanism.

6.6. Electron Beam Instabilities

Field-aligned electron beams have been observed in the plasmasheet boundary layers (PSBL). The electron beams can excite high frequency electrostatic modes. From ISEE 1 and 2 particle and wave data, *Parks et al.* [1984] and *Onsager et al.* [1993] have shown that broadband electrostatic noise is closely associated with electron beams rather than with ion beams. *Schriver and Ashour-Abdalla* [1989] have studied electrostatic instabilities driven by a cold electron beam streaming relative to a hot background plasma analytically and also by computer simulation. They found that the low-frequency waves are excited by the electron-beam driven ion acoustic instability whereas the high frequency waves are generated by the electron-beam driven electron acoustic modes. *Baumjohann et al.* [1989, 1990] have also discussed the possibility of high-frequency wave generation by electron beams. *Matsumoto et al.* [1994] and *Omura et al.* [1996] studied nonlinear evolution of several kinds of electron beam instabilities by 1D full particle codes. They found that electron beam instabilities evolved into isolated electrostatic potential structures similar to BGK modes. These structures travel along the magnetic field and would be observed as electrostatic solitary waves by the spacecraft.

6.7. Loss Cone Instabilities

6.7.1. Whistler Instability. Electromagnetic waves of whistler-type can be generated by the electron loss cone instability which is driven by velocity space gradients [*Kennel and Petschek*, 1966]. However, the required anisotropy in the electron distribution function has not been observed for the case of LLBL waves [*Gurnett et al.*, 1979]. Another difficulty with this mechanism is to explain the broadband nature of the BL waves.

6.7.2. Electrostatic Electron Cyclotron Instability. This instability excites electrostatic emissions with frequencies above the electron cyclotron frequency, e.g., $(n + \frac{1}{2})f_{ce}$ (n being the harmonic number) emission. The instability requires the presence of at least two electron populations, namely, a hot, weak loss-cone component, and a cold dense component. The hot electron component, which contains regions of velocity space where $\partial f/\partial v_\perp > 0$, provides the free energy for the instability, while the cold electron component helps destabilization and controls the dispersion of the waves. The instability is strongest in the vicinity of the cold plasma upper-hybrid frequency, f_{uhc} [*Young et al.*, 1973; *Ashour-Abdalla and Kennel*, 1978; *Rönmark et al.*, 1978; *Kennel and Ashour-Abdalla*, 1982]. The broadband nature of the waves can be explained by assuming excitation of many harmonics and strong Doppler shifts. The main difficulty with this mechanism is that it is difficult to explain the strongest wave power at low-frequencies (i.e., $f \sim f_{ci}$ or smaller).

6.8. Velocity Shear Instabilities

The presence of velocity shear in the boundary layer can excite the Kelvin-Helmholtz (KH) instability [*Chandrasekhar*, 1961]. The KH instability generates low-frequency ($f \ll f_{ci}$), long-wavelength (i.e., $\lambda \gg \rho_i$, where λ and ρ_i are, respectively, the wavelength of the mode and the ion Larmor radius) waves, and it can produce high anomalous

viscosity at the magnetopause BL [*D'Angelo*, 1973; *Miura*, 1987; *Lakhina*, 1994; *Ganguli et al.*, 1994]. However, in the presence of field-aligned ion beams with sufficiently strong velocity shear, a short wavelength kinetic KH instability having frequencies near ion cyclotron harmonics ($f \approx n\, f_{ci}$, where n is the harmonic number), can be excited [*Lakhina*, 1987].

Similarly, the gradient of the field-aligned current can excite an electrostatic current convective instability [*Drake et al.*, 1994a] and a whistler instability [*Drake et al.*, 1994b; *Drake* , 1995; Zhu et al., 1996]. The mechanism of current convective instability demands thickness of the magnetopause current layer, L, to be very narrow such that $L < \delta_e$, where $\delta_e = c/\omega_{pe}$ (c and ω_{pe} are the speed of light and the electron plasma frequency, respectively) is the electron skin depth. The whistler instability on the other hand requires that $L < \delta_i$, where $\delta_i = c/\omega_{pi}$ is the ion skin depth. The observed thickness of the magnetopause is typically several times the ion skin depth. Although all these mechanisms can explain the strongest wave power at the lowest frequencies, they suffer from a common drawback as to how to cascade the power upto VLF frequencies.

6.9. Coupled Velocity Shear-Lower Hybrid Instabilities Model

All the models described above consider only one free energy source at a time. As mentioned above, several free energy sources could simultaneously be present in the boundary layers. This could couple various modes excited by different free energy sources, or even lead to some new modes altogether. *Lakhina and Tsurutani* [1999b] have presented a linear theory for the generation of broadband PCBL plasma waves. The theory is based on two-fluid equations, is fully electromagnetic and takes into account the free energy available due to the presence of field-aligned currents, and gradients in the currents, the plasma densities and the magnetic fields. The dispersion relation generalizes the dispersion relations for several plasma modes, including the lower hybrid

[*Gary and Eastman,* 1979], the modified-two stream instability [*Lakhina and Sen,* 1973], beam modes [*Dum,* 1989; *Lakhina,* 1993], current convective and whistler instabilities [*Drake et al.,* 1994a; *Drake,* 1995]. In general, the beam driven modes, the current convective and the lower hybrid drift modes are coupled, and the dispersion relation has to be solved numerically. It is found that density gradients tend to stabilize both the current convective and the whistler instabilities, at the same time these modes develop real frequencies. On the other hand, sharp density gradients can lead to the excitation of a lower hybrid drift instability when the hot ions are present in the boundary layer.

Figure 24 shows the dispersion relation for the coupled lower hybrid and current convective modes in a hot plasma. Here, the equilibrium magnetic field varies along x-direction, the direction of inhomogeneity, and is directed along the z axis, i.e., $\mathbf{B}_0 = B_0(x)\,\mathbf{z}$. There is a finite field-aligned current carried by electrons streaming with a nonuniform velocity $\mathbf{V}_0(x)$ relative to ions. The waves are propagating obliquely to the ambient magnetic field in the y-z plane, i.e., the wave vector, $\mathbf{k}$, can be written as $\mathbf{k} = k_z\,\mathbf{z} + k_y\,\mathbf{y}$. The velocity shear is defined as $S = (dV_0/dx)\omega_{ce}^{-1}$, $\beta_i = 8\pi n_0 T_i/B_0^2$, is the ratio of ion pressure to the magnetic field pressure, and $a = k_y V_{ti}/\omega_{ci}$ is the perpendicular wave number normalized by the ion gyroradius $\rho_i = V_{ti}/\omega_{ci}$. Further, $\kappa_n = d\ln n_0/dx$ is the inverse of equilibrium density gradient, and $\kappa_B = d\ln B_0/dx$ is the inverse of the ambient magnetic field gradient.

The coupled lower hybrid -current convective modes tend to be stabilized by an increase in the value of β_i (cf. curves 1, 5 and 6). The velocity shear S can have either a destabilizing or a stabilizing effect on these modes depending on the sign of the parameter k_z/k_y (cf. curves 1, 2, 3 and 4).

6.9.1. Physical mechanism of the instability. In the model by *Lakhina and Tssurutani* [1998], the density gradients tend to reduce the growth rate of the current convective and whistler instabilities Since the density gradients provide a free energy

source, normally one would expect the density gradients to increase the growth rate of the instabilities, for example, the modified two-stream and lower hybrid instabilities discussed above. However, in general, the effect of the density gradients, or any other free energy source, could be destabilizing for some modes and stabilizing for the others, depending upon the nature of the excited modes. It has been shown that density gradients tend to stabilize the Kelvin-Helmholtz instability which is driven by a velocity shear [*D'Angelo*, 1965; *Rome and Briggs*, 1972; *Catto et al.*, 1973; *Huba*, 1981]. Both the current convective and whistler modes, like the Kelvin-Helmholtz modes, are driven by a parallel velocity shear, and therefore their basic nature is expected to be similar to the latter. Physical mechanism of the velocity shear instability is explained in Figure 25. In a uniform plasma, a perturbation electric field causes the electrons to $\mathbf{E} \times \mathbf{B}$ drift along x. In the presence of velocity gradients, the convection of the electron flow v_z brings regions of different parallel flow to the same magnetic field line [*Drake et al.*, 1994a]. The resultant bunching of electrons along this magnetic field line produces an electric field which reinforces the initial perturbation, thereby producing an instability . The presence of a local density gradient would alter the nature of the bunching process. It introduces perturbations in the electron density, which in turn produce perturbations in the parallel electron velocity which are in the opposite direction to the perturbations in v_z produced by the velocity gradients. Thus, the presence of density gradients tend to debunch the electrons along $\mathbf{B}$ and reduce growth of the velocity shear modes.

6.9.2. Generation of PCBL waves. The typical real frequencies generated by the *Lakhina and Tsurutani* [1999b] model are in the range of 10 to 400 ω_{ci} with the parameter a lying in the range of $5 \leq a \leq 50$. The plasma density at the Polar apogee is highly variable. The density can vary from 0.05 to 10 particles cm^{-3}, or even more Similarly, the currents can vary considerably during a given pass, and from one pass to the next. There are indications of vary sharp current gradients (as narrow as 3 ρ_e,

where ρ_e is the electron gyroradius) in the cusp region. For the PCBL region, typically ω_{ci} is $\sim$ 4 -5 Hz [*Russell et al.*, 1995, *Tsurutani et al.*, 1998], $T_i \sim 200$ eV, and $\beta_i \leq 0.05$. The typical ion gyroradius would be $\rho_i \approx 5.0$ km. A range of parameters need to be considered to reflect the variability in the observed plasma and field quantities near Polar apogee. For example, the values of $\kappa_n/k_y = (0.01 - 0.2)$ corresponds to density gradient scale lengths of $L_n \simeq$ (0.5 to 100) km, $S = (0.01 - 0.3)$ translate to velocity gradients of $L_v \simeq$ (0.5 - 20) km on assuming typical energies of 10 eV for the field-aligned electron beams. In view of the above parameters, the plasma rest frame frequencies of the excited modes would be of the order of 40 to 2000 Hz. In the satellite frame of reference, this frequency range would be broadened due to Doppler shifts and this could explain the observed frequency range of the broadband waves. The typical perpendicular wavelengths associated with the unstable modes would be $\lambda_\perp = 2\pi/k_y \simeq$ (0.6 - 6.0) km. Since the model describes coupled electrostatic and electromagnetic modes, the waves excited by the instabilities would have a mixture of electrostatic and electromagnetic modes, thus, naturally explaining an important characteristic of the PCBL waves.

6.9.3. Generation of Jovian BL waves. *Lakhina and Tsurutani* [1999b] model can be applied to explain the Jovian boundary layer waves. Taking typical parameters for the Jovian boundary layer as $B_0 = 5$ nT, $n_0 = 0.1$ cm^{-3}, $T_e = 3 \times 10^{5\circ}$ K, and $T_i = 5 \times 10^{5\circ}$ K (although there can be considerable variability in all of these parameters) [*Phillips et al.*, 1993; *Tsurutani et al.*, 1997], one gets $\omega_{ci} = 76$ mHz, $\rho_i \approx$ 133 km, $\beta_i \sim 0.06$, $T_e/T_i = 0.6$ and $\omega_{pe}/\omega_{ce} \approx 20$. Unfortunately, reliable estimates of the gradients in density and field-aligned currents at the Jovian magnetopause boundary layer are not available. Assuming that sufficiently strong density, magnetic fields or current gradients, such that $\kappa_n/k_y = (0.01 - 0.2)$ and/or $S = (0.01 - 0.3)$, exist in the JBL, the model would predict excitation of modes with frequencies of about 0.5 Hz to

30 Hz in the plasma rest frame with perpendicular wavelengths of 15 to 150 km. This agrees fairly well with the observed frequency band ($\sim 10^{-3}$ to 10^{2} Hz) of the JBL waves. Once again the Doppler shifts could broaden the frequency range, thus further improving the agreement between the prediction of the theory and the observation.

7. Conclusion

We have described the main characteristics of the broadband plasma waves observed in the Earth's magnetopause BL, Jovian BL, plasma sheet BL, and in the PCBL. The waves are spiky signals spanning a broad frequency range from less than the ion cyclotron frequency to probably greater than electron cyclotron frequency. As of now, the PSBL BEN appears to be electrostatic (i.e., no associated magnetic component has been identified unambiguously). On the other hand, the broadband waves observed in the LLBL, PCBL, and in Jovian LB have both the electric and magnetic components that on the average follow a rough power law spectral shape. The frequency dependence and the amplitude ratio B/E suggest that the waves are most likely a mixture of electrostatic and electromagnetic modes.

It appears that the broadband plasma waves discussed here are ubiquitous to the plasma flow boundary layers. It is interesting to point out that broadband electrostatic noise (BEN), with frequencies extending from the local lower hybrid frequency up to the local electron plasma frequency (or even above), has been observed in other regions of the Earth's magnetosphere not discussed in this review. For example, BEN has been observed in the magnetotail [*Cattell et al.*, 1986; *Gurnett and Frank*, 1977; *Matsumoto et al.*, 1994; *Kojima et al.*, 1997], on cusp and auroral field lines [*Scarf et al.*, 1972; *Gurnett and Frank*, 1977; 1978; *Pottelette et al.*, 1990; *Dubouloz et al.*, 1991; *Ergun et al.*, 1998a], and in the magnetosheath [*Anderson et al.*, 1982]. The magnetotail BEN emissions are correlated with ion and electron beams, whereas auroral region

BEN emissions are usually associated with ion conics and field-aligned electron beams. *Dubouloz et al.* [1991] have proposed a generation mechanism for auroral field line BEN in terms of electron acoustic solitons. The waveform observations by the plasma wave instrument on board the Geotail spacecraft have shown that BEN consists of a series of bipolar solitary pulses [*Matsumoto et al.*, 1994]. As discussed earlier, the broadness of the BEN frequency spectra arises from the solitary waveforms. A likely generation mechanism for BEN is based on the nonlinear evolution of the electron beam instabilities leading to the formation of the isolated Bernstein-Greene-Kruskal (BGK) potential structures which reproduce well the observed electrostatic solitary waveforms [*Omura et al.*, 1996; *Kojima et al.*, 1997].

The high time resolution measurements of the broadband plasma waves in the PCBL region by Polar and in the auroral ionosphere by FAST have just started to come out, and they have given very useful information on the fine structure of the BL waves. Recent results on the PCBL wave using the high time resolution of the POLAR shown in Figure 26 indicate the presence of large amplitude bipolar pulses (bpp) in the parallel electric component of the wave, similar to PSBL BEN, at high altitudes ($\sim$ 6 R_E) [*Franz et al.*, 1998; *Tsurutani et al.*, 1998b] as well as low altitudes ($\sim$ 1-2 R_E) [*Mozer et al.*, 1997]. There are magnetic signatures associated with these electric pulses. Offset bipolar pulses (obpp), where the positive pulse does not follow immediately after the negative pulse, but are delayed somewhat, are also seen in this figure. Further, the monopolar pulses (mpp) in the parallel electric field component are seen in the right-hand inset of Figure 26. The monopolar pulses are found to alternate between one polarity and the opposite polarity, and to occur in pairs. These three types of parallel electric field (bipolar, offset bipolar and monopolar) structures can be explained by a 1-D model of the spatial distribution of charges involving an electron hole and neutralizing charge as sketched in Figure 27. The spacecraft flying through the center

of this spatial distribution of charge would see the electric field signatures detected by Polar. The charge distribution of the left panels, i.e., an electron hole plus surrounding neutralizing charge, would result in the observed bipolar structure [*Franz et al.*, 1998; *Tsurutani et al.*, 1998b]. The middle panels show an offset bipolar structure and a possible charge distribution, essentially a broadened electron hole due to dispersion, that could give rise to the observed obpp electric fields. The right panels show a pair of monopolar pulses (mpp) that can result from the charge distribution consisting of a split electron hole and the neutralizing charges [*Tsurutani et al.*, 1998b]. It has been shown theoretically that hole splitting can occur due to the interaction of holes with density gradients [*Mohan and Buti*, 1979].

Similarly, recent measurements from FAST [*Ergun et al.*, 1998a, b] have revealed the presence of intense localized electrostatic wave structures at altitudes of 2000 to 4000 km on the auroral field lines. *Muschietti et al.* [1999] have interpreted these solitary structures [*Ergun et al.*, 1998a, 1998b] in terms of BGK phase-space electron holes drifting along the magnetic field lines. *Goldman et al.* [1999] have given an explanation for these bipolar structures in terms of nonlinear two-stream instabilities, a mechanism similar to that of PSBL BEN proposed by [*Omura et al.*, 1996; *Kojima et al.*, 1997].

We would like to point out that the mechanism discussed by *Dubouloz et al.* [1991] predict negatively charged structures whereas the Geotail [*Matsumoto et al.*, 1994], the POLAR [*Franz et al.*, 1998] as well as FAST [*Ergun et al.*, 1998a,b] observations indicate positively charged flowing potential structures. It is important to note that a potential structure, whether positive or negative, must inherently be a part of some nonlinear wave where the charges are trapped, otherwise it would rapidly disrupt due to the repulsive forces of the charges. Depending on the free energy available, some of the instabilities discussed in the previous section could evolve nonlinearly into solitary waves, for example, whistler-type solitons. If this happens it would naturally explain the

recent observations on the waveform of the coherent structures (including the associated magnetic component ,if any) as reported by POLAR [*Mozer et al.*, 1997; *Franz et al.*, 1998; *Tsurutani et al.*, 1998b] and FAST [*Ergun et al.*, 1998a, b] teams. Further analyses of the high time resolution plasma and wave data from Polar, FAST and Geotail would advance our knowledge about the generation and saturation mechanisms of the BL waves as well as about their fine structures. This would lead to better understanding about the BL waves and their role in cross-field particle diffusion leading to the formation of the boundary itself, and in the process of heating/acceleration and precipitation of the BL plasma causing the dayside aurora.

Acknowledgments. A part of this research effort was performed at the Jet Propulsion Laboratory, California Institute of Technology, Pasadena, under contract with the National Aeronautics and Space Administration. The research in Kyoto University was supported by Grant-in-Aid 10044081 from the Japanese Ministry of Education, Science, and Culture. The research at Indian Institute of Geomagnetism, Mumbai was supported by the Department of Science and Technology, Government of India.

References

Akasofu, S.-I., E. W., Hones, Jr., S. J. Bame, J. R. Asbridge, A. T. Y. Lui, Magnetotail and boundary layer plasma at geocentric distance of 18 R_E: Vela 5 and 6 observations, *J. Geophys. Res., 78,* 7257, 1973.

Akimoto, K. and N. Omidi, The generation of broadband electrostatic noise by an ion beam in the magnetotail, *Geophys. Res. Lett., 13,* 97, 1986.

Anderson, K.A., Binsack, J.H., and Fairfield, D.H., Hydromagnetic disturbances of 3 to 15 minute period on the magnetopause and their relation to Bow Shock Spikes, *J. Geophys. Res., 73,* 2371, 1968.

Anderson, R.R., C.C. Harvey, M.M. Hoppe, B.T. Tsurutani, T.E. Eastman, and J. Etcheto, Plasma waves near the magnetopause, *J. Geophys. Res., 87,* 2087, 1982.

Anderson, B.J., ULF signals observed near the magnetopause in *Physics of the magnetopause,* AGU Monograph 90, edited by P. Song, B.U.O. Sonnerup, and M.F. Thomsen, AGU, Washington, D.C., p. 269, 1995.

Ashour-Abdalla, M. and C. F. Kennel, Nonconvective and convective electron cyclotron harmonic instabilities, *J. Geophys. Res., 83,* 1531, 1978.

Ashour-Abdalla, M. and R. M. Thorne, The importance of electrostatic ion cyclotron instability for quiet-time proton auroral precipitation, *Geophys. Res. Lett., 4,* 45, 1977.

Ashour-Abdalla, M. and R. M. Thorne, Towards a unified view of diffuse auroral precipitation, *J. Geophys. Res., 83,* 4775, 1978.

Ashour-Abdalla, M., and H. Okuda, Electron acoustic instabilities in the geomagnetic tail, *Geophys. Res. Lett.,* it 13, 366-369, 1986a.

Ashour-Abdalla, M. and H. Okuda, Theory and simulations of broadband electrostatic noise in the geomagnetic tail, *J. Geophys. Res., 91,* 6833-6844, 1986b.

Ashour-Abdalla, M., T. Chang, and P. Dusenbury, eds., *Space Plasmas: Coupling Between Small and Medium Scale Processes, Geophys. Mono.,* Vol. 86, 1995.

Aubry, M.P., M.G. Kivelson, and C. T. Russell, Motion and structure of the magnetopause, *J.*

Geophys. Res. 76, 1673, 1971.

Axford, W. I. and C. O. Hines, A unifying theory of high-latitude geophysical phenomena and geomagnetic storms, *Can. J. Phys., 39,* 1433, 1961.

Axford, W. I., Viscous interaction between the solar wind and the earth's magnetosphere, *Planet. Space Sci., 13,* 45, 1964.

Bahnsen, A., Recent techniques of observations and results from the magnetopause regions, *J. Atmospheric Terrest. Phys. 40,* 235, 1978.

Balogh, A. T., J. Beek, R. J .Forsyth, P. C. Hedgecock, R.J.Marquedant, E.j.Smith, D.J.Southwood and B.T.Tsurutani, The magnetic field investigation on the Ulysses mission : Instrumentation and preliminary scientific results, *Astron, Astrophys. Suppl. Ser., 92,* 221, 1992.

Bame, S. J., B. L. Barraclough, W. D. Feldman, G.R.Gisler, J.T. Gosling, D.J.McComas, J.L.Phillips, and M.F.Thomsen, Jupiter's magnetosphere : Plasma description from the ulysses flyby, *Science, 257,* 1539, 1992.

Baumjohann, W., and G. Paschmann, Solar wind magnetosphere coupling, Processes and Observations, *Phys. Scripta, T18,* 61, 1987.

Baumjohann, W., R. A. Treumann, J. LaBelle, and R. R. Anderson, Average electric wave spectra across the plasma sheet and their relation to ion bulk speed, *J. Geophys. Res., 94,* 15221, 1989.

Baumjohann, W., R. A. Treumann, and J. LaBelle, Average electric wave spectra in the plasma sheet: dependence on ion density and ion beta, *J. Geophys. Res., 95,* 3811, 1990.

Belmont, G. F. Rebeac, and L. Rezeau, Resonant amplification of magnetosheath MHD fluctuations at the magnetopause, *Geophys. Res. Let., 22,* 295, 1995.

Bernstein, I. B., J. M. Greene, and M. D. Kruskal, Exact nonlinear plasma pscillations, *Phys. Rev., 108,* 546-550, 1957.

Bohm, D., Quantitative description of the arc plasma in the magnetic field, in *Characteristics*

of Electrical Discharges in Magnetic fields, edited by A. Guthrie and R. Walkerling, p.1, McGraw Hill, New York, 1949.

Burinskaya, T. M. and C. -V. Meister, Contribution of the ion-beam acoustic instability to the generation of broadband electrostatic noise in the earth's magnetotail, *Planet. Space Sci., 37*, 145-150, 1989.

Burinskaya, T. M. and C. -V. Meister, Contribution of the ion-beam acoustic instability to the generation of broadband electrostatic noise -Three dimensional quasilinear approach-, *Planet. Space Sci., 38*, 695-700, 1990.

Catto, P. J., M. N. Rosenbluth, and C. S. Liu, Parallel velocity shear instabilities in an inhomogeneous plasma with a sheared magnetic field, *Phys. Fluids, 16*, 1719, 1973.

Cattel, C. A., F. S. Mozer, R. R. Anderson, E. W. Hones, Jr., and R. D. Sharp, ISEE observations of the plasma sheet boundary, plasma sheet, and neutral sheet, 2, Waves, *J. Geophys. Res., 91,* 5681, 1986.

Cattell, C. J. Wygant, F. S. Mozer, T. Okada, K. Tsuruda, S. Kokubun, and T. Yamamoto, ISEE 1 and Geotail observations of low-frequency waves at the magnetopause, *J. Geophys. Res., 100,* 11823, 1995.

Chandrasekhar, S., *Hydrodynamic and Hydromagnetic Stability,* Clarendon, Oxford, 1961.

Chmyrev, V. M., S. V. Bilichenko, O. A. Pokhotelov, V. A. Marchenko, V. I. Lazarev, A. V. Streltsov, and L. Stenflo, Alfvén vortices and related phenomena in the ionosphere and the magnetosphere, *Phys. Scr., 38,* 841, 1988.

Cummings, W.D. and Coleman, P.J., Jr. Magnetic fields in the magnetopause and vicinity at synchronous altitude, *J. Geophys. Res. 73,* 5699, 1968.

D'Angelo, N., Kelvin-Helmholtz instability in a fully ionized plasma in a magnetic field, *Phys. Fluids, 8*, 1748, 1965.

D'Angelo, N., Ultra low-frequency fluctuations At the polar cusp: A review, *Rev. Geophys., 15*, 299, 1973.

Davidson, R. C., Quasilinear stabilization of Lower-hybrid drift instability, *Phys. Fluids, 21,*

1375, 1978.

Drake, J. F., J. Gerber, and R. G. Kleva, Turbulence and transport in the magnetopause current layer, *J. Geophys. Res., 99,* 11211, 1994a.

Drake, J. F., R. G. Kleva, and M. E. Mandt, Structure of thin current layers: Implications for magnetic reconnection, *Phys. Rev. Lett., 73,* 1251, 1994b.

Drake, J. F., Magnetic reconnection, a kinetic treatment, in *Physics of the Magnetopause, Geophys. Mon. 90,* Amer. Geophys. Union, Washington, DC, 155, 1995.

Dubouloz, N., R.Pottelette, M. Malingre, G.Holmgren, and P.A.Lindqvist, Detailed analysis of broadband electrostatic noise in the dayside auroral zone, *J.Geophys. Res., 96,* 3565, 1991.

Dum, C. T., and T. H. Dupree, Nonlinear stabilization of high-frequency instabilities, *Phys. Fluids., 13,* 2064, 1970.

Dum, C. T., Transition in the dispersive properties of beam-plasma and two-stream instabilities, *J. Geophys. Res., 94,* 2429, 1989.

Dusenbery, P. B. and L. R. Lyons, The generation of electrostatic noise in the plasma sheet boundary layer, *J. Geophys. Res., 90,* 10935-10943, 1985.

Dusenbery, P. B. and L. R. Lyons, Ion diffusion coefficients from resonant interactions with broadband turbulence in the magnetotail, *J. Geophys. Res., 94,* 2484-2496, 1989.

Dusenbery, P. B., Generation of broadband noise in the magnetotail by the beam acoustic instability, *J. Geophys. Res., 91,* 12005-12016, 1986.

Eastman, T. E., E. W. Hones, Jr., S. J. Bame, and J. R. Asbridge, The magnetospheric boundary layer: Site of plasma, momentum and energy transfer, from the magnetosheath into magnetosphere, *Geophys. Res. Lett, 3,* 685, 1976.

Eastman, T. E., L. A. Frank, W. K. Peterson,a dn W. Lennartsson, The plasma sheet boundary layer, *J. Geophys. Res., 89,* 1553-1572, 1984.

Ergun, R. E. *et al.*, FAST satellite observations of large-amplitude solitary structures, *Geophys. Res. Lett., 25,* 2041, 1998a.

Ergun, R. E., C. W. Carlson, J. P. Fadden, F. S. Mozer, L. Muschietti, I. Roth, and R. Strangeway, Debye-scale plasma structures associated with magnetic-field-aligned electric fields, *Phys. Rev. Lett., 81*, 826, 1998b.

Eviatar, A. and R. A. Wolf, Transfer processes in the magnetopause, *J. Geophys. Res., 73*, 5561, 1968.

Fairfield, D.H., Magnetic fields of the magnetosheath, *Rev. Geophys. Space Phys., 14*, 117, 1976.

Franz, J. R., Kintner, P. M., Pickett, J. S., Polar observations of coherent electric field structures, *Geophys. Res. Lett., 25*, 1277, 1998.

Galeev, A. A., M. M. Kuznetsova, and L. M. Zelenyi, Magnetopause stability threshold for patchy reconnection, *Space Sci. Rev., 44*, 1, 1986.

Ganguli, G., M. J. Keskinen, H. Romero, R. Heelis, T. Moore, and C. Pollock, Coupling of microprocesses and macroprocesses due to velocity shear: An application to the low-altitude ionosphere, *J. Geophys. Res., 99*, 8873, 1994.

Gary, S.P. and T.E. Eastman, The lower hybrid drift instability at the magnetopause, *J. Geophys. Res., 84*, 7378, 1979.

Gary, S.P., C. W. Smith, M. A. Lee, M. L. Goldstein, and D. W. Forslund, Electromagnetic ion beam instabilities, *Phys. Fluids, 27*, 1852, 1984. (Erratum, *Phys. Fluids, 28*, 438, 1985).

Gary, S. P. and A. G. Sgro, The lower hybrid drift instability at the magnetopause, *J. Geophys. Res., 17*, 909, 1990.

Gendrin, R., Magnetic turbulence and diffusion processes in the magnetopause boundary layer, *J. Geophys. Res., 84*, 7043, 1979.

Gendrin, R., Magnetic turbulence and diffusion processes in the magnetopause boundary layer, *Geophys. Res. Lett., 10*, 769, 1983.

Goldman, M. V., M. M. Oppenheim, and D. L. Newman, Nonlinear two-stream instabilites as an explanation for the auroral bipolar wave structures, *Geophys. Res. Lett., 26*, 1821,

1999.

Glassmeier, K. H., N. F. Ness, M. H. Acuna and F.M.Neubauer, Studying hydromagnetic waves in the Io plasma torus : Voyager 1 observations, *J.Geophys. Res., 94,* 15, 063, 1989.

Goldstein, M.L., C.W.Smith and W.H.Mattaeus, large amplitude MHD waves upstream of the Jovian bow shock, *J.Geophys. Res., 88,* 9989, 1983.

Grabbe, C. L., New results on the generation of broadband electrostatic waves in the magnetotail, *Geophys. Res. Lett., 12,* 483-486, 1985.

Grabbe, C. L., Numerical study of the spectrum of broadband electrostatic noise in the magnetotail, *J. Geophys. Res., 92,* 1185-1192, 1987.

Grabbe, C. L., Wave propagation effects of broadband electrostatic noise in the magnetotail, *J. Geophys. Res., 94,* 17299-17304, 1989.

Grabbe, C. L., and T. E. Eastman, Generation of broadband electrostatic noise by ion beam instabilities in the magnetotail, *J. Geophys. Res., 89,* 3865-3872, 1984.

Gurnett, D.A., L.A. Frank, and R.P. Lepping, Plasma waves in the distant magnetotail, *J. Geophys. Res., 81,* 6059, 1976.

Gurnett, D.A., and L.A. Frank, A region of intense plasma wave turbulence on auroral field lines, *J. Geophys. Res., 82,* 1031, 1977.

Gurnett, D.A., and L.A. Frank, Plasma waves in the polar cusp: Observations from Hawkeye 1, *J. Geophys. Res., 82,* 1447, 1978.

Gurnett, D.A., R.R. Anderson, B.T. Tsurutani, E.J. Smith, G. Paschmann, G. Haerendel, S.J. Bame, and C.T. Russell, Plasma wave instabilities at the magnetopause: Observations from ISEE 1 and 2, *J. Geophys. Res., 84,* 7043, 1979.

Gurnett, D.A., W.S.Kurth, and F.L.Scarf, The structure of the Jovian magnetotail for plasma waves observation, *Geophys. Res. Lett., 1,* 53, 1980.

Gurnett, D.A., R.L. Huff, J.D. Menietti, J.L. Burch, J.D. Winningham, and S.D. Shawhan, Correlated low-frequency electric and magnetic noise along the auroral field lines, *J.*

Geophys. Res., 89, 8971, 1984.

Gurnett, D.A., The Polar plasma wave instrument, *Space Sci. Rev., 71,* 597, 1995.

Gonzalez, W. D., B. T. Tsurutani, A. L. C. Gonzalez, E. J. Smith, F. Tang, and S.-I. Akasofu, Solar wind magnetosphere coupling during intense magnetic storms (1978-1979), *J. Geophys. Res., 94,* 8835, 1989.

Haerendel, G., G. Paschmann, N, Sckopke, H. Rosenbauer, and P. C. Hedgecock, The frontside boundary layer of the magnetopause and the Problem of reconnection, *J. Geophys. Res., 83,* 3195, 1978.

Haerendel, G., and G. Paschmann, Interaction of the solar wind with the dayside magnetosphere, in *Magnetospheric Plasma Physics,* edited by A. Nishida, Center for Academic Publications Japan, Tokyo, 1982.

Heikkila, W. J., Impulsive plasma transport through the magnetopause, *Geophys. Res. Lett., 9,* 159, 1982.

Ho, C. M., B.T.tsurutani, D.A.Gurnett, J.S.Pickett, Wideband plasma waves in the polar cap boundary layer: Polar observations, *Proceedings of Third SOLTIP Symposium,* in Beijing, in press, 1997.

Holzer, R.E., M.G. Mcleod, and E.J. Smith, Preliminary results from the Ogo 1 search coil magnetometer: Boundary positions and magnetic noise spectra, *J. Geophys. Res., 71,* 1481, 1966.

Hones, E. W., Jr., J. R. Asbridge, S. J. Bame, M. D. Montgomery, S. Singer, and S.-I. Akasofu, Measurements of the magnetotail plasma flow made by VELA-4B, *J. Geophys. Res., 77,* 5503, 1972.

Huba, J. D., The Kelvin-Helmholtz instability in inhomogeneous plasma, *J. Geophys. Res., 86,* 3653, 1981.

Huba, J.D., N.T. Gladd, and J.F. Drake, On the role of the lower hybrid drift instability in substorm dynamics, *J. Geophys. Res., 86,* 5881, 1981.

Horwitz, J. L., N. Singh, and J. L. Burch, eds., *Cross-Scale Coupling in Space Plasmas,*

Geophys. Mono., Vol. 93, 1996.

Ichimaru, S., *Basic Principles of Plasma Physics*, W. A. Benjamin, Inc., Reading, Mass., 1973.

Johnson, J. R. and C. Z. Cheng, Global structure of mirror modes in the magnetosheath, *J. Geophys. Res., 102,* 7179, 1997.

Kennel, C.F., and H.E. Petschek, Limit on stably trapped particle fluxes, *J. Geophys. Res., 71,* 1, 1966.

Kennel, C.F. and M. Ashour-Abdalla, Electrostatic waves and the strong diffusion of magnetospheric electrons, in *Magnetospheric Plasma Physics*, ed. A. Nishida, Center for Academic Publications Japan, Tokyo, p.245, 1982.

Kindel and C. F. Kennel, Topside current instabilities, *J. Geophys. Res., 76,* 3055, 1971.

Kojima, H., H. Matsumoto, T. Miyatake, I. Nagano, A. Fujita, L. A. Frank, T. Mukai, W. R. Paterson, Y. Saito, S. Machida, and R. R. Anderson, Relation between electrostatic solitary waves and hot plasma flow in the plasma sheet boundary layer: GEOTAIL Observations, *Geophys. Res. Lett., 21,* 2919-2922, 1994.

Kojima, H., H. Matsumoto, S. Chikuba, S. Horiyama, M. Ashour-Abdalla, and R. R. Anderson, Geotail waveform observations of broadband/narrowband electrostatic noise in the distant tail, *J. Geophys. Res., 102,* 14439, 1997.

Kojima, H., Study on plasma waves in the geomagnetic tail region via spacecraft observations, *PhD. thesis in Kyoto university, Japan*, 1998.

Kojima, H., Y. Omura, H. Matsumoto, K. Miyaguti, and T. Mukai, Characteristics of electrostatic solitary waves: Statistical analyses, *submitted to Nonlinear Processes in Geophyhsics*, 1999.

Krall, N. A. and P. C. Liewer, Low-frequency instabilities in magnetic pulses, *Phys. Rev. A 4,* 2094, 1971.

LaBelle, J., and R.A. Treumann, Plasma Waves at the dayside magnetopause, *Space Sci. Revs., 47,* 175, 1988.

Lakhina, G. S. and A. Sen, Electromagnetic and ∇B effects on the modified two stream

instability, *Nucl. Fusion, 13,* 913, 1973.

Lakhina, G.S., Low-frequency electrostatic noise due to velocity shear instabilities in the regions of magnetospheric flow boundaries, *J. Geophys. Res., 92,* 12161, 1987.

Lakhina, G.S., Generation of low-frequency electric field fluctuations on auroral field lines, *Annales Geophysicae, 64,* 660, 1993.

Lakhina, G.S., P. K. Shukla, and L. Stenflo, Ultra-low-frequency fluctuations at the magnetopause, *Geophys. Res. Lett., 20,* 2419, 1993.

Lakhina, G.S., Linear macroscopic instabilities in space plasmas, *Phys. Scripta, T50,* 114, 1994.

Lakhina, G. S. and K. Schindler, Tearing modes at the magnetopause, *J. Geophys. Res., 101,* 2707, 1996.

Lakhina, G. S., B. T. Tsurutani, J. K. Arballo, C. M. Ho, and A. Boonsiriseth, Generation of broadband plasma waves in the polar cap boundary layer, *EOS, 78,* S297, 1997.

Lakhina, G. S., B. T. Tsurutani, Broadband plasma waves in the magnetopause and polar cap boundary layers, *Surveys Geophys.*, in press, 1999a.

Lakhina, G. S., B. T. Tsurutani, A generation mechanism for the polar cap boundary layer broadband plasma waves, *J. Geophys. Res., 104,* 279, 1999b.

Lanzerotti, L.J., S.M.Krimigis, C.O.Bostrom, W.I.Axford, R.P.Lepping and N.F.Ness, Measurements of plasma flow at the dawn magnetopause by Voyager 1, *J. Geophys. Res., 84,* 6483, 1979.

Lee, L. C., J. R. Johnson, and Z. W. Ma, Kinetic Alfvén waves as a source of plasma transport at the dayside magnetopause, *J. Geophys. Res., 99,* 17405, 1994.

Lemaire, J., and M. Roth, Penetration of solar wind plasma elements into the magentosphere, *J. Atmos. Terr. Phys., 40,* 331, 1978.

Lundin, R., Processes in the magnetospheric boundary layer, *Physica Scripta, 18,* 85, 1987.

Matsumoto, H., H. Kojima, T.Miyatake, Y. Omura, M.Okada, and M.Tsutsui, Electrostatic solitary waves (ESW) in the magnetotail- BEN wave forms observed by GEOTAIL,

Geophys. Res. Lett., 21, 2915, 1994.

McBride, J. B., E. Ott, J. P. Boris, and J. H. Orens, Theory and simulation of turbulent heating by the modified two-stream instability, *Phys. Fluids, 15*, 2367, 1972.

Miura, A., Simulation of the Kelvin-Helmholtz instability at the magnetospheric boundary, *J. Geophys. Res., 92,* 3195, 1987.

Mohan, M. and B. Buti, Modulated ion acoustic waves in inhomogeneous plasmas, *Plasma Phys., 21*, 713, 1979.

Mozer, F. S., R. Ergun, M. Temerin, C. Cattell, J. Dombeck, and J. Wygant, New features of time domain electric-field structures in the auroral acceleration region, *Phys. Rev. Lett., 79*, 1281, 1997.

Muschietti, L., R. E.Ergun, I. Roth, and C. W. Carlson, Phase-space electron holes along magnetic field lines, *Geophys. Res. Lett., 26*, 1093, 1999.

Neugebauer, M., C.T. Russell, and E.J. Smith, Observations of the internal structure of the magnetopause, *J. Geophys. Res., 79,* 499, 1974.

Nishida, A., T. Hada, K. A. Anderson, R. R. Anderson, S. J. Bame, and E. W. Hones, Jr., Broadband electrostatic noise in the magnetotail: Its relation to plasma sheet dynamics, *J. Geophys. Res., 90*, 4453-4460, 1985.

Omidi, N., Broadband electrostatic noise produced by ion beams in the Earth's magnetotail, *J. Geophys. Res., 90*, 12330-12334, 1985.

Omura, Y., H. Kojima, and H. Matsumoto, Computer simulation of Electrostatic Solitary Waves: A nonlinear model of broadband electrostatic noise, *Geophys. Res. Lett., 21*, 2923-2926, 1994.

Omura, Y., H. Matsumoto, T.Miyake, and H. Kojima, Electron beam instabilities as generation mechanism of electrostatic solitary waves in the magnetotail, *J. Geophys. Res., 101,* 2685, 1996.

Onsager, T. G., M. F. Thomsen, R. C. Elphic, J. T. Gosling, R. R. Anderson, and G. Kettmann, Electron generation of electrostatic waves in the plasma sheet boundary

layer, *J. Geophys. Res.*, *98*, 15509-15519, 1993.

Owen, C. J., and S. W. H. Cowley, Heikkila's mechanism for impulsive plasma transport through the magnetopause: a re-examination, *J. Geophys. Res.*, *96*, 273, 1991.

Papadopoulos, K., The role of microturbulence on collisionless reconnection, in *Dynamics in the Magnetosphere*, ed. S. I. Akasofu, D. Reidel Publ. Co., Dordrecht, Holland, 289, 1979.

Parks, G. K., M. McCarthy, R. J. Fitzenreiter, J. Etcheto, K. A. Anderson, R. R. Anderson, T. E. Eastman, L. A. Frank, D. A. Gurnett, C. Huang, R. P. Lin, A. T. Y. lui, K. W. Oglivie, A. Pedersen, H. Reme, and D. J. Williams, Particle and field characteristics of the high-latitude plasma sheet boundary layer, *J. Geophys. Res.*, *89*, 8885-8906, 1984.

Phillips, J.L., S.J. Bame, M.F.Thomsen, B,.E.Goldstein, and E.J.Smith Ulysses plasma observations in the Jovian magnetosheath, *J. Geophys. Res.*, *98*, 21, 189, 1993.

Pickett, J.S., R.R. Anderson, L.A. Frank, D.A. Gurnett, W.R. Paterson, J.D. Scudder, J.B. Sigworth, B.T. Tsurutani, C.M. Ho, G.S. Lakhina, W.K. Peterson, E. G. Shelley, C.T. Russell, G. K. Parks, M.J. Brittnacher, H. Matsumoto, K. Hashimoto, I. Nagano, S. Kokubun, and T. Yamamoto, II. Correlative magnetopause boundary layer observations, *EOS, 78*, S291, 1997.

Pottelette, R., M. Malingre, N. Dubouloz, B. Aparicio, R. Lundin, G. Holmgren, and G. Marklund, High-frequency waves in the cusp/cleft regions, *J. Geophys. Res.*, *95*, 5957, 1990.

Revathy, P. and G. S. Lakhina, Ion and electron heating in the Earth's bow shock, *J. Plasma Phys.*, *17*, 133, 1977.

Rezeau, L., S. Perraut, and A. Roux, Electromagnetic fluctuations in the vicinity of the magnetopause, *Geophys. Res. Lett.*, *13*, 1093, 1986.

Rezeau, L., A. Morane, S. Perraut, A. Roux, and R. Schmidt, Characterization of Alfvénic fluctuations in the magnetopause boundary layer, *J. Geophys. Res.*, *94*, 101, 1989.

Rezeau, L., G. Belmont, N. Cornilleau-Wehrlin, F. Reberac, and C. Briand, Spectral law and polarization properties of the low-frequency waves at the magentopause, *Geophys. Res. Lett., 26,* 651, 1999.

Rome, J. A. and R. Briggs, Stability of sheared electron flow, *Phys. Fluids, 15*, 796, 1972.

Rönnmark, K., H. Borg, P. J. Christiansen, M. P. Gough, and D. Jones, Banded electron cyclotron harmonic instability - A first comparison of theory and experiment, *Space Sci. Rev., 22,* 401, 1978.

Rosenbauer, H., Grunwaldt, H., Montgomery, M.D., Paschmann, G. and Sckopke, N., HEOS 2 plasma observations in the distant polar magnetosphere: The Plasma Mantle, *J. Geophys. Res., 80,* 2723, 1975.

Russell, C.T., R.C. Snare, J.D. Means, D. Pierce, D. Dearborn, M. Larson, G. Barr and G. Le, The GGS/POLAR magnetic fields investigation, *Space Sci. Revs., 71,* 563, 1995.

Scarf, F.L., R.W. Fredricks, I.M. Green, and C.T. Russell, Plasma waves in the dayside polar cusp, *J. Geophys. Res., 77*, 2274, 1972.

Scarf, F. L., L. A. Frank, K. L. Ackerson, and R. P. Lepping, Plasma wave turbulence at distant crossings of the plasma sheet boundaries and the neutral sheet, *Geophys. Res. Lett., 1*, 189-192, 1974.

Schindler, K., On the role of irregularities in plasma entry into the magnetosphere, *J. Geophys. Res., 84*, 7257, 1979.

Schriver, D., and M. Ashour-Abdalla, Generation of high-frequency broadband electrostatic noise: The role of cold electrons, *J. Geophys. Res., 92*, 5807-5819, 1987.

Schriver, D., and M. Ashour-Abdalla, Broadband electrostatic noise due to field-aligned currents, *Geophys. Res. Letts., 16*, 899, 1989.

Schriver, D., M. Ashour-Abdalla, R. Treumann, M. Nakamura, and L. M. Kistler, The lobe to plasma sheet boundary layer transition: theory and observations, *Geophys. Res. Lett., 17*, 2027-2030, 1990.

Sckopke, N.G., Paschmann, G. Harendel, B.U.O. Sonnerup, S.J. Bame, T.G. Forbes, E.W.

Hones, Jr., and C.T. Russell, Structure of the low-latitude boundary layer, *J. Geophys. Res., 86,* 2099, 1981.

Shelley, E. G., et al.,The toroidal imaging Mass-angle spectrograph (TIMAS) for the Polar Mission, *Space Sci. Rev., 71,* 497, 1995.

Smith, E.J. and Davis, L., Magnetic measurements in the Earth's magnetopause and magnetosheath: Mariner 5, *J. Geophys. Res., 75,* 1233, 1970.

Smith, E. J., and B. T. Tsurutani, D. L. Chenette, T. F. Conlon, and J. A. Simpson, Jovian electron bursts: Correlation with the interplanetary field directions and hydromagnetic waves, *J. Geophys. Res., 81,* 65, 1976.

Smith, C. W., M. L., Goldstein and W. H. Mathaeus, Turbulence analysis of the Jovian upstream wave phenomenon, *J. Geophys. Res., 88,* 5581, 1983.

Smith, C. W., and M. C. Lee, Coupled hydromagnetic wave excitation and ion acceleration upstream of Jovian bow shock, *J. Geophys. Res., 91,* 81, 1986.

Smith, E. J., and B. T. Tsurutani, Saturn's magnetosphere : Observations of ion cyclotron waves near the Dione L shell, *J.Geophys, Res., 88,* 7831, 1983.

Song, P., J. Zhu, C. T. Russell, R. R. Anderson, D. A. Gurnett, K. W. Ogilvie, R. J. Strangeway, Properties of ELF emission in the dayside magnetopause, *J. Geophys. Res., 103,* 26495, 1998.

Sonnerup, B. U, Theory of the low latitude boundary layer, *J. Geophys. Res., 85,* 2017, 1980.

Sonnerup, B.U.O., E. J. Smith, B. T. Tsurutani and J. H. Wolfe, Structure of Jupiter's magnetopause : Pioneer 10 and 11 observations, *J. Geophys. Res. 86,* 3321, 1981.

Stone, R. G., et al., The unified radio and plasma wave (URAP) instrument, *Astron, Astrophys. Suppl. Ser., 92,* 291, 1992.

Swift, D. F., Turbulent generation of electrostatic fields in the magnetosphere, *J. Geophys. Res., 82,* 5143, 1977.

Thorne, R. M. and B. T. Tsurutani, Wave-particle interactions in the magnetopause boundary layer, in *Physics of Space Plasmas (1990)*, ed. T. Chang, et al., Sci. Publ. Inc.,

Cambridge, MA, 10, 119, 1991.

Treumann, R.A., J. LaBelle, and R. Pottelette, Plasma diffusion at the magnetopause, The case of lower hybrid draft waves, *J. Geophys. Res., 96,* 16009, 1991.

Treumann, R. A., J. LaBelle, and T. M. Bauer, Diffusion processes: An observational perspective, in *Physics of the Magnetopause, Geophys. Mon. 90,* Amer. Geophys. Union, Washington, DC, 331, 1995.

Treumann, R. A., Theory of super-diffusion for the magnetopause, *Geophys. Res. Lett, 24,* 1727, 1997.

Tsurutani, B. T., A. L. Brinca, E. J. Smith, R. T. Okida, R. R. Anderson and T. E. Eastman, A statistical study of ELF-VLF plasma waves at the magnetopause, *J. Geophys. Res., 94,* 1270, 1989.

Tsurutani, B. T., D. J. Southwood, E. J. Smith and A. Balogh, A survey of low-frequency waves at Jupiter : The Ulysses encounter, *J. Geophys. Res., 98,* 21, 203, 1993.

Tsurutani, B. T., G. S. Lakhina, C. M. Ho, J. K. Arballo, C. Galvan, A. Boonsiriseth, J. S. Pickett, D. A. Gurnett, W. K. Peterson, and R. M. Thorne, Broadband plasma waves observed in the polar cap boundary layer: Polar, *J. Geophys. Res., 103,* 17,351, 1998.

Tsurutani, B.T., E.J. Smith, R.M. Thorne, R.R. Anderson, D.A. Gurnett, G.K. Parks, C.S. Lin, and C.T. Russell, Wave-particle interaction at the magnetopause: Contribution to the dayside aurora, *Geophys. Res. Lett., 8,* 183, 1981.

Tsurutani, B.T., and R.M. Thorne, Diffusion processes in the magnetopause boundary layer, *Geophys. Res. Lett., 22,* 663, 1982.

Tsurutani, B. T. and W. D. Gonzalez, The efficiency of "viscous interaction" between the solar wind and the magnetosphere during intense northward IMF events, *Geophys. Res. Lett., 22,* 663, 1995.

Tsurutani, B. T., J. K. Arballo, B. E. Goldstein, C. M. Ho, G. S. Lakhina, E. J. Smith, N. Cornilleau-Wehrlin, R. Prangé, N. Lin, P. Kellogg, J. L. Phillips, A. Balogh, N. Krupp, and M. Kane, Plasma wave characteristics of the Jovian magnetopause boundary layer:

Relationship to the Jovian aurora, *J. Geophys. Res., 102,* 4751, 1997.

Tsurutani, B.T., and G. S. Lakhina, Some basic Concepts of wave-particle interaction in collisionless plasmas, *Rev. Geophys., 35,* 491, 1997.

Tsurutani, B.T., G. S. Lakhina, C.M. Ho, J. K. Arballo, C. Galvan, A. Boonsiriseth, J. S. Pickett, D. A. Gurnett, W. K. Peterson, and R. M. Thorne, Broadband plasma waves observed in the polar cap boundary layer (PCBL): Polar, *J. Geophys. Res., 103,* 17351, 1998a.

Tsurutani, B.T., J. K. Arballo, G. S. Lakhina, C.M. Ho, B. Buti, J. S. Pickett, and D. A. Gurnett, Plasma waves in the dayside polar cap boundary layer: Bipolar and monopolar electric pulses and whistler mode waves, *Geophys. Res. Lett., 25,* 4117, 1998b.

Tsutsui, M., R. J. Strangeway, B. T. Tsurutani, H. Matsumoto, J. L. Phillips, and M. Ashour-Abdalla, Wave mode identification of electrostatic noise observed with ISEE 3 in the deep tail boundary layer, *J. Geophys. Res., 96,* 14065-14073, 1991.

Verheest, F. and **G. S. Lakhina**, Nonresonant low-frequency instabilities in multibeam plasmas : applications to cometary environments and plasma sheet boundary layers, *J. Geophys. Res., 96,* 7905, 1991.

Verheest, F. and **G. S. Lakhina**, Resonant electromagnetic ion-ion beam turbulence at comet P/Grigg-Skjellerup, *J. Geophys. Res., 98,* 21,017, 1993.

Weiss, L. A., P. H. Reiff, J. J. Moses, and B. D. Moore, Energy dissipation in substorms, *Eur. Space Agency Spec. Publ., ESA-SP-335,* 309, 1992.

Winske, D. and N. Omidi, Diffusion at the magnetopause: hybrid simulations, *J. Geophys. Res., 100,* 11923, 1995.

Winske, D., V. A. Thomas, and N. Omidi, Diffusion at the magnetopause: A theoretical perspective, in *Physics of the Magnetopause, Geophys. Mon. 90,* Amer. Geophys. Union, Washington, DC, 321, 1995.

Winske, D. and N. Omidi, Diffusion at the magnetopause: Hybrid simulations, *J. Geophys. Res., 100,* 11923, 1995.

Young, T. S. T., J. D. Callen, and J. E. McCune, High frequency electrostatic waves in the magnetosphere, *J. Geophys. Res., 78,* 1082, 1973.

Zhu, Z., P. Song, J.F. Drake, C.T. Russell, R.R. Anderson, D.A. Gurnett, K.W. Ogilvie, and R.J. Fitzenreiter, The relationship between ELF-VLF waves and magnetic shear at the dayside magnetopause, *Geophys. Res., Lett., 23,* 773, 1996.

G. S. Lakhina, Indian Institute of Geomagnetism, Colaba, Bombay 400005, India. (e-mail: lakhina@iig.iigm.res.in)

B.T. Tsurutani, Jet Propulsion Laboratory, California Institute of Technology, 4800 Oak Grove Drive, Pasadena, California 91109. (e-mail:btsurutani@jplsp.jpl.nasa.gov)

H. Kojima, and H. Matsumoto, Radio Atmospheric Science Center, Kyoto University, Uji, Kyoto 611, Japan. (e-mail:kojima@kurasc.kyoto-u.ac.jp; matsumot@kurasc.kyoto-u.ac.jp)

Received _____

Submitted to *Journal of Geophysical Research*, 1999.

Spacecraft	Location	Date	B $(nT)^2$ Hz^{-1}	E V^2 m^{-2} Hz^{-1}
POLAR[1]	$\sim$ 7-8 R_E altitude	day 098, 1996	$1.17 \times 10^{-2} f^{-2.6}$	$1.19 \times 10^{-7} f^{-1.8}$
	$\sim$ 2 R_E altitude	day 103, 1996	$1.34 \times 10^{-2.5} f^{-2.5}$	$1.22 \times 10^{-6} f^{-1.8}$
ULYSSES[2]	Jovian LLBL	day 043, 1992	$2.0 \times 10^{-4} f^{-2.4}$	$4.0 \times 10^{-9} f^{-2.4}$
ISEE[3] 1	Earth's LLBL	day 314, 1977	$\sim f^{-3.3}$	$\sim f^{-2.2}$
ISEE[4] 1, 2	Earth's LLBL	1977	$1.0 \times 10^{1} f^{-3.9}$	$3.0 \times 10^{-5} f^{-2.8}$
ISEE[5] 1, 2	Earth's LLBL	1977	$7.90 \times 10^{-2} f^{-2.9}$	$6.3 \times 10^{-6} f^{-2.2}$
GEOS[6] 2	Earth's LLBL	day 240, 1978	$3.60 \times 10^{1} f^{-2.6}$	$1.2 \times 10^{-6} f^{-2.6}$
ISEE[7] 1	Earth's LLBL	1977-1978	$3.0 \times 10^{-1} f^{-3.3}$	$6.0 \times 10^{-7} f^{-2.1}$

[1] *Tsurutani et al.* [1998a]; [2] *Tsurutani et al.* [1997]

[3] *Gurnett et al.* [1979] ; [4] *Tsurutani et al.* [1981]

[5] *Anderson et al.* [1982] ; [6] *Rezeau et al.* [1989]

[7] *Tsurutani et al.* [1989]

Table 1. Comparison of broadband plasma wave properties in various boundary layers.

Figure 1. Schematics of the Earth's Magnetosphere with various boundary layers. The plasma mantle, the exterior cusp, the entry layer, the low-latitude boundary layer, and the plasma sheet boundary layers are indicated.

Figure 2. The plasma wave electric and magnetic field data from ISEE 1 for a representative pass through the magnetospere. The enhanced electric and magnetic field intensities at the inbound and outbound magnetopause crossings are clearly indicated. From *Gurnett et al.* [1979, Figure 1].

Figure 3. Shows the typical electric and magnetic field spectra of the enhanced plasma wave turbulence obseved near the magnetopause. From *Gurnett et al.* [1979, Figure 10].

Figure 4. A comparison between the GEOS 2 Magnetopause BL magnetic wave spectrum (bottom) and and the magnetosheath magnetic wave spectrum (top). The average magnetosheath spectrum is shown by the dahed line in the bottom panel. The BL wave spectrum is enhanced above the magnetosheath spectrum (except below 10 Hz). From *Rezeau et al.* [1986, Figure 3].

Figure 5. Shows the AMPTE/IRM wave, particle and field data from three magnetopause crossing on October 9, 1984. The top panel shows electric field fluctuations from 30 Hz to 10 kHz, the next panel shows the magnetic field fluctuations (0 - 16 Hz), next three panels show ion density, ion temperature, and ion flow velocity, respectively, the last four panels show the magnetic field magnitude, and magnetic field component expressed in LMN coordinates [*Paschmann et al.*, 1986]. Vertical lines indicate the position of the three magnetopauses. A dashed vertical line indicate the location of the magnetic 'hole'. From *LaBelle and Treumann* [1988, Figure 1].

Figure 6. a) The spectrum of magnetic fluctuations observed at the magnetopause from various different satellite. b) The spectrum of electric fluctuations observed at the magnetopause from ISEE and from AMPTE/IRM. The IRM data comes from a single day; the maximum value at the magnetopause is shown, along with the spectrum averaged over the magnetopause region. The IRM data from below 30 Hz are only upper limits on the wave amplitude. Also shown is the typical value of electric field fluctuations below 0.1 Hz corresponding to the velocity fluctuations reported from the HEOS satellite. From *LaBelle and Treumann* [1988, Figures 2 and 3].

Figure 7. Average wave three-point electric field spectra (at 10^1, 10^3, and 10^5 Hz) for three different local times (dawn, noon, and dusk). The average spectra are remarkably similar to each other in both shape and intensity. From *Tsurutani et al.* [1989, Figure 6].

Figure 8. Same as Figure 7 except for the wave magnetic component. From *Tsurutani et al.* [1989, Figure 7].

Figure 9. The amplitude of the normalized wave magnetic field (asterisks) and wave electric field (closed squares) as function of local magnetic shear angle. Vertical bars indicate the deviations of the means. Solid and dashed lines are the linear fits to the wave magnetic and electric data respectively. From *Zhu et al.* [1996, Figure 2].

Figure 10. Dispersion relation of ELF-VLF waves under different shear levels. The two dotted lines (v_{w1} and v_{w2}) show the theoretical dispersion curves of whistler mode with a magnetic field strength of 50 nT and electron density of 1 cm^{-3} and 10 cm^{-3} respectively. Ω_{ce} and Ω_{lh} are the electron cyclotron frequency and the lower-hybrid frequency respectively. From *Zhu et al.* [1996, Figure 3].

Figure 11. The correlation of the normalized magnetic (closed squares and solid lines) and electric (open triangles and dashed lines) amplitudes with the electron plasma beta (upper panel) and the electron temperature anisotropy (lower panel). From *Song et al.* [1998, Figure 13].

Figure 12. Different microscopic diffusion coefficients and their dependencies on the total electric wave intensity. The shaded region marks the range of the observed electric wave field strengths. The horizontal dashed line at $D = 10^9 m^2 s^{-1}$ is the diffusion required to maintain LLBL according to the theory of Sonnerup (1980). The dots indicate the diffusion coefficients according to theoretical saturation levels of the various instabilities. The double shaded regions mark the uncertainties in measured wave intensity and in the estimate of the diffusion coefficient. From *Treumann et al.* [1995, Figure 5].

Figure 13. The POLAR orbit and the region of wave detection (solid bar) in the magnetosphere. POLAR has a perigee at 1.8 R_E and apogee at 9 R_E. Waves on the field lines that map into the low latitude boundary layer (LLBL) are the topic of this study. From *Tsurutani et al.* [1998a, Figure 1].

Figure 14. Occurrence frequency of northern dayside PCBL waves as a function of local time. The polar cap boundary layer waves are present on the dayside 96% of the time (05-18 LT). The statistics are listed at the top. From *Tsurutani et al.* [1998a, Figure 3].

Figure 15. a) The geomagnetic latitude of the footpoint of the B field line passing through the spacecraft versus local time (GMT). Regions of wave activity are primarily located on the field lines whose footpoint geomagnetic latitudes lie between 70° - 80°. b) L-value distribution of the PCBL waves versus GMT. The wave region is located for L = 10. From *Tsurutani et al.* [1998a, Figure 4].

Figure 16. The electric field a) and magnetic field b) spectra for the events occurring on Day 098, 1996. The background noise is indicated. The electric component of the waves extend beyond the electron cyclotron frequency ($\sim 6 \times 10^3$ Hz). From *Tsurutani et al.* [1998a, Figure 5].

Figure 17. The B/E wave amplitude ratio for two events, one on day 98 (panel a) and the other on day 114 (panel b). Two curves corresponding to propagation angles of $\psi = 0°$ and $\psi = 60°$ for the whistler wave refractive index, η, are also shown. These ratios are highly variable but lie between the values 10 to 100. For parallel propagating whistler modes, the ratio B/E should lie along the $\psi = 0°$ curve. From *Tsurutani et al.* [1998a, Figure 7].

Figure 18. A northern polar view of the mapping of polar cap boundary layer (PCBL) waves to the low latitude boundary layer (LLBL). From *Tsurutani et al.* [1998a, Figure 8].

Figure 19. A typical frequency spectrum of the broadband electrostatic noise observed by the IMP 8 spacecraft [Figure 5 in Gurnett et al., 1976].

Figure 20. Time evolution of the bump-on-tail instability. Right and left four panels show the time series of electron phase diagrams and electron velocity distribution [Figure 7 in Omura et al., 1996]

Figure 21. An overview of the low-frequency E and B wave amplidtudes for all 14 Jovian BL events encountered by Ulysses The inbound pass is shown on the left and the outbound on the right. The top 4 panels show the spin average E from 9.3-, 14-, 19-, and 28-Hz channel wave intensities, the next 4 panels show the spin average B wave intensities for the same frequency channels, the next 2 panels show the dc magnetometer 1-min and 10-min variances, and the bottom two panels show the spacecraft location relative to Jupiter. The BL events are shaded and numbered at the top. The vertical dashed lines indicate the bow shock crossings, and magnetosheath/BL interval are shown by horizontal bars in the top panel. From *Tsurutani et al.* [1997, Figure 1].

Figure 22. The electric (left) and magnetic field (right) wave spectra for the Jovian BL event 10. The spectra are broadband with no obvious peaks. From *Tsurutani et al.* [1997, Figures 5 and 6].

Figure 23. Ratio of B/E as a function of frequency for the JBL event 10 shown in Figure 21. Since the $f^{-1/2}$ frequency depence is not seen throughout the interval, it is speculated that the waves may be propagating off-axis to the ambient magnetic field. From *Tsurutani et al.* [1997, Figure 7].

Figure 24. Variation of normalized growth rate, γ/ω_{ci}, (upper panel) and normalized real frequency, ω_r/ω_{ci},(lower panel) versus normalized wavenumber number $a = k_y V_{ti}/\omega_{ci}$ for the coupled lower hybrid drift and current convective instability for the case of hot plasma with $\omega_{pe}/\omega_{ce} = 10.0$, V_0=0, and $\kappa_n/k_y = 0.1$. The curves 1, 2, and 3 are for $\beta_i =$ 0.0, k_z/k_y = -0.1 and $S = \frac{1}{\omega_{ce}}\frac{dV_0}{dx} = 0.0$, 0.05, and 0.1, respectively. The curv 4 is for β_i = 0.0, $S = 0.1$, and $k_z/k_y = 0.1$. The curves 4 and 5 are for $S = 0.1$, k_z/k_y = -0.1 and $\beta_i = 0.05$ and 0.2, respectively. From *Lakhina and Tsurutani et al.* [1999b, Figure 6].

Figure 25. Schematics of the physical mechanism of the velocity shear instability. The equilibrium magnetic field $\mathbf{B_0}$ is taken along the z axis. The equilibrium electrons flow $\mathbf{V_0}$ is parallel to the magnetic field $\mathbf{B_0}$. The parallel electron velocity gradients ∇V_0, which derives the instability, and the density gradient ∇n_0 are in the x direction. The assumed form of the perturbing field $\mathbf{E} = E_z\,\mathbf{z} + E_y\,\mathbf{y}$ is shown in the $y - z$ plane. The convection of the electron flow v_z brings regions of different parallel flow to the same magnetic field line The resultant bunching of electrons along this magnetic field line (shown in the $x - z$ plane) produces an electric field which reinforces the initial perturbation, thereby producing an instability . The presence of density gradients tends to debunch the electrons along $\mathbf{B}$ (i.e., the particles shown as shaded in the $x - z$ plane are removed), thereby reducing growth of the velocity shear modes. From *Lakhina and Tsurutani et al.* [1999b, Figure 7].

Figure 26. Bipolar (bpp), offset bipolar (obpp), and monopolar (mpp) wave structures in parallel electric field component. From *Tsurutani et al.* [1998b, Figure 3].

Figure 27. A schematic showing a bipolar electric field structure (left), an offset bipolar structure (middle), and a pair of oppositely polarized monopolar structures (right). The bipolar pulse is modeled by an electron hole plus surrounding neutralizing charge. The offset bipolar pulse is modeled by a broadened electron hole. The two monopolar pulses are modeled by an electron hole that has split into two into two. From *Tsurutani et al.* [1998b, Figure 4].

Plate 1. Color spectrogram of wave electric field from $\sim 10^1$ to 10^4 Hz and above. The boundary layer waves are indicated. In between the two boundary layer (dayside and nightside) crossings is the polar cap (quiet wave region). From *Tsurutani et al.* [1998a, Plate 1].

Plate 2. Color spectrogram of the H^+, O^+, He^+ and He^{++} ion fluxes observed by the TIMAS experiment (top 4 panels) and the electric component of the PWI broadband plasma wave event (lower panel) on day 98, 1996. The values of eccentric dipole magnetic local time (EDMLT), magnetic latitude (MAGLAT), invariant latitude (INVLAT) and local time (LT) are also shown at the bottom of the Plate. From *Tsurutani et al.* [1998a, Plate 3].

Plate 3. Typical frequency-time spectrogram of the BEN and corresponding ESW waveforms.

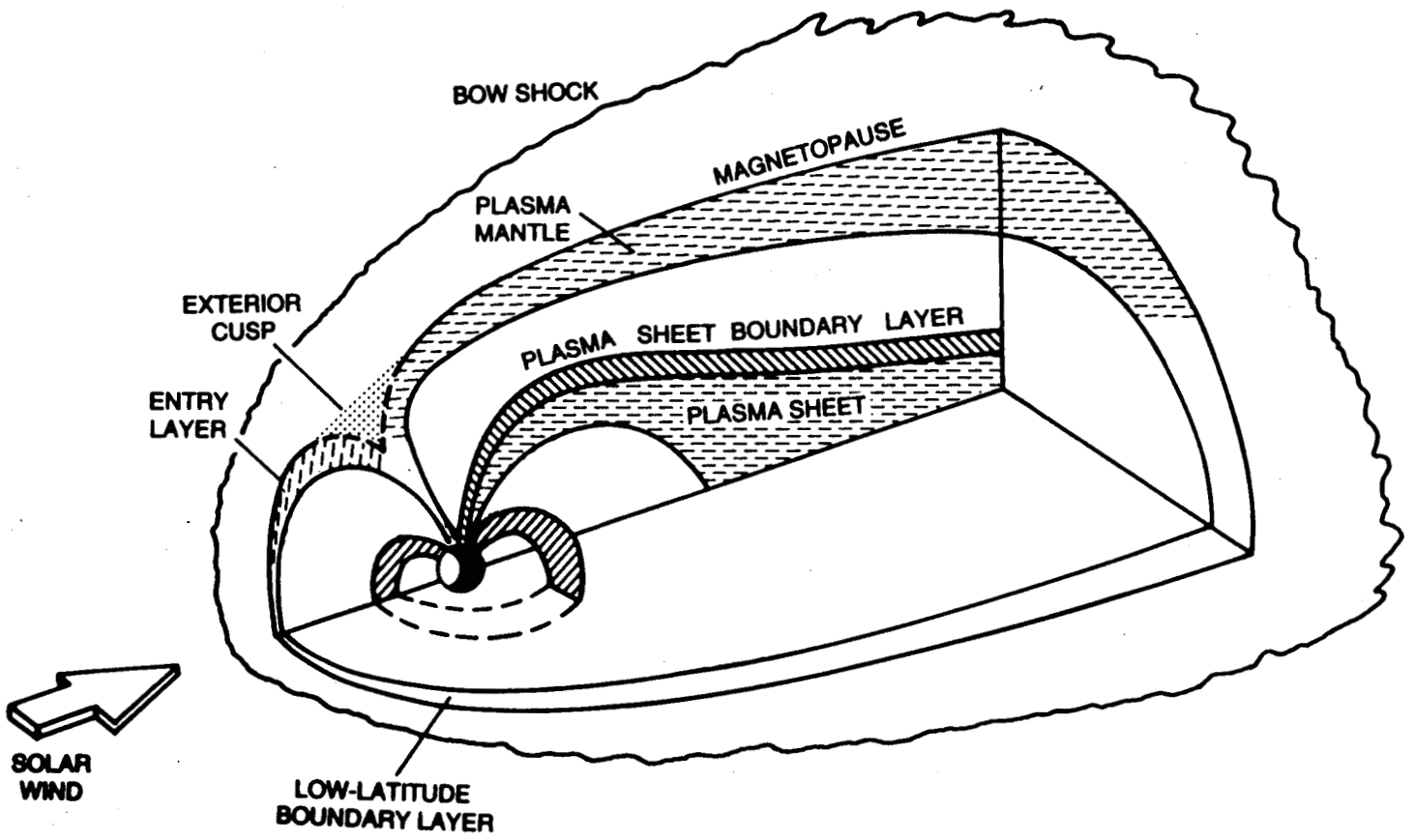
BOW SHOCK
MAGNETOPAUSE
PLASMA MANTLE
EXTERIOR CUSP
PLASMA SHEET BOUNDARY LAYER
ENTRY LAYER
PLASMA SHEET
SOLAR WIND
LOW-LATITUDE BOUNDARY LAYER

Figure 1

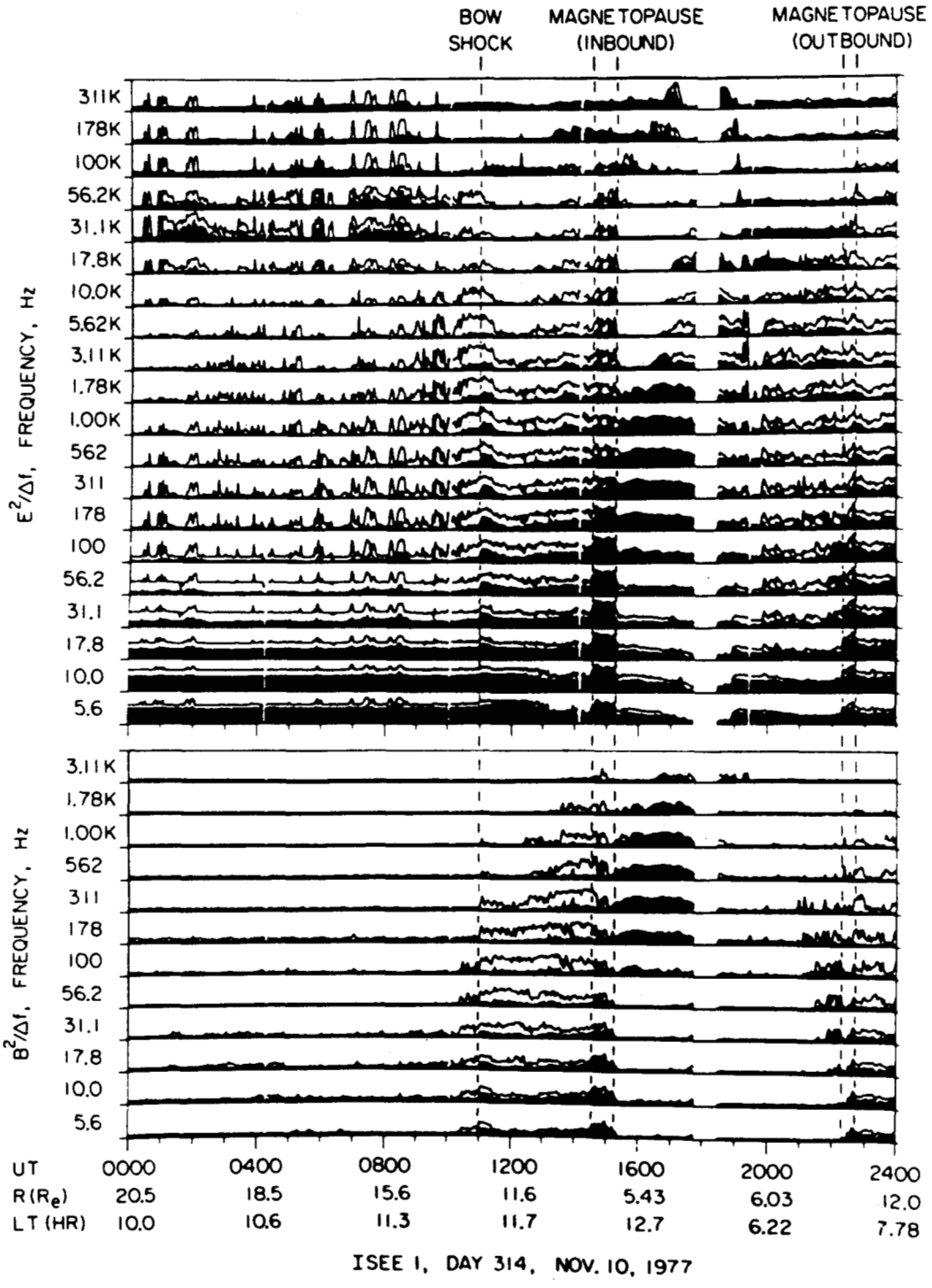
BOW SHOCK
MAGNETOPAUSE (INBOUND)
MAGNETOPAUSE (OUTBOUND)
E²/Δf, FREQUENCY, Hz
311K
178K
100K
56.2K
31.1K
17.8K
10.0K
5.62K
3.11K
1.78K
1.00K
562
311
178
100
56.2
31.1
17.8
10.0
5.6
B²/Δf, FREQUENCY, Hz
3.11K
1.78K
1.00K
562
311
178
100
56.2
31.1
17.8
10.0
5.6
UT 0000 0400 0800 1200 1600 2000 2400
R(Re) 20.5 18.5 15.6 11.6 5.43 6.03 12.0
LT (HR) 10.0 10.6 11.3 11.7 12.7 6.22 7.78
ISEE 1, DAY 314, NOV. 10, 1977

Fig. 2

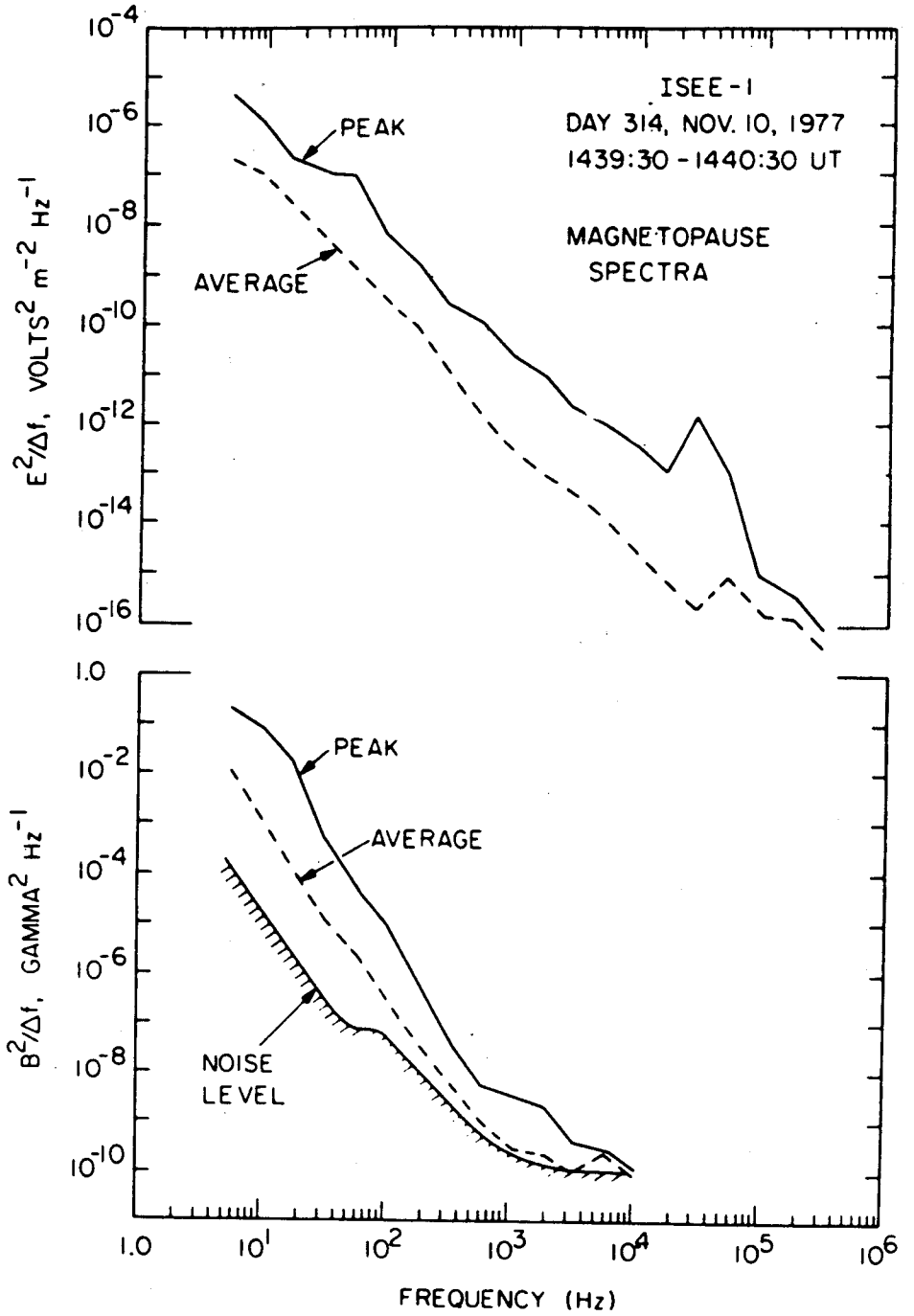
ISEE-1
DAY 314, NOV. 10, 1977
1439:30 - 1440:30 UT
MAGNETOPAUSE
SPECTRA
PEAK
AVERAGE
$E^2/\Delta f$, VOLTS^2 m^{-2} Hz^{-1}
10^{-4}
10^{-6}
10^{-8}
10^{-10}
10^{-12}
10^{-14}
10^{-16}
PEAK
AVERAGE
NOISE
LEVEL
$B^2/\Delta f$, GAMMA^2 Hz^{-1}
1.0
10^{-2}
10^{-4}
10^{-6}
10^{-8}
10^{-10}
1.0
10^1
10^2
10^3
10^4
10^5
10^6
FREQUENCY (Hz)

Fig. 3

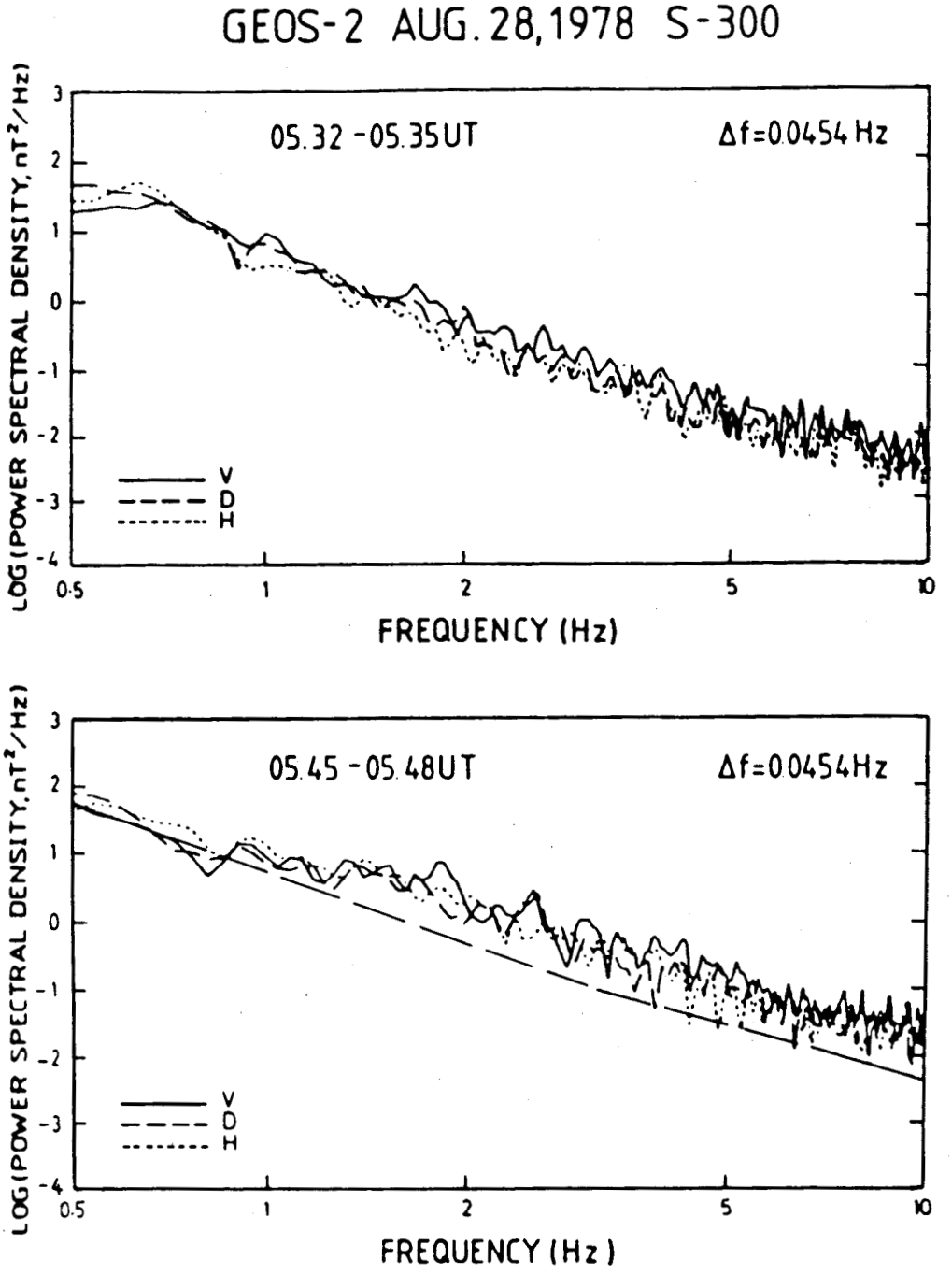
GEOS-2 AUG. 28, 1978 S-300
05.32 - 05.35UT
Δf=0.0454 Hz
LOG(POWER SPECTRAL DENSITY, nT²/Hz)
FREQUENCY (Hz)
V
D
H
05.45 - 05.48UT
Δf=0.0454Hz
LOG(POWER SPECTRAL DENSITY, nT²/Hz)
FREQUENCY (Hz)
V
D
H

Fig. 4

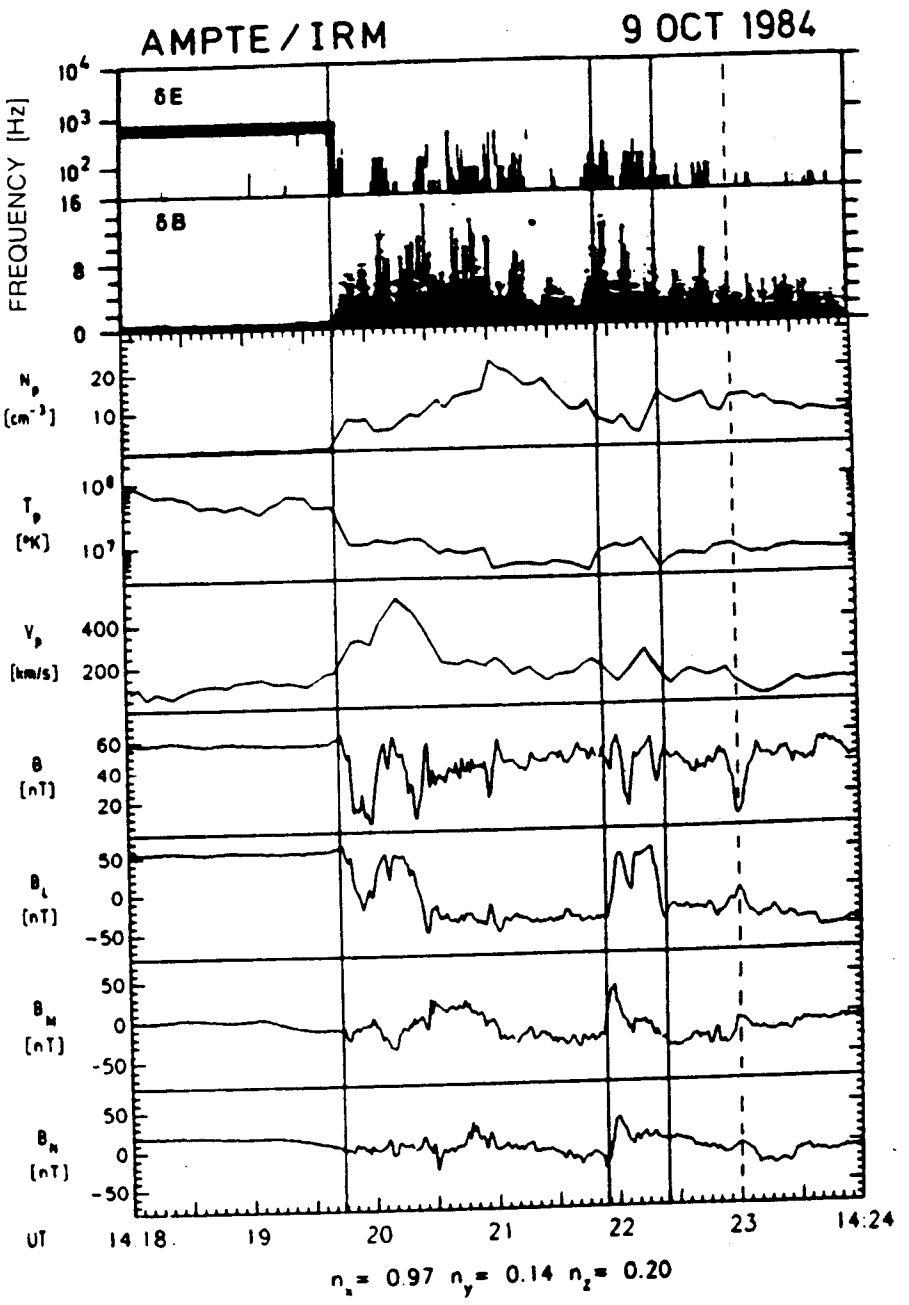
AMPTE / IRM
9 OCT 1984
FREQUENCY [Hz]
δE
δB
N_p [cm^{-3}]
T_p [°K]
V_p [km/s]
B [nT]
B_L [nT]
B_M [nT]
B_N [nT]
UT
14 18 19 20 21 22 23 14:24
n_x= 0.97 n_y= 0.14 n_z= 0.20

Figure 5

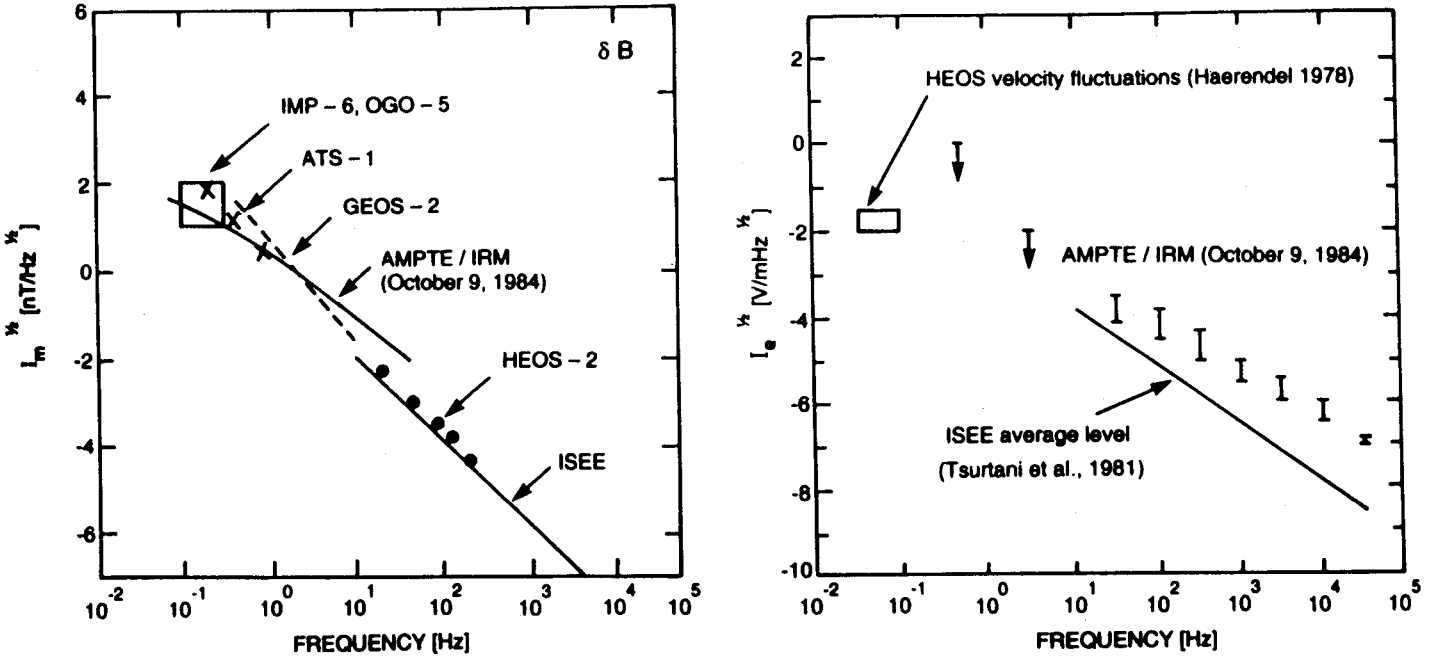
δ B
IMP – 6, OGO – 5
ATS – 1
GEOS – 2
AMPTE / IRM
(October 9, 1984)
HEOS – 2
ISEE
FREQUENCY [Hz]
HEOS velocity fluctuations (Haerendel 1978)
AMPTE / IRM (October 9, 1984)
ISEE average level
(Tsurtani et al., 1981)
FREQUENCY [Hz]

Figure 6

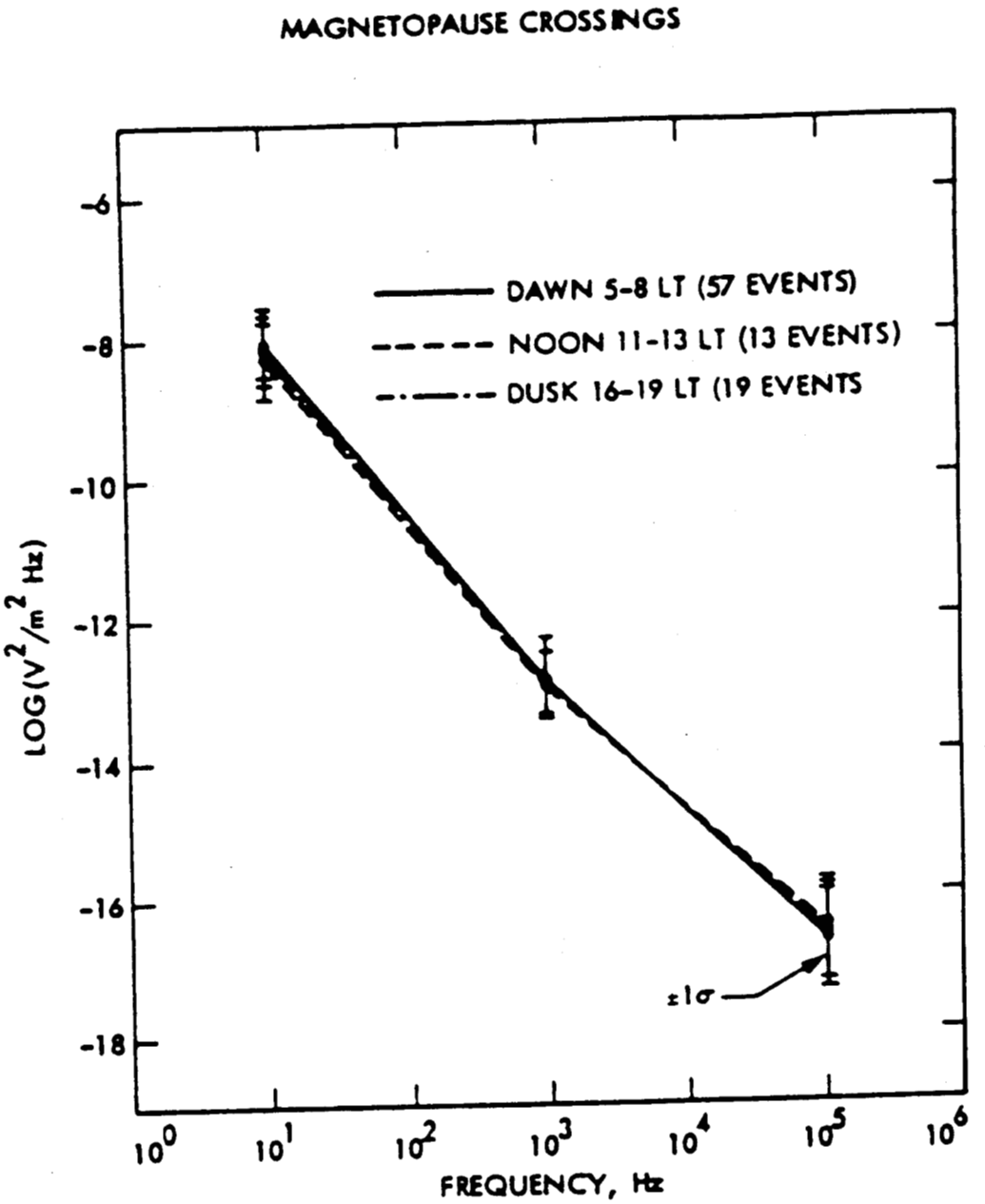
MAGNETOPAUSE CROSSINGS
DAWN 5-8 LT (57 EVENTS)
NOON 11-13 LT (13 EVENTS)
DUSK 16-19 LT (19 EVENTS
±1σ
LOG(V²/m² Hz)
-6
-8
-10
-12
-14
-16
-18
10⁰
10¹
10²
10³
10⁴
10⁵
10⁶
FREQUENCY, Hz

Figure 7

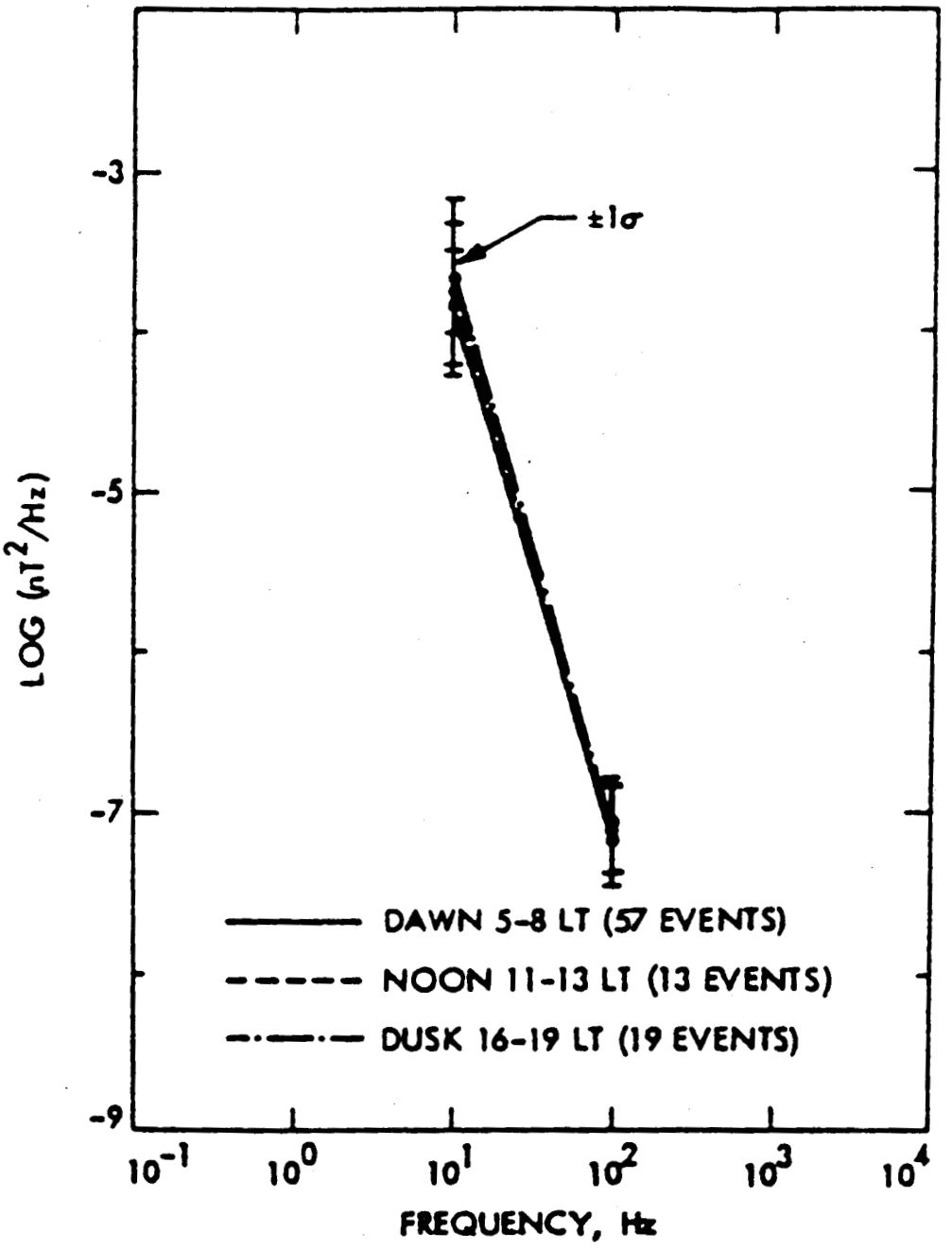
MAGNETOPAUSE CROSSINGS
±1σ
-3
-5
-7
-9
LOG (nT²/Hz)
DAWN 5-8 LT (57 EVENTS)
NOON 11-13 LT (13 EVENTS)
DUSK 16-19 LT (19 EVENTS)
10⁻¹
10⁰
10¹
10²
10³
10⁴
FREQUENCY, Hz

Figure 8

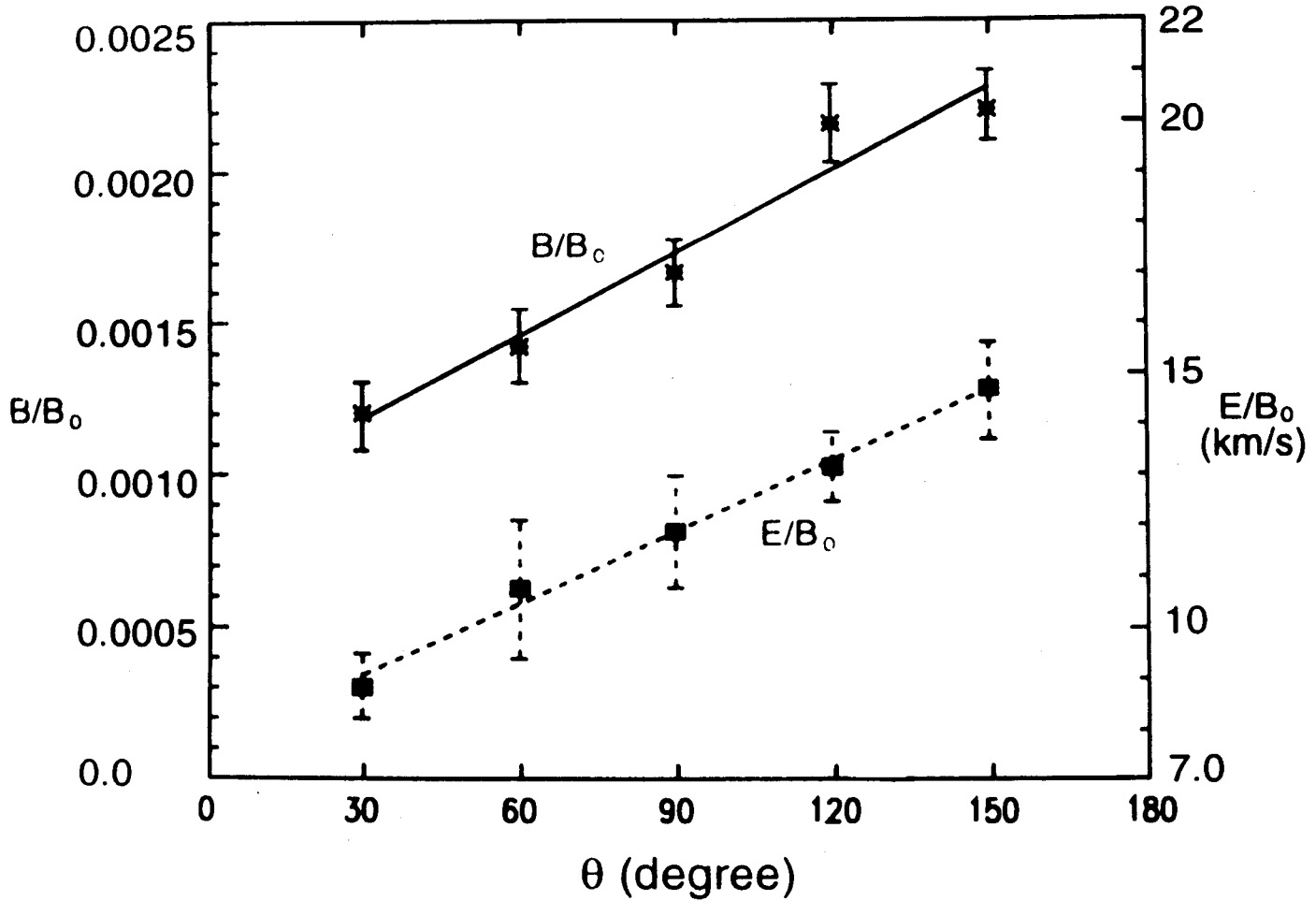
0.0025
0.0020
0.0015
0.0010
0.0005
0.0
B/B0
22
20
15
10
7.0
E/B0
(km/s)
B/B0
E/B0
0
30
60
90
120
150
180
θ (degree)

Fig. 9

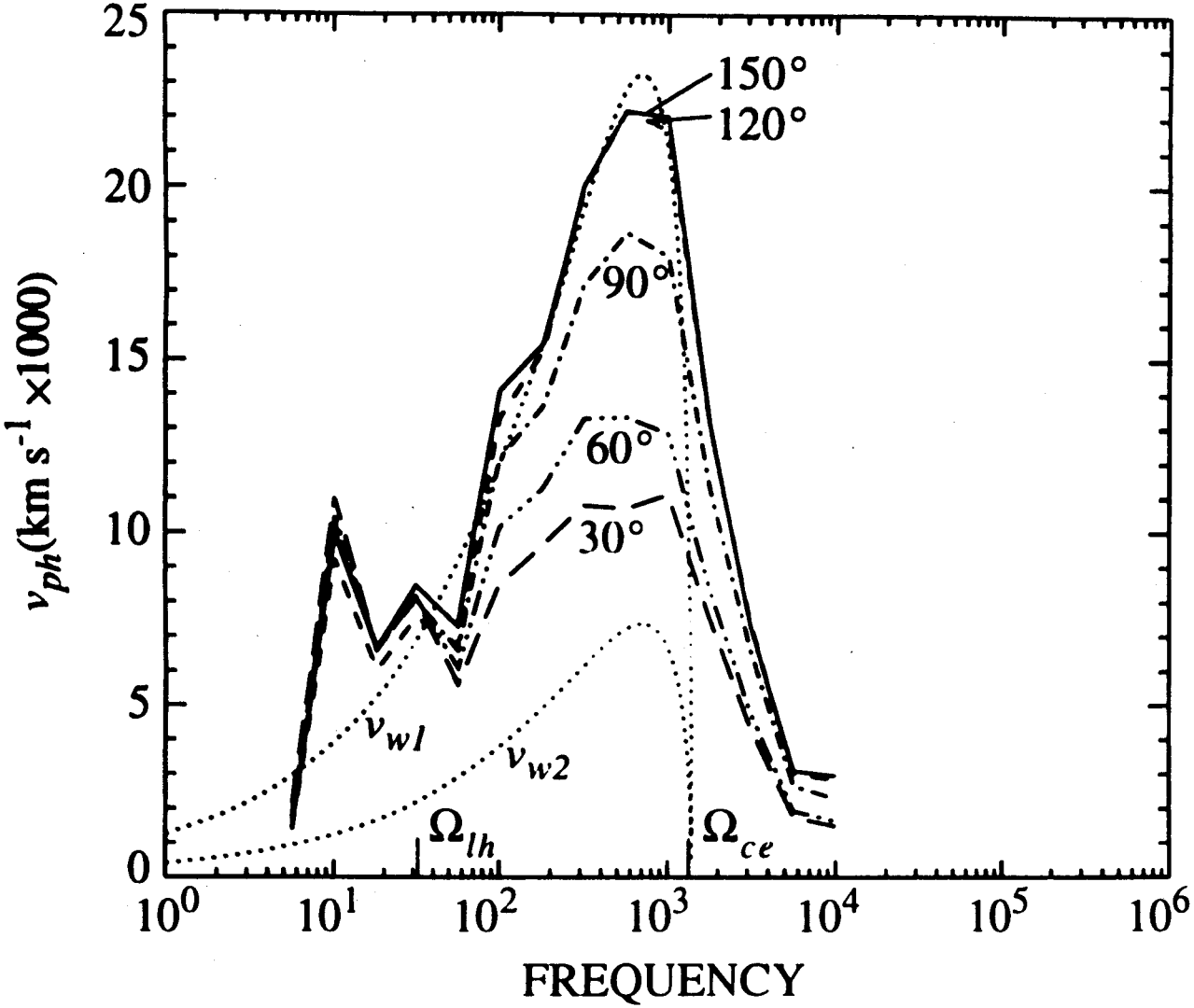
25
20
15
10
5
0
v_{ph}(km s^{-1} ×1000)
150°
120°
90°
60°
30°
v_{w1}
v_{w2}
Ω_{lh}
Ω_{ce}
10^0
10^1
10^2
10^3
10^4
10^5
10^6
FREQUENCY

FIGURE 10

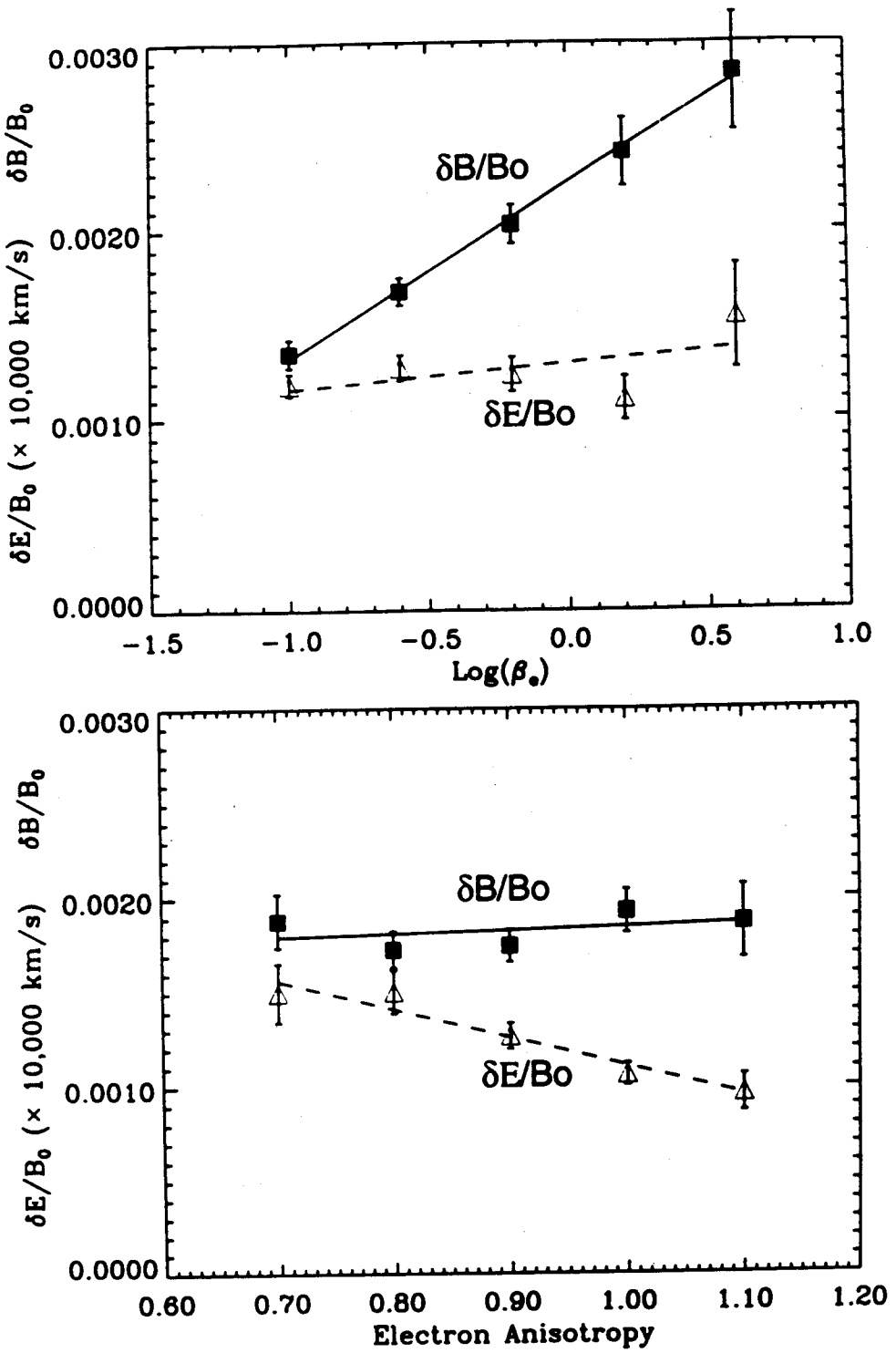
0.0030
0.0020
0.0010
0.0000
δE/B₀ (× 10,000 km/s)
δB/B₀
δB/Bo
δE/Bo
−1.5
−1.0
−0.5
0.0
0.5
1.0
Log(β∥)
0.0030
0.0020
0.0010
0.0000
δE/B₀ (× 10,000 km/s)
δB/B₀
δB/Bo
δE/Bo
0.60
0.70
0.80
0.90
1.00
1.10
1.20
Electron Anisotropy

Figure 11

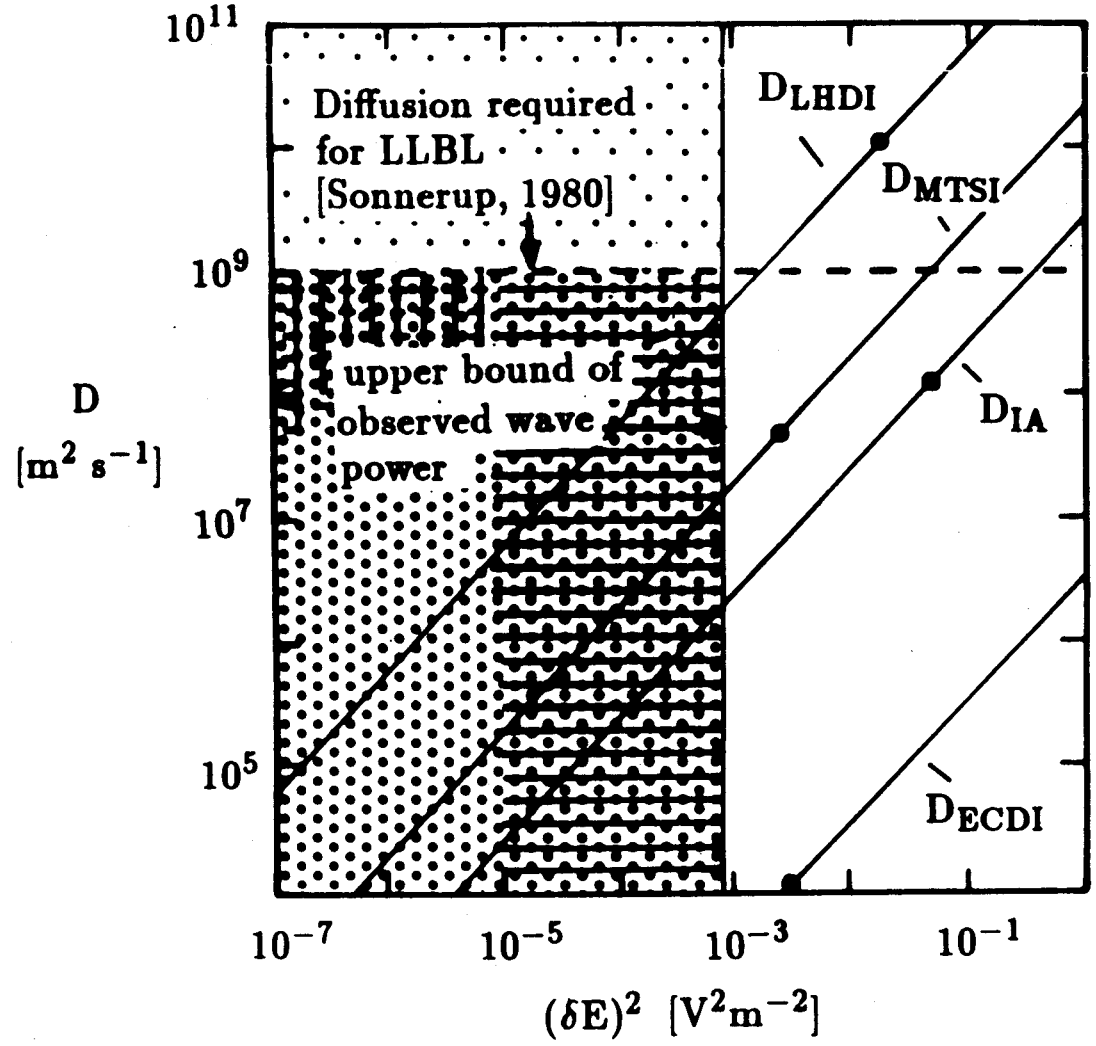
Diffusion required
for LLBL
[Sonnerup, 1980]
upper bound of
observed wave
power
D_{LHDI}
D_{MTSI}
D_{IA}
D_{ECDI}
10^{11}
10^{9}
10^{7}
10^{5}
D
$[m^2\ s^{-1}]$
10^{-7}
10^{-5}
10^{-3}
10^{-1}
$(\delta E)^2$ $[V^2 m^{-2}]$

Figure 12

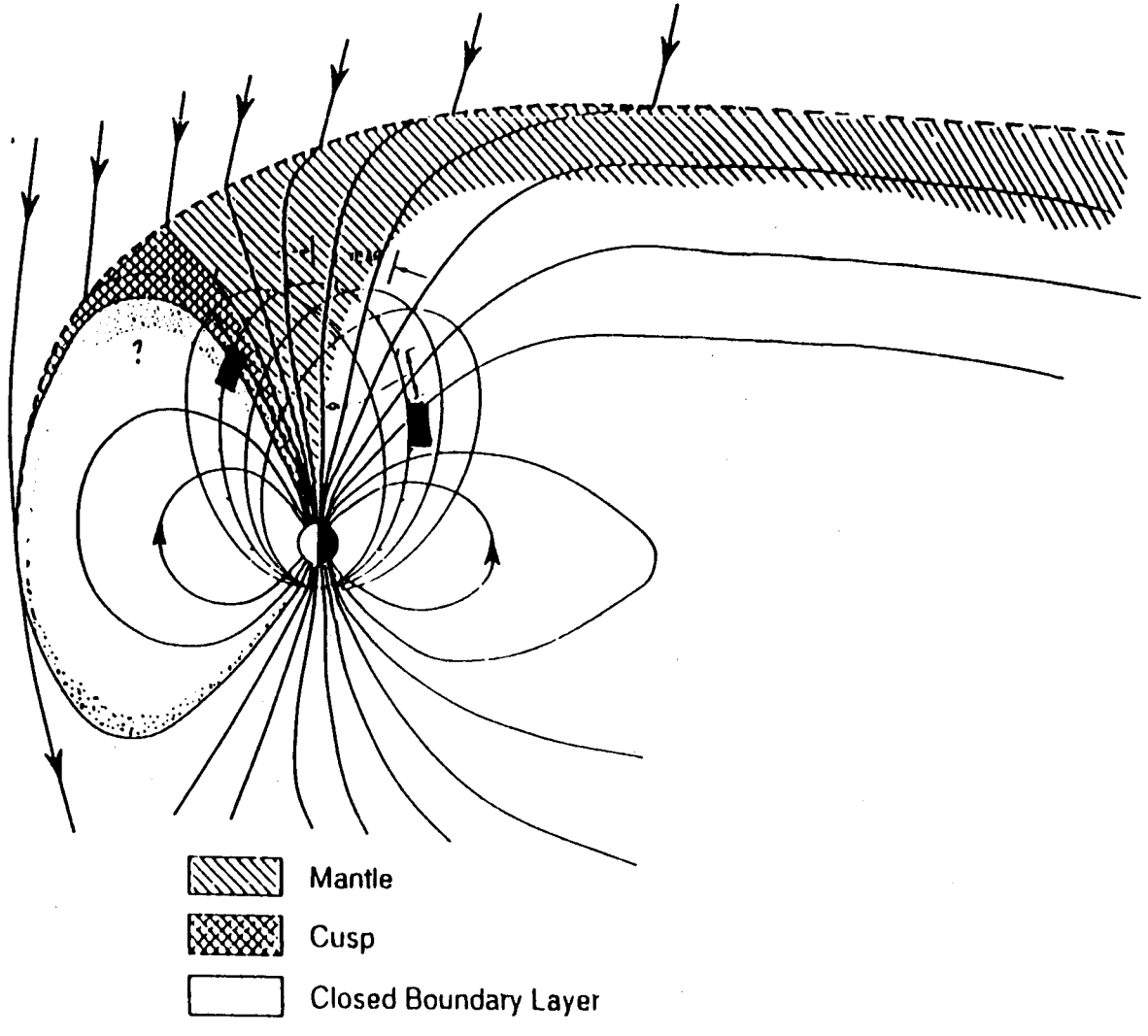

Figure 12

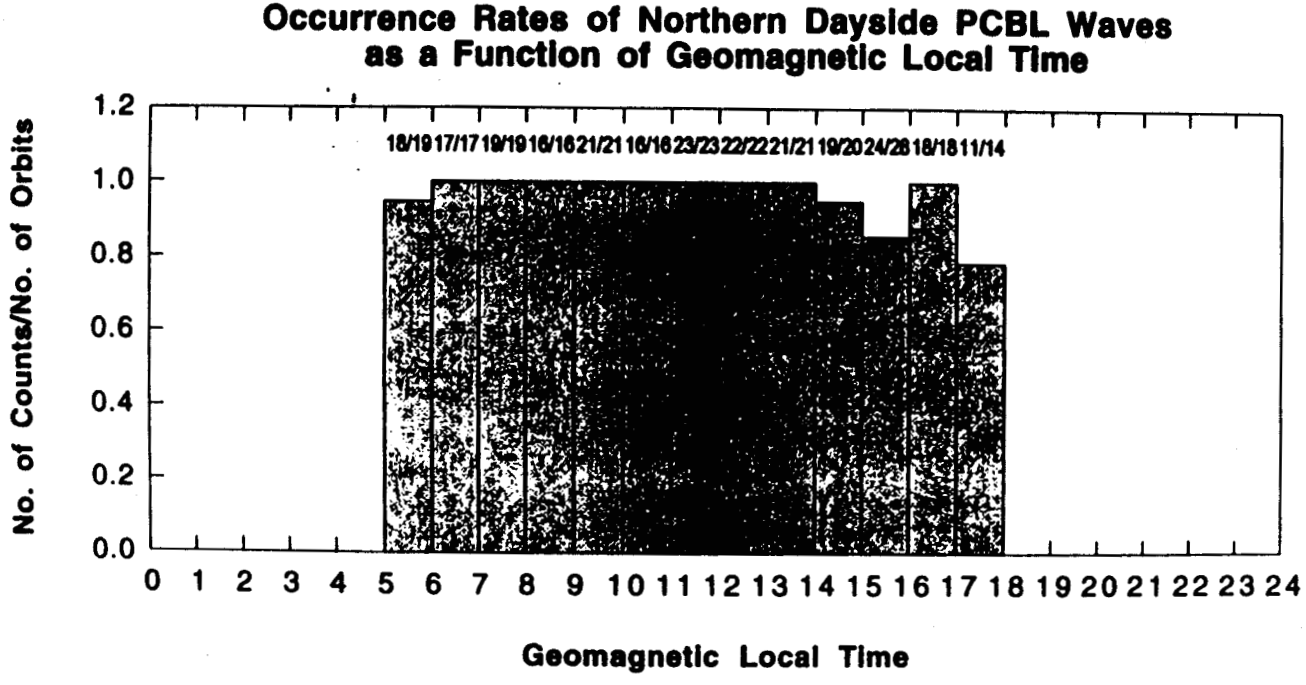
Occurrence Rates of Northern Dayside PCBL Waves
as a Function of Geomagnetic Local Time
18/19 17/17 19/19 16/16 21/21 16/16 23/23 22/22 21/21 19/20 24/28 18/18 11/14
No. of Counts/No. of Orbits
1.2
1.0
0.8
0.6
0.4
0.2
0.0
0 1 2 3 4 5 6 7 8 9 10 11 12 13 14 15 16 17 18 19 20 21 22 23 24
Geomagnetic Local Time

Figure 12

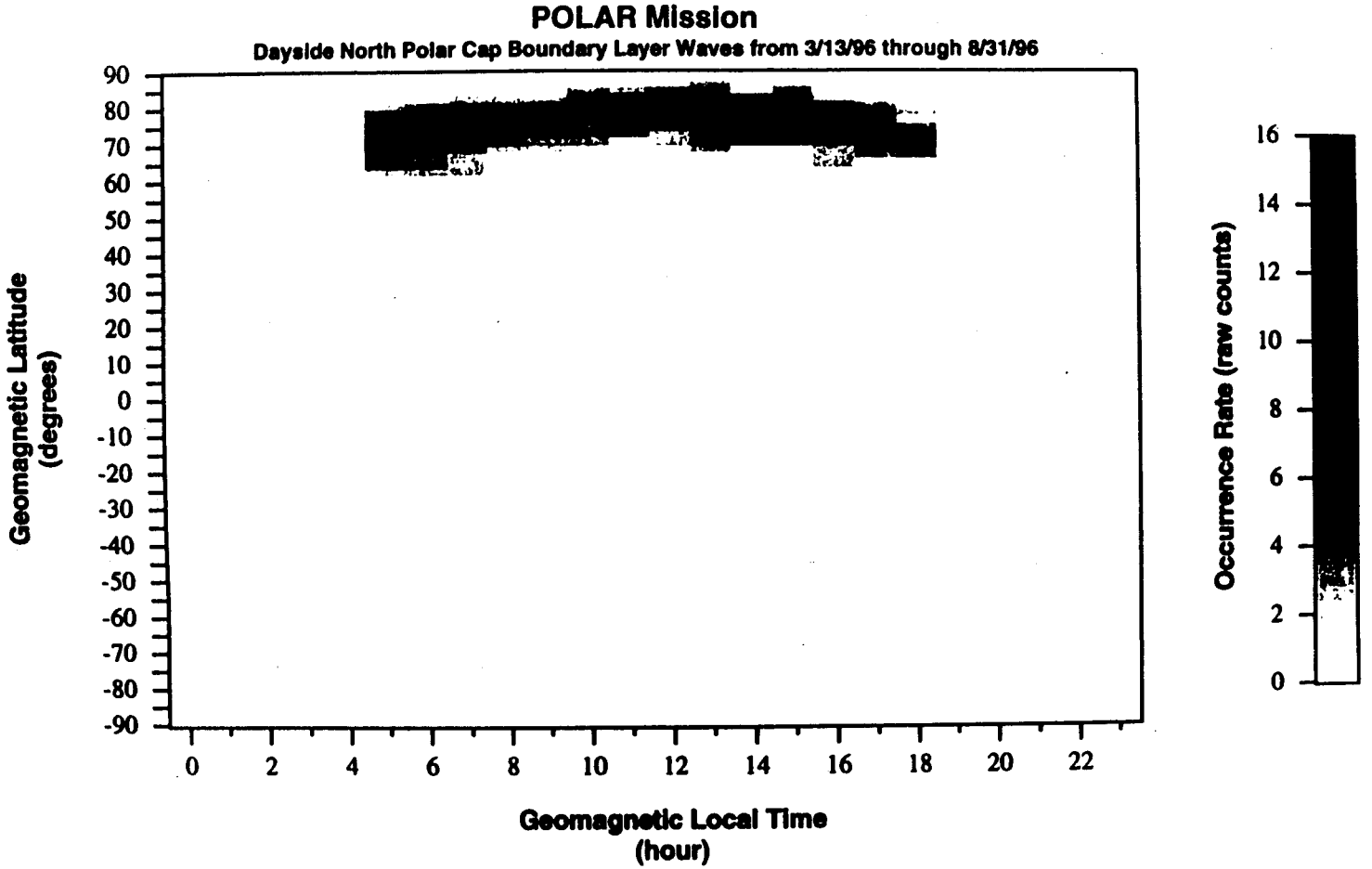
POLAR Mission
Dayside North Polar Cap Boundary Layer Waves from 3/13/96 through 8/31/96
Geomagnetic Latitude (degrees)
90
80
70
60
50
40
30
20
10
0
-10
-20
-30
-40
-50
-60
-70
-80
-90
0
2
4
6
8
10
12
14
16
18
20
22
Geomagnetic Local Time (hour)
Occurrence Rate (raw counts)
16
14
12
10
8
6
4
2
0

Figure 1

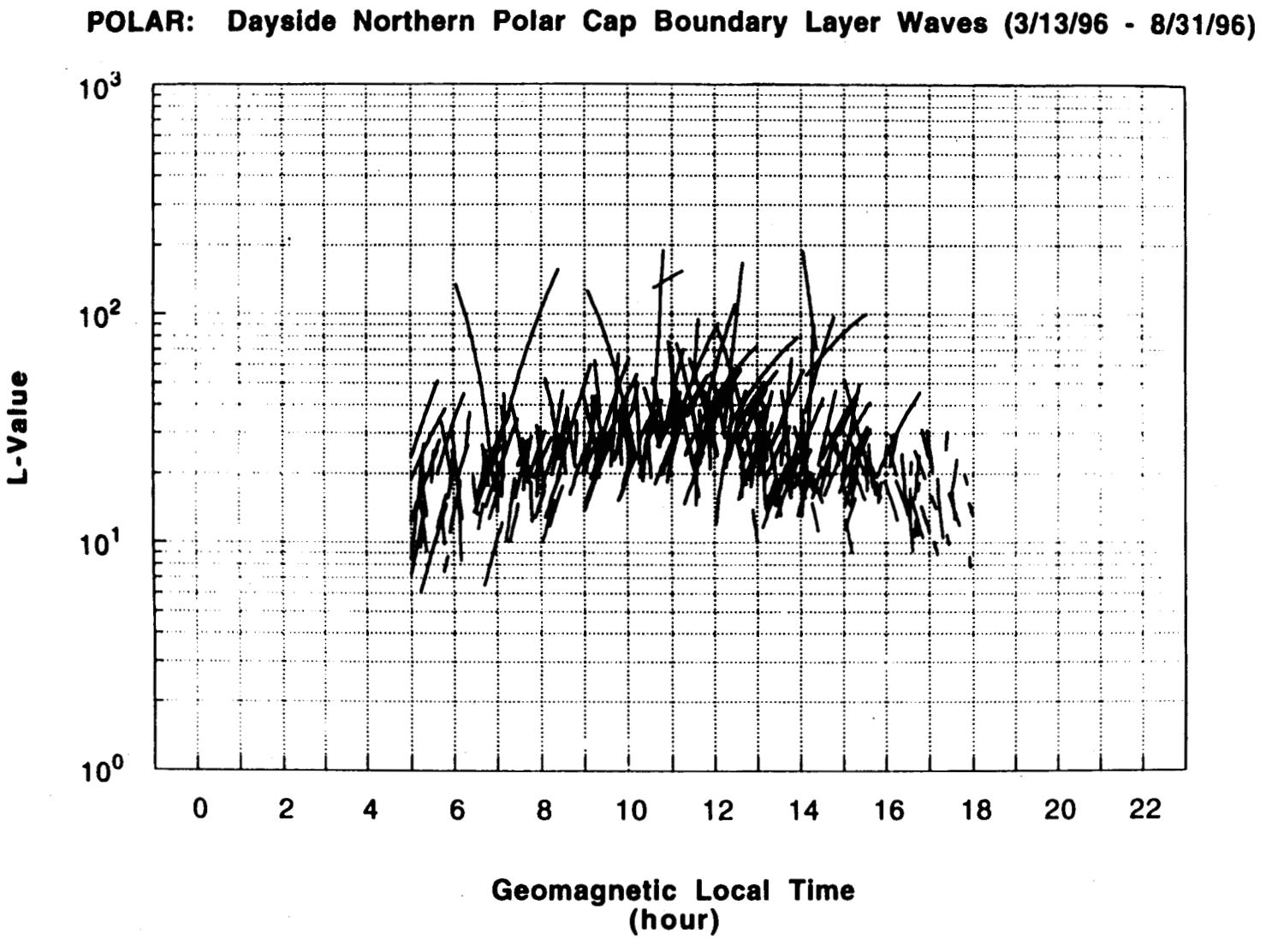
POLAR: Dayside Northern Polar Cap Boundary Layer Waves (3/13/96 - 8/31/96)
L-Value
10^3
10^2
10^1
10^0
0
2
4
6
8
10
12
14
16
18
20
22
Geomagnetic Local Time
(hour)

Figure 15b

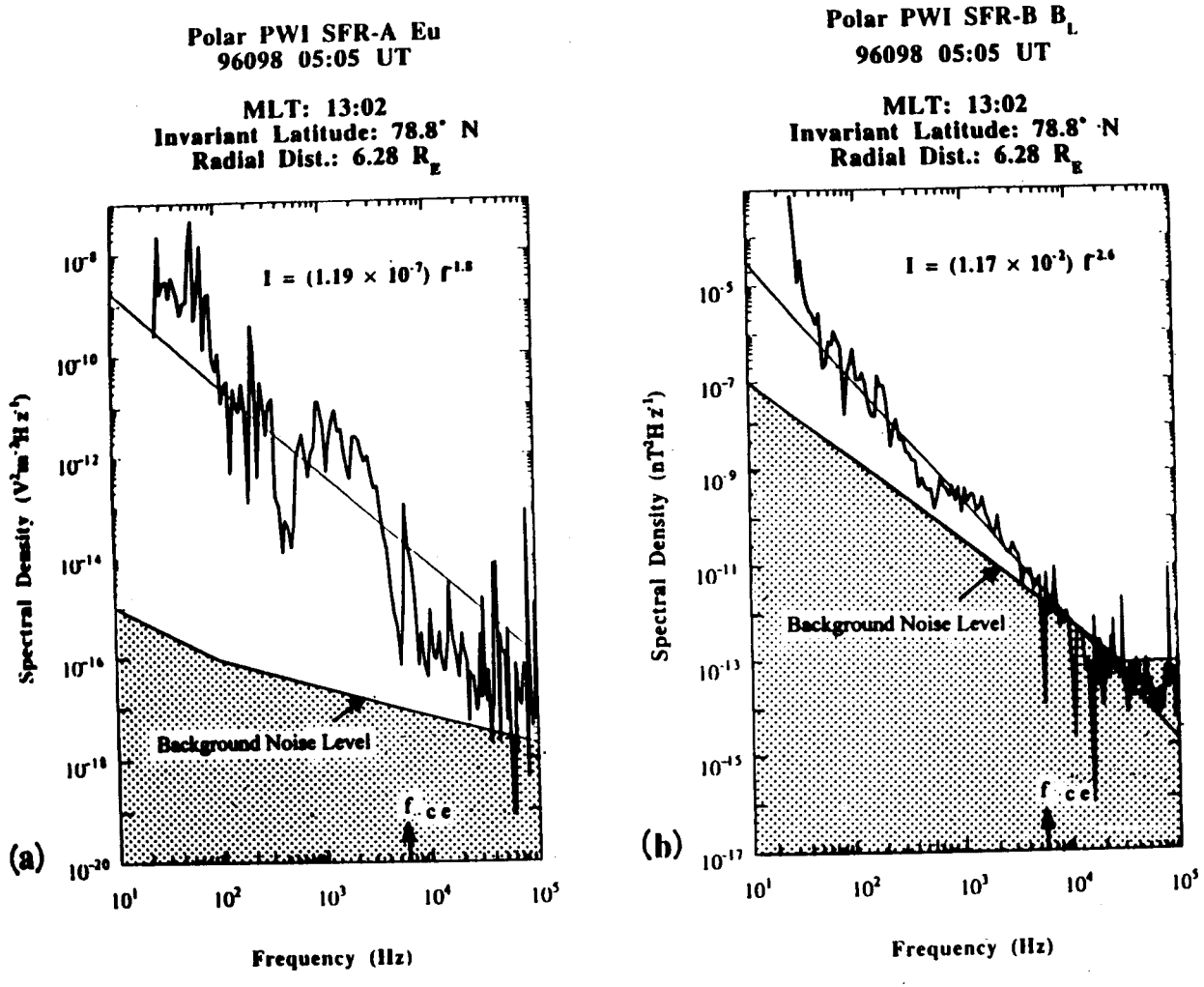
Polar PWI SFR-A Eu
96098 05:05 UT
MLT: 13:02
Invariant Latitude: 78.8° N
Radial Dist.: 6.28 R_E
I = (1.19 × 10^-7) f^1.8
Spectral Density (V²m⁻²Hz⁻¹)
Background Noise Level
f_ce
(a)
Frequency (Hz)
Polar PWI SFR-B B_L
96098 05:05 UT
MLT: 13:02
Invariant Latitude: 78.8° N
Radial Dist.: 6.28 R_E
I = (1.17 × 10^-2) f^2.6
Spectral Density (nT²Hz⁻¹)
Background Noise Level
f_ce
(b)
Frequency (Hz)

Figure 16

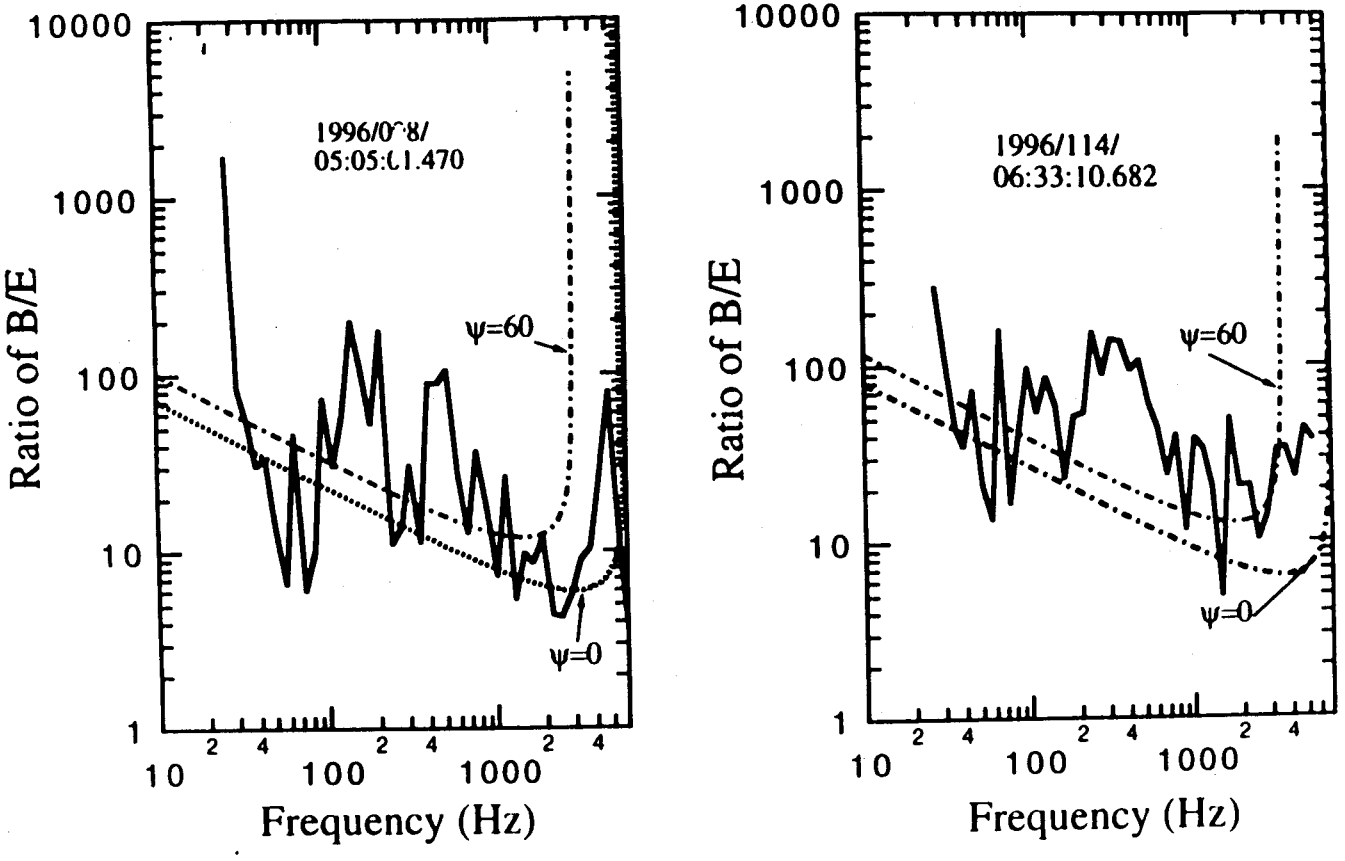
10000
1000
100
10
1
Ratio of B/E
1996/0?8/
05:05:01.470
ψ=60
ψ=0
10
100
1000
Frequency (Hz)
10000
1000
100
10
1
Ratio of B/E
1996/114/
06:33:10.682
ψ=60
ψ=0
10
100
1000
Frequency (Hz)

Figure 17

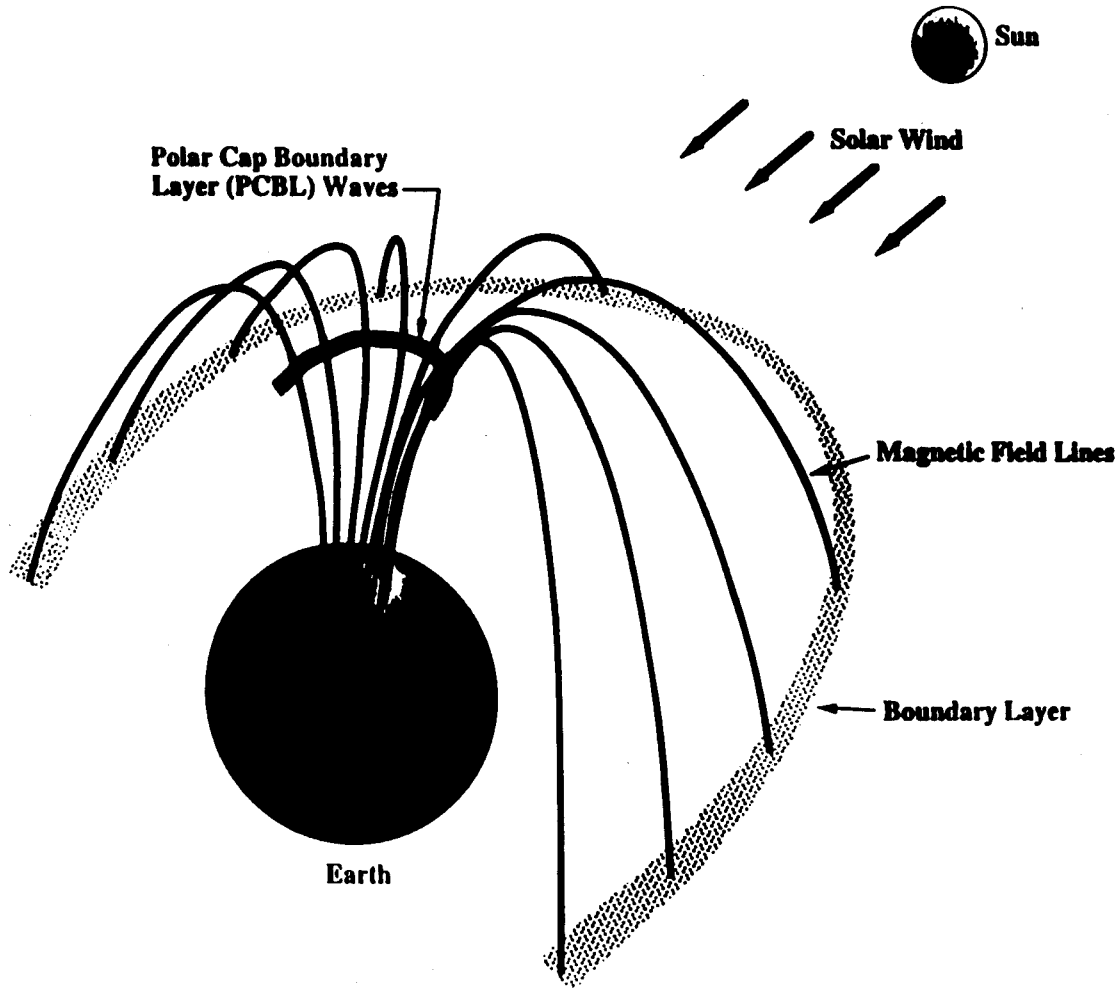
Sun
Solar Wind
Polar Cap Boundary
Layer (PCBL) Waves
Magnetic Field Lines
Boundary Layer
Earth

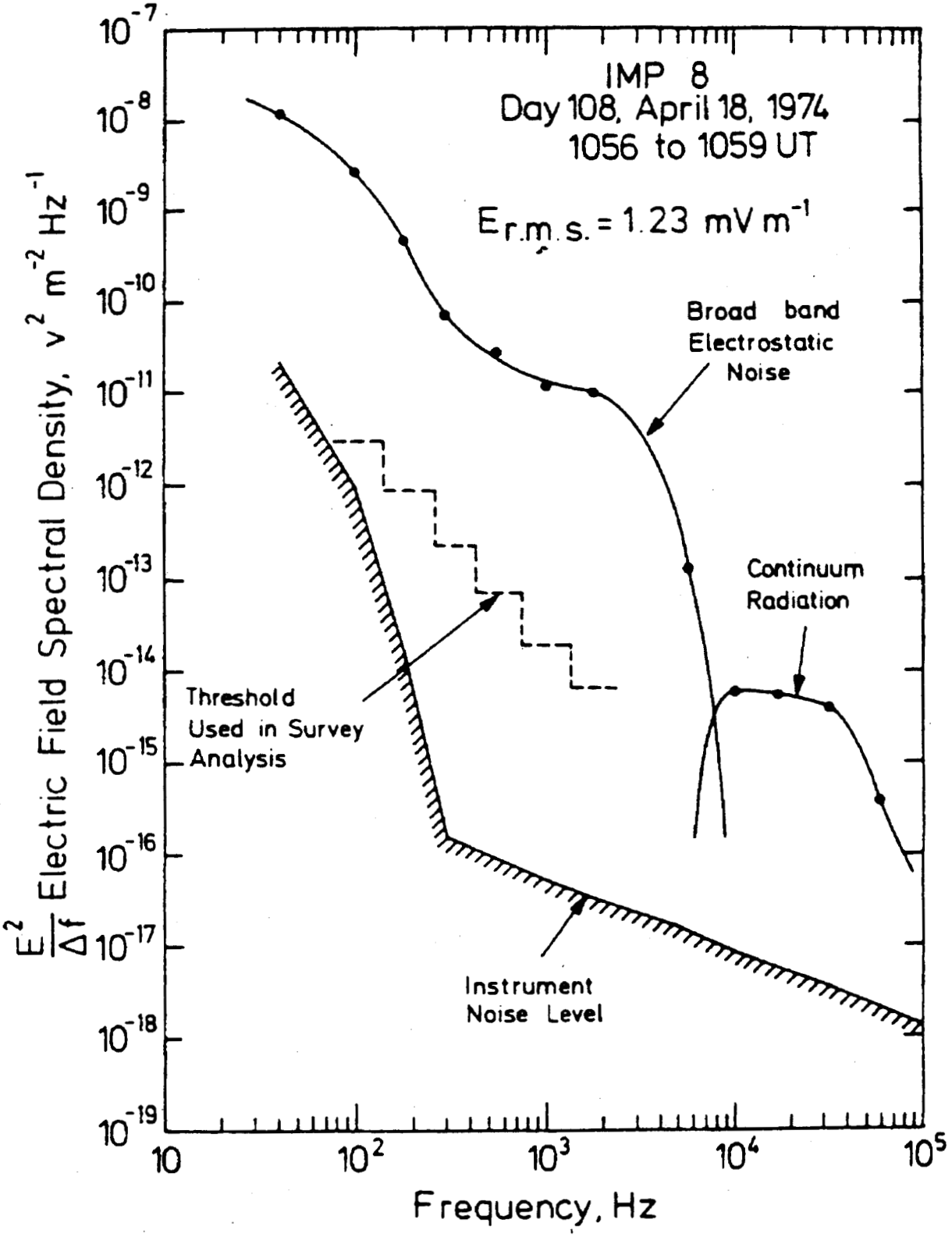
IMP 8
Day 108, April 18, 1974
1056 to 1059 UT
$E_{r.m.s.} = 1.23\ mV\ m^{-1}$
Broad band
Electrostatic
Noise
Continuum
Radiation
Threshold
Used in Survey
Analysis
Instrument
Noise Level
$\frac{E^2}{\Delta f}$ Electric Field Spectral Density, $v^2\ m^{-2}\ Hz^{-1}$
10^{-7}
10^{-8}
10^{-9}
10^{-10}
10^{-11}
10^{-12}
10^{-13}
10^{-14}
10^{-15}
10^{-16}
10^{-17}
10^{-18}
10^{-19}
10
10^2
10^3
10^4
10^5
Frequency, Hz

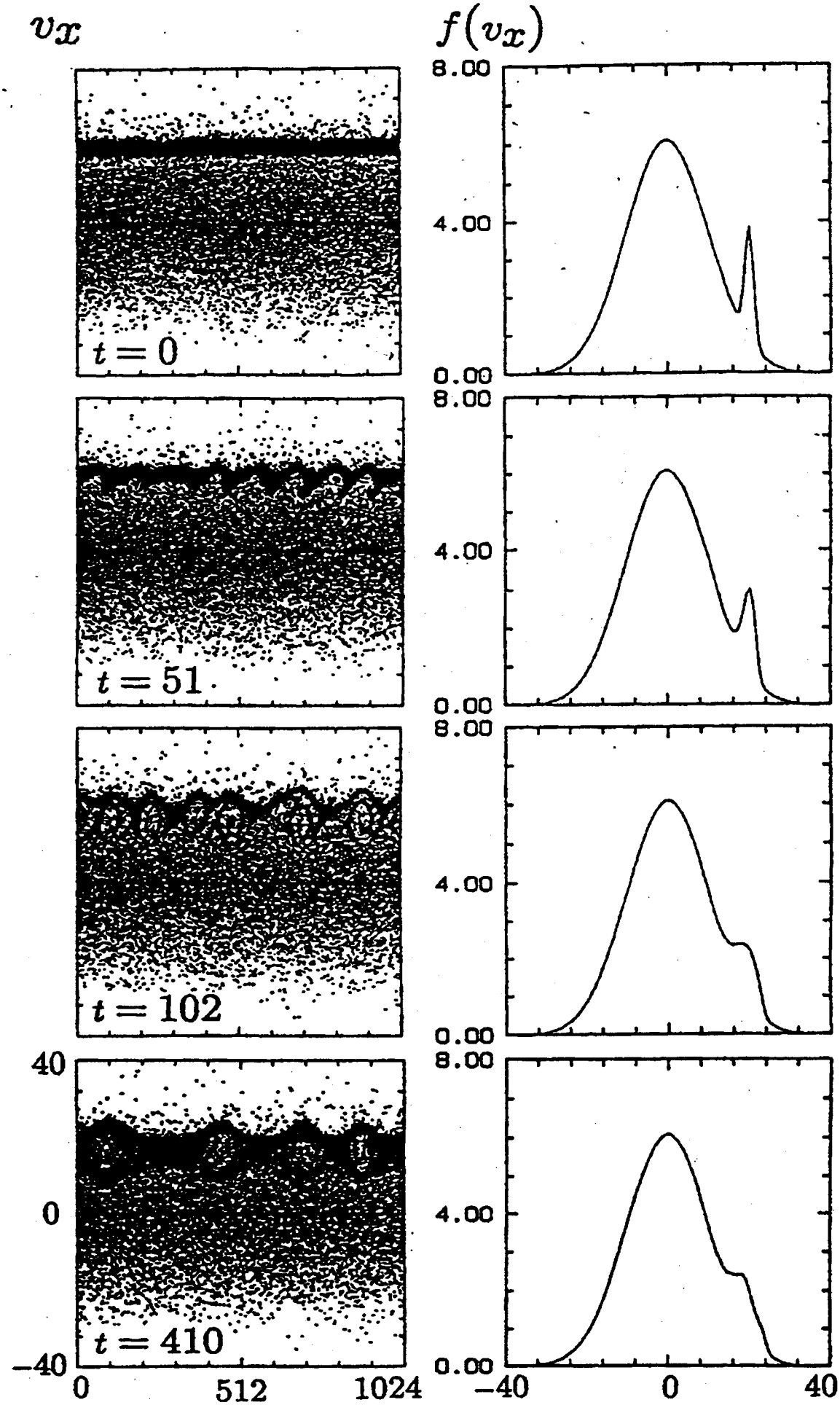
v_x
$f(v_x)$
$t = 0$
$t = 51$
$t = 102$
$t = 410$
8.00
4.00
0.00
40
0
−40
0
512
1024
−40
0
40

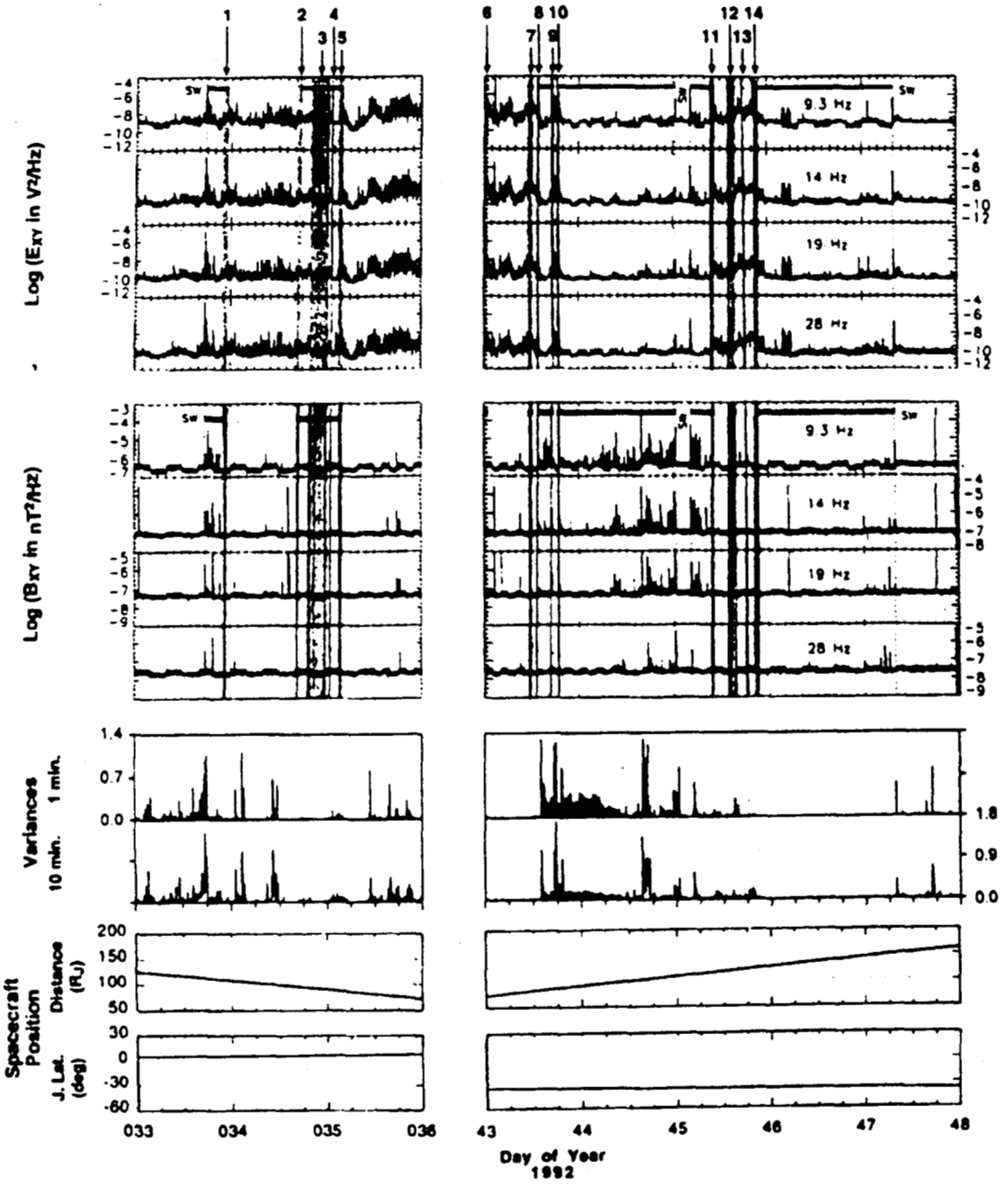
1
2
3
4
5
6
7
8
9
10
11
12
13
14
Log (Exy in V²/Hz)
Log (Bxy in nT²/Hz)
9.3 Hz
14 Hz
19 Hz
28 Hz
SW
Variances
10 min.
1 min.
Spacecraft Position
Distance (RJ)
J. Lat. (deg)
033
034
035
036
43
44
45
46
47
48
Day of Year
1992

21

Figure 21

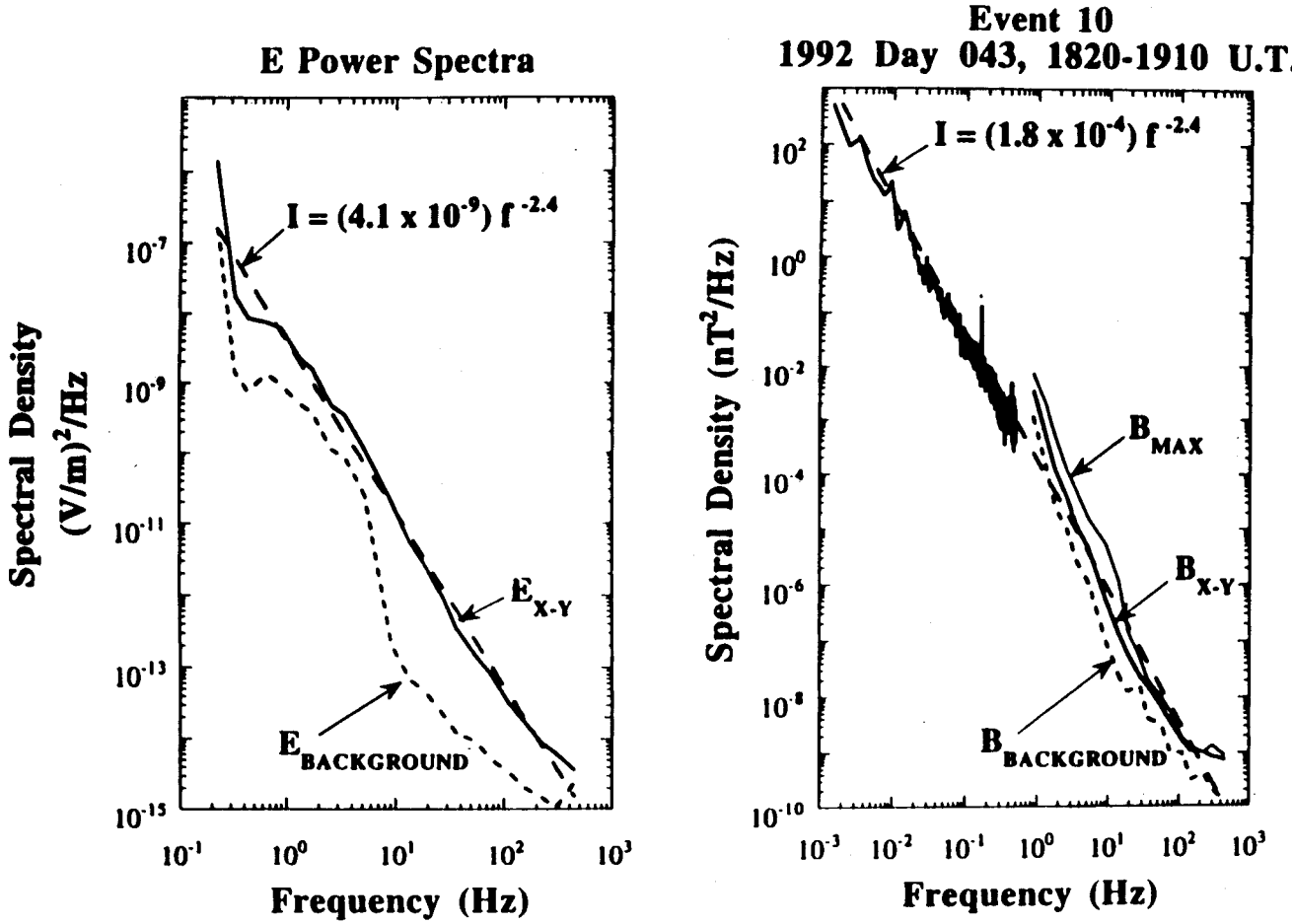
E Power Spectra
I = (4.1 x 10^-9) f^-2.4
E_X-Y
E_BACKGROUND
Spectral Density (V/m)^2/Hz
Frequency (Hz)
Event 10
1992 Day 043, 1820-1910 U.T.
I = (1.8 x 10^-4) f^-2.4
B_MAX
B_X-Y
B_BACKGROUND
Spectral Density (nT^2/Hz)
Frequency (Hz)

Figure 3a

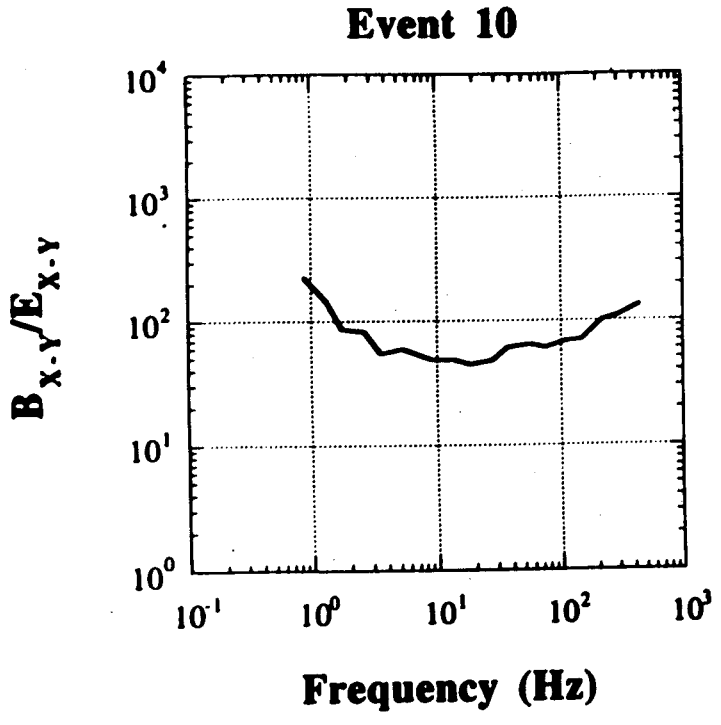

B_{X-Y}/E_{X-Y} at selected frequencies

Frequency (Hz)	B_{X-Y}/E_{X-Y}
1	2.0×10^2
3	7.0×10^1
10	4.9×10^1
30	5.1×10^1
100	6.6×10^1

FIGURE 23

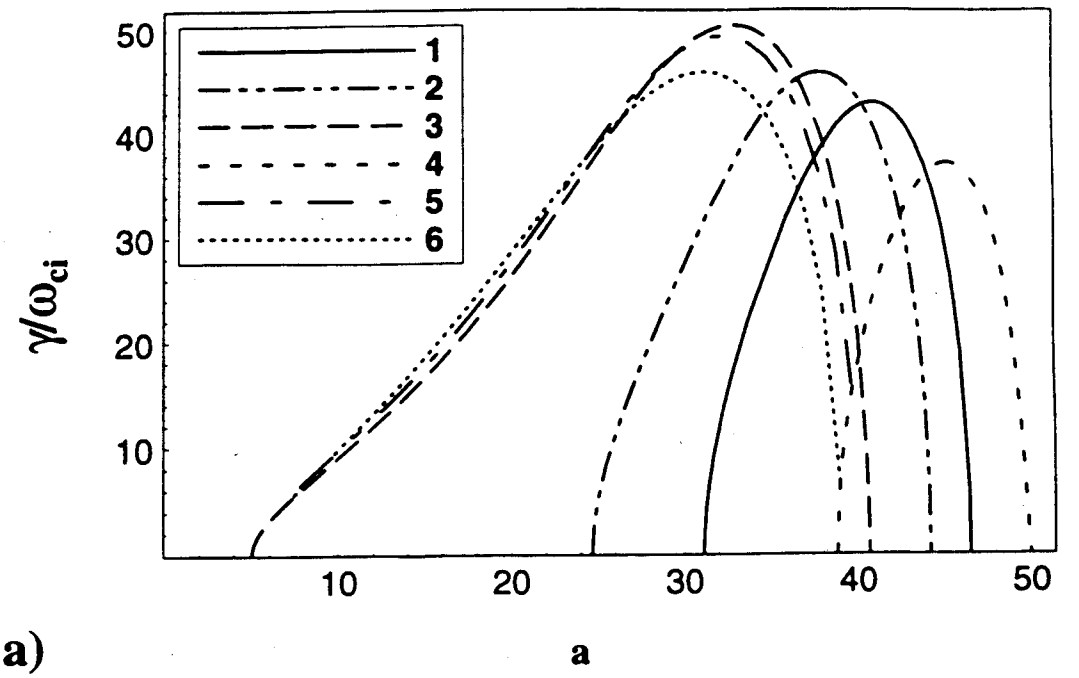
50
40
30
20
10
γ/ω_{ci}
1
2
3
4
5
6
10
20
30
40
50
a

a)

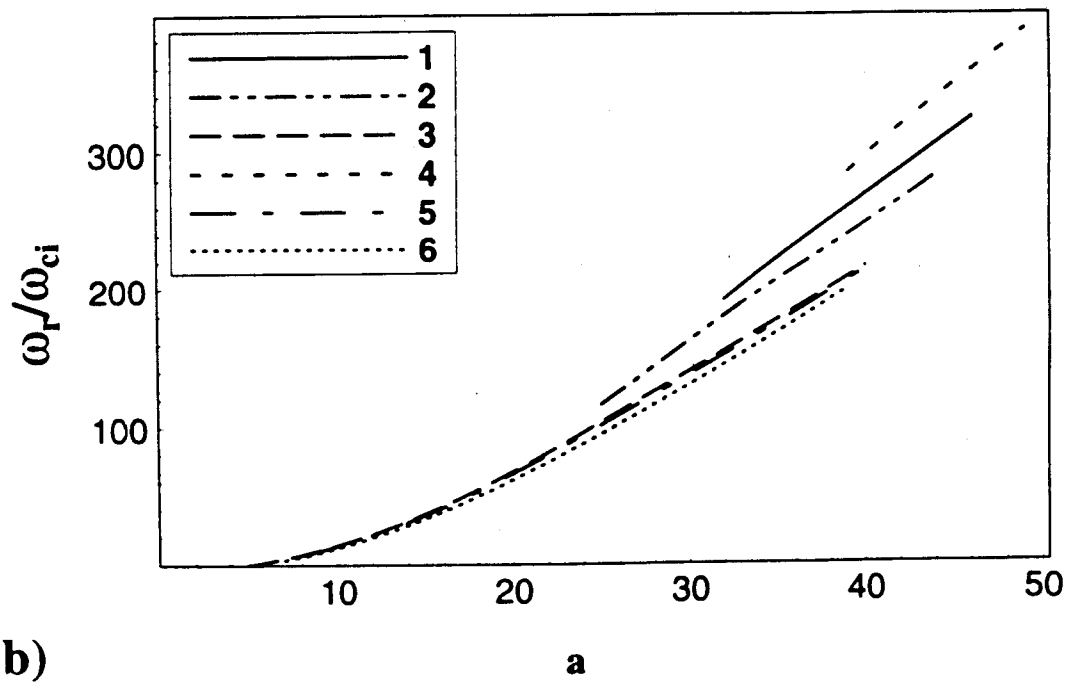
300
200
100
ω_r/ω_{ci}
1
2
3
4
5
6
10
20
30
40
50
a

b)

Figure 2b

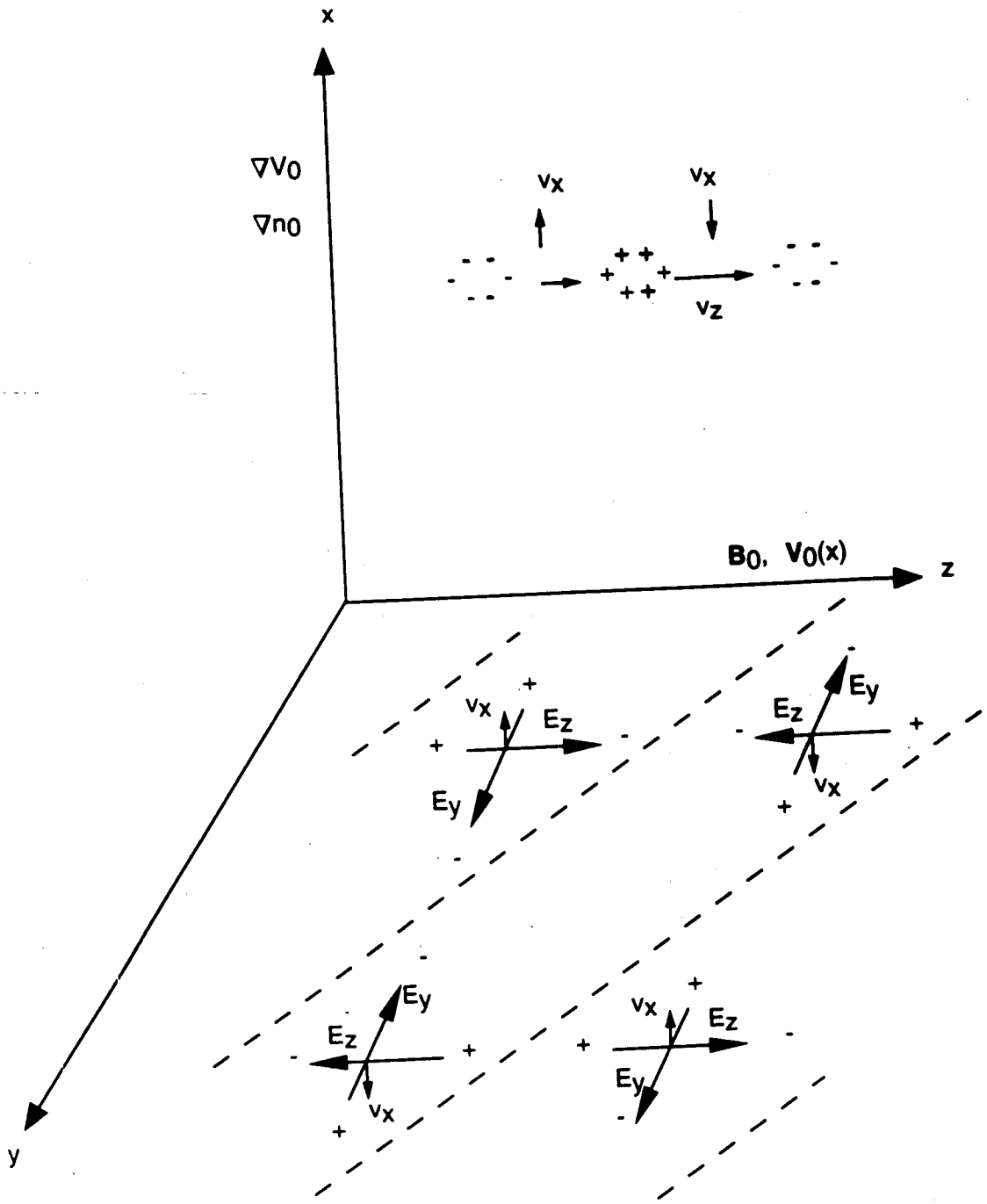

Figure 25

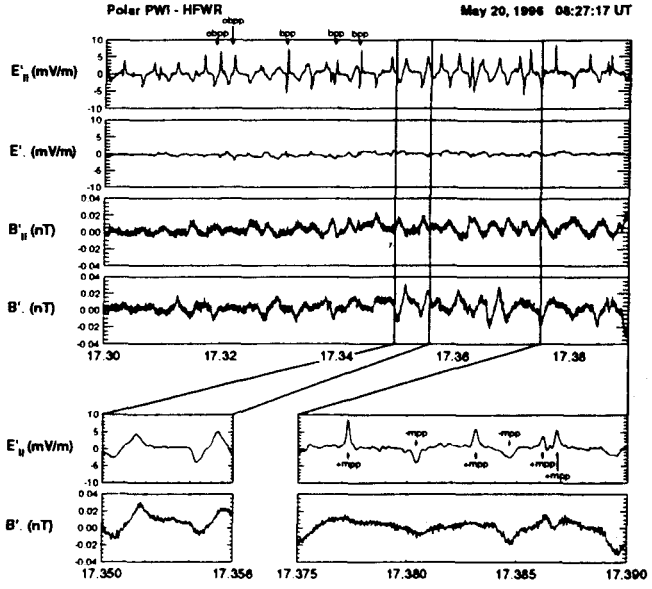
Polar PWI - HFWR
May 20, 1996 08:27:17 UT
obpp
bpp
bpp
bpp
E'll (mV/m)
E'⊥ (mV/m)
B'll (nT)
B'⊥ (nT)
17.30
17.32
17.34
17.36
17.38
E'll (mV/m)
B'⊥ (nT)
mpp
17.350
17.355
17.375
17.380
17.385
17.390

Figure 2b

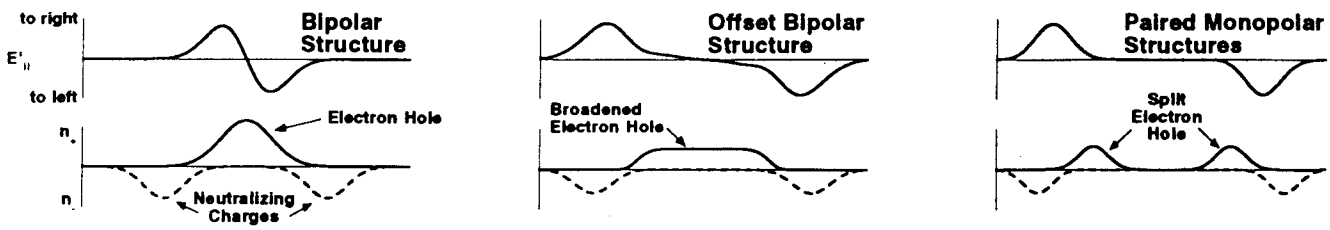
to right
E'||
to left
Bipolar Structure
Electron Hole
n+
n-
Neutralizing Charges
Offset Bipolar Structure
Broadened Electron Hole
Paired Monopolar Structures
Split Electron Hole

Figure 27

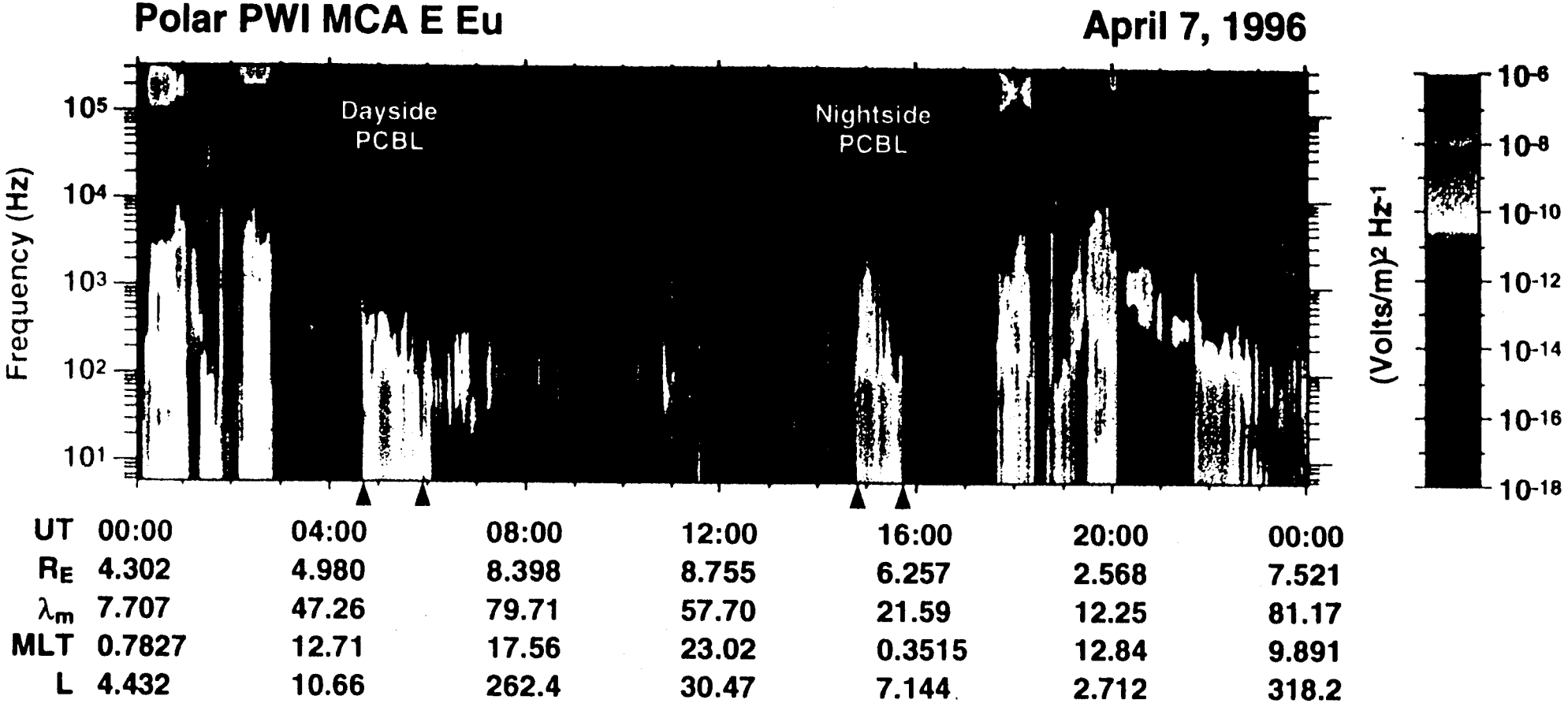
Polar PWI MCA E Eu
April 7, 1996
Dayside
PCBL
Nightside
PCBL
Frequency (Hz)
10^5
10^4
10^3
10^2
10^1
(Volts/m)^2 Hz^-1
10^-6
10^-8
10^-10
10^-12
10^-14
10^-16
10^-18
UT 00:00 04:00 08:00 12:00 16:00 20:00 00:00
R_E 4.302 4.980 8.398 8.755 6.257 2.568 7.521
λ_m 7.707 47.26 79.71 57.70 21.59 12.25 81.17
MLT 0.7827 12.71 17.56 23.02 0.3515 12.84 9.891
L 4.432 10.66 262.4 30.47 7.144 2.712 318.2

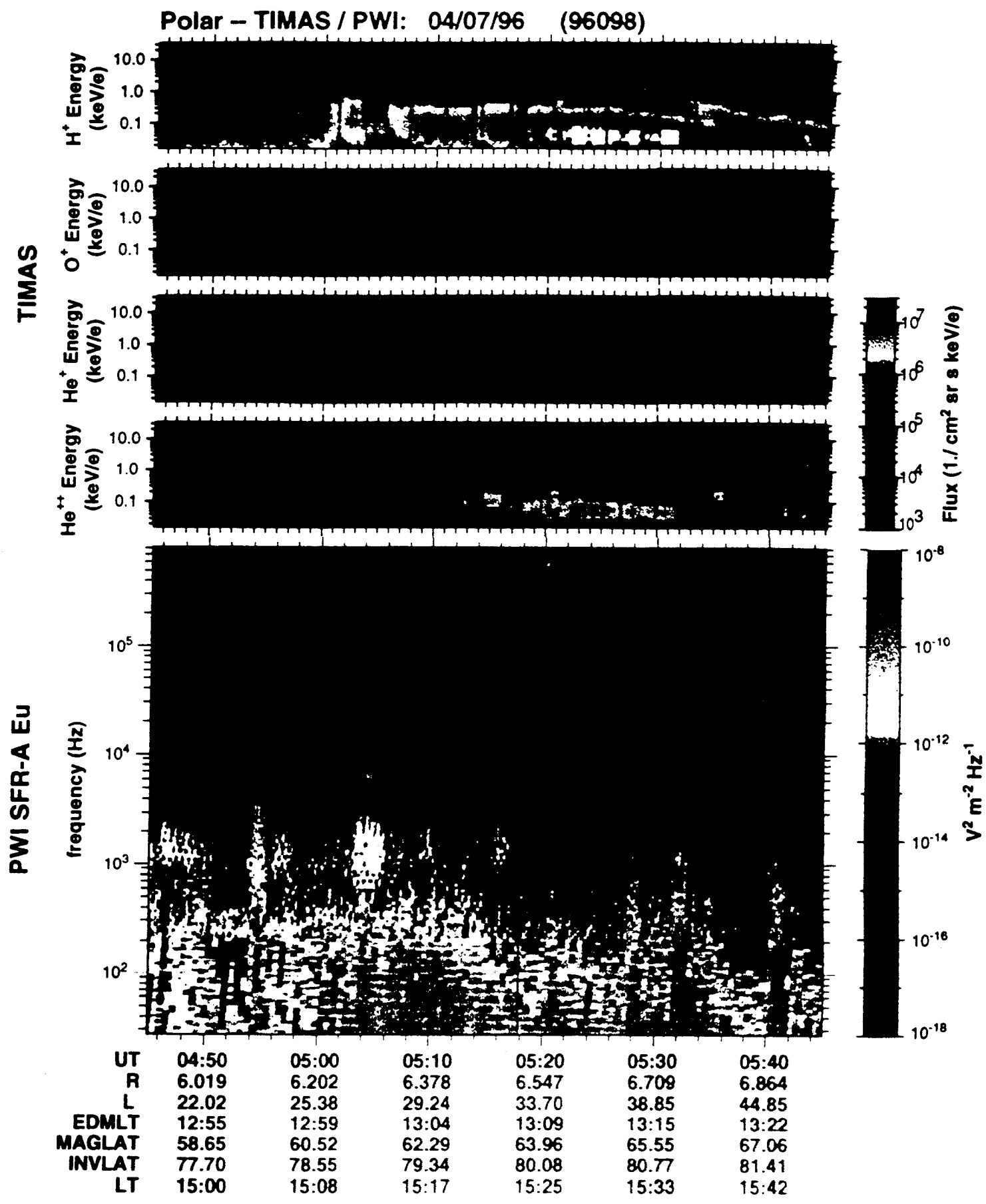
Polar – TIMAS / PWI: 04/07/96 (96098)
TIMAS
PWI SFR-A Eu
H+ Energy (keV/e)
O+ Energy (keV/e)
He+ Energy (keV/e)
He++ Energy (keV/e)
10.0
1.0
0.1
Flux (1./cm2 sr s keV/e)
frequency (Hz)
V2 m-2 Hz-1
UT 04:50 05:00 05:10 05:20 05:30 05:40
R 6.019 6.202 6.378 6.547 6.709 6.864
L 22.02 25.38 29.24 33.70 38.85 44.85
EDMLT 12:55 12:59 13:04 13:09 13:15 13:22
MAGLAT 58.65 60.52 62.29 63.96 65.55 67.06
INVLAT 77.70 78.55 79.34 80.08 80.77 81.41
LT 15:00 15:08 15:17 15:25 15:33 15:42

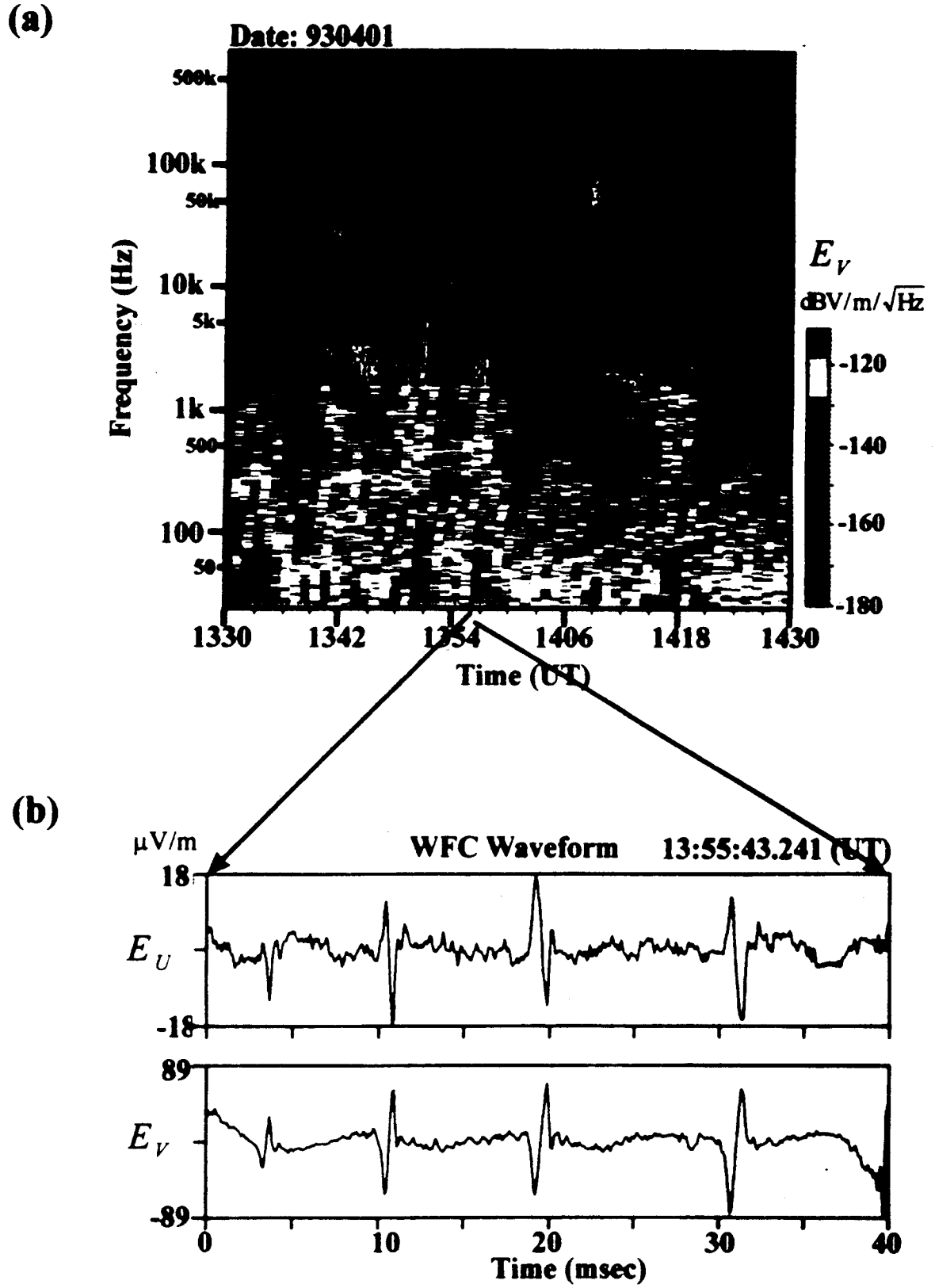
(a)
Date: 930401
500k
100k
50k
10k
5k
1k
500
100
50
Frequency (Hz)
E_V
dBV/m/√Hz
-120
-140
-160
-180
1330
1342
1354
1406
1418
1430
Time (UT)
(b)
μV/m
WFC Waveform
13:55:43.241 (UT)
18
E_U
-18
89
E_V
-89
0
10
20
30
40
Time (msec)